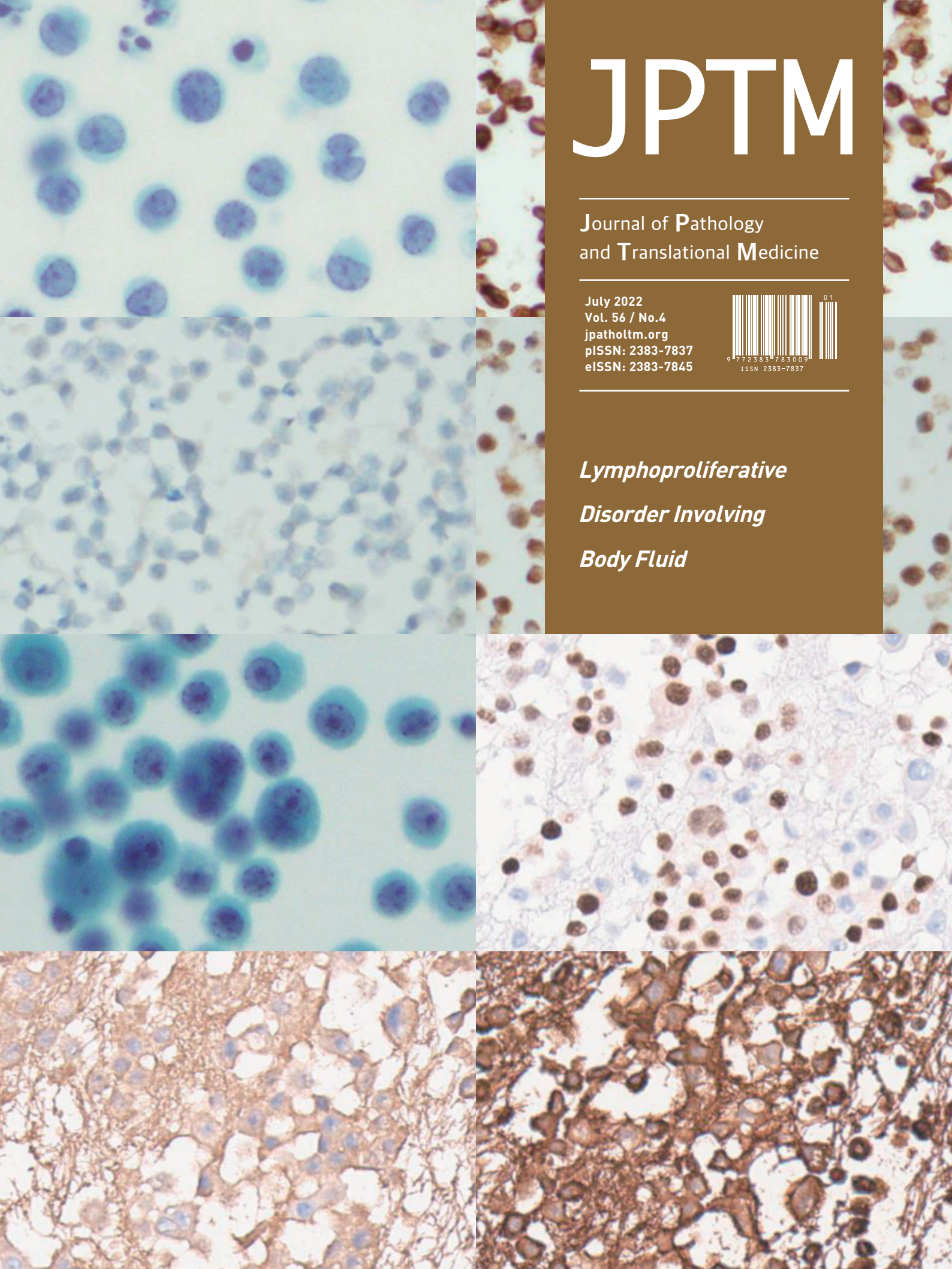

JPTM

Journal of Pathology and Translational Medicine

July 2022
Vol. 56 / No.4
jpatholtm.org
pISSN: 2383-7837
eISSN: 2383-7845

Lymphoproliferative Disorder Involving Body Fluid

Journal of Pathology and Translational Medicine

Volume 56 • Number 4 • July 2022 (bimonthly)
Published since 1967
Printed on 11 July 2022 Published on 15 July 2022

J Pathol Transl Med
pISSN: 2383-7837
eISSN: 2383-7845

Aims & Scope

The Journal of Pathology and Translational Medicine is an open venue for the rapid publication of major achievements in various fields of pathology, cytopathology, and biomedical and translational research. The Journal aims to share new insights into the molecular and cellular mechanisms of human diseases and to report major advances in both experimental and clinical medicine, with a particular emphasis on translational research. The investigations of human cells and tissues using high-dimensional biology techniques such as genomics and proteomics will be given a high priority. Articles on stem cell biology are also welcome. The categories of manuscript include original articles, review and perspective articles, case studies, brief case reports, and letters to the editor.

Subscription Information

To subscribe to this journal, please contact the Korean Society of Pathologists/the Korean Society for Cytopathology. Full text PDF files are also available at the official website (https://jpatholtm.org). *Journal of Pathology and Translational Medicine* is indexed by Emerging Sources Citation Index (ESCI), PubMed, PubMed Central, Scopus, KoreaMed, KoMCI, WPRIM, Directory of Open Access Journals (DOAJ), and CrossRef. Circulation number per issue is 50.

Contact the Korean Society of Pathologists/the Korean Society for Cytopathology

Publishers: Nam, Jong Hee, MD, Gong, Gyungyub, MD
Editors-in-Chief: Jung, Chan Kwon, MD, Park, So Yeon, MD
Published by the Korean Society of Pathologists/the Korean Society for Cytopathology

Editorial Office
Room 1209 Gwanghwamun Officia, 92 Saemunan-ro, Jongno-gu, Seoul 03186, Korea
Tel: +82-2-795-3094 Fax: +82-2-790-6635 E-mail: office@jpatholtm.org

#1508 Renaissancetower, 14 Mallijae-ro, Mapo-gu, Seoul 04195, Korea
Tel: +82-2-593-6943 Fax: +82-2-593-6944 E-mail: office@jpatholtm.org

Printed by iMiS Company Co., Ltd. (JMC)
Jungang Bldg. 18-8 Wonhyo-ro 89-gil, Yongsan-gu, Seoul 04314, Korea
Tel: +82-2-717-5511 Fax: +82-2-717-5515 E-mail: ml@smileml.com

Manuscript Editing by InfoLumi Co.
210-202, 421 Pangyo-ro, Bundang-gu, Seongnam 13522, Korea
Tel: +82-70-8839-8800 E-mail: infolumi.chang@gmail.com

Front cover image: Use of immunocytochemistry in differential diagnosis of hematolymphoid malignancy involving body fluid (p181).

This work was supported by the Korean Federation of Science and Technology Societies Grant funded by the Korean Government (Ministry of Education).

Journal of Pathology and Translational Medicine

J Pathol Transl Med
pISSN: 2383-7837
eISSN: 2383-7845

Volume 56, Number 4, July 2022

CONTENTS

JPTM
Journal of Pathology and Translational Medicine 2022; 56: 173-186
https://doi.org/10.4132/jptm.2022.05.16

REVIEW

Lymphoproliferative disorder involving body fluid: diagnostic approaches and roles of ancillary studies

Jiwon Koh[1], Sun Ah Shin[1,2], Ji Ae Lee[1], Yoon Kyung Jeon[1,3]

[1]Department of Pathology, Seoul National University Hospital, Seoul National University College of Medicine, Seoul;
[2]Department of Pathology, National Cancer Center, Goyang; [3]Cancer Research Institute, Seoul National University, Seoul, Korea

Lymphocyte-rich effusions represent benign reactive process or neoplastic condition. Involvement of lymphoproliferative disease in body cavity is not uncommon, and it often causes diagnostic challenge. In this review, we suggest a practical diagnostic approach toward lymphocyte-rich effusions, share representative cases, and discuss the utility of ancillary tests. Cytomorphologic features favoring neoplastic condition include high cellularity, cellular atypia/pleomorphism, monomorphic cell population, and frequent apoptosis, whereas lack of atypia, polymorphic cell population, and predominance of small T cells usually represent benign reactive process. Involvement of non-hematolymphoid malignant cells in body fluid should be ruled out first, followed by categorization of the samples into either small/medium-sized cell dominant or large-sized cell dominant fluid. Small/medium-sized cell dominant effusions require ancillary tests when either cellular atypia or history/clinical suspicion of lymphoproliferative disease is present. Large-sized cell dominant effusions usually suggest neoplastic condition, however, in the settings of initial presentation or low overall cellularity, ancillary studies are helpful for more clarification. Ancillary tests including immunocytochemistry, in situ hybridization, clonality test, and next-generation sequencing can be performed using cytologic preparations. Throughout the diagnostic process, proper review of clinical history, cytomorphologic examination, and application of adequate ancillary tests are key elements for successful diagnosis.

Key Words: Cytology; Body fluid; Malignant lymphoma; Lymphoproliferative disorder; Immunocytochemistry; Polymerase chain reaction; Next-generation sequencing

Received: April 5, 2022 **Revised:** May 10, 2022 **Accepted:** May 16, 2022
Corresponding Author: Yoon Kyung Jeon, MD, PhD, Department of Pathology, Seoul National University Hospital, Seoul National University College of Medicine, 101 Daehak-ro, Jongno-gu, Seoul 03080, Korea
Tel: +82-2-740-8323, Fax: +82-2-743-5530, E-mail: ykjeon@snu.ac.kr

Effusions in the body cavities occur as the common complication in patients with various types of diseases including benign condition and malignancy. Among the cytologically proven malignant body fluid effusions, involvement of malignant lymphoma is not uncommon. It is reported that about 10%–15% of all malignant pleural effusions and ascites were caused by malignant lymphoma [1-4], after more common causes including carcinomas of lung, breast, and ovary.

Lymphocyte-rich effusions pose a diagnostic challenge in cytopathology, because effusions can be caused by non-neoplastic etiology [2], consisting of predominantly small lymphocytes, thereby mimicking low-grade indolent lymphomas [3-5]. It is often hard to discriminate lymphoma cells from reactive activated lymphocytes based on cytomorphology and cellular atypia. In addition, lymphoma is a very heterogeneous disease composed of tens of entities, and thus their cytomorphogical features are highly variable across disease entities and even in a single disease entity as well. Therefore, careful review of clinical history and precise cytologic examination along with proper use of ancillary testings are essential for accurate diagnosis of lymphoproliferative disease (LPD) involving body fluid. In this review, we aim to discuss the clinical pathological characteristics, diagnostic strategies, ancillary studies, and special considerations regarding LPD involving body fluid. It should be noted that specific diagnosis of hematolymphoid malignancy diagnosis should be based on tissue material and is not necessarily the scope of cytologic diagnosis in practice, except for a few rare conditions (i.e., lymphoma initially or solely presented with effusion, such as primary vitreoretinal lymphoma). However, understanding of unique cytomorphology of lymphoma entities may be very helpful and thus will

pISSN 2383-7837
eISSN 2383-7845

be partly addressed in this review.

CLINICOPATHOLOGICAL CHARACTERISTIC OF LYMPHOPROLIFERATIVE DISEASE INVOLVING BODY FLUID

Body fluid effusions are common complication of LPD and are generally associated with poor prognosis [6-8]. Pleural effusion complicates about 6%–20% of patients with non-Hodgkin lymphoma (NHL), where the proportion is higher with mediastinal involvement [9,10]. Significant age variation is reported in lymphomatous effusions; LPD accounted for the most common cause of malignant body fluid in the children under age 18 years, while only a minority of malignant pleural effusion was caused by LPD in the patients over 40 years of age [3].

Lymphomatous effusions can be either primary or secondary. Primary effusion lymphoma (PEL) is a rare disease entity presenting as serous effusions without detectable nodal disease or tumor masses, which will be discussed later in this review. Secondary involvement of body fluid by LPDs are much more common than PEL. A study in a tertiary medical center in Taiwan [11] reported that the lymphomatous effusions were more commonly caused by B-cell NHL (27/36, 75.0%) than T-cell NHL (8/36, 22.2%) or classic Hodgkin lymphoma (1/36, 2.8%). Most common causes included diffuse large B-cell lymphomas (DLBCL) and high-grade B-cell lymphomas (16/36, 44.4%), followed by peripheral T-cell lymphomas (6/36, 16.7%) and mantle cell lymphomas (MCL) (5/36, 13.9%) [11].

To have a glance at the real world data of lymphomatous effusions, we collected the consecutive cases of cytologically diagnosed LPDs involving body fluid and cerebrospinal fluid (CSF) in Seoul National University Hospital in the year 2020 (Table 1). Samples definitely diagnosed with involvement of hematolymphoid malignancy were included, and those with indeterminate diagnosis such as 'atypical cells' were excluded from the collection to provide clearer view. Our results on body fluid also showed the predominance of B-cell NHLs (12/24, 50.0%) including DLBCLs and high-grade B-cell lymphomas. On the other hand, CSF involvement by leukemic conditions (9/17, 52.9%) outweighed that by lymphoid neoplasm (7/17, 41.2%) or myeloma (1/17, 5.9%).

Table 1. Subtypes of hematolymphoid malignancies in body fluid and CSF diagnosed at Seoul National University Hospital in 2020

	No. (%)
Body fluid	
B-cell NHL	12 (50.0)
DLBCL/LBCL	7 (29.2)
HG B-NHL	2 (8.3)
MCL	1 (4.2)
Effusion-based lymphoma	2 (8.3)
T-cell NHL	3 (12.5)
T-prolymphocytic leukemia	3 (12.5)
cHL	1 (4.2)
Multiple myeloma	3 (12.5)
Leukemia	5 (20.8)
AML	3 (12.5)
T-LBL	2 (8.3)
Total	24 (100)
CSF	
B-cell NHL	7 (41.2)
DLBCL/PCNSL	5 (29.4)
HG B-NHL	1 (5.9)
BL	1 (5.9)
T-cell NHL	0
cHL	0
Multiple myeloma	1 (5.9)
Leukemia	9 (52.9)
B-ALL	5 (29.4)
AML	3 (17.6)
BPDCN	1 (5.9)
Total	17 (100)

CSF, cerebrospinal fluid; NHL, non-Hodgkin lymphoma; DLBCL, diffuse large B-cell lymphoma; LBCL, large B-cell lymphoma; HG B-NHL, high-grade B-cell non-Hodgkin lymphoma; MCL, mantle cell lymphoma; cHL, classic Hodgkin lymphoma; AML, acute myelogenous leukemia; T-LBL, T-cell lymphoblastic lymphoma; PCNSL, primary central nervous system lymphoma; BL, Burkitt lymphoma; B-ALL, B-cell acute lymphoblastic leukemia; BPDCN, blastic plasmacytoid dendritic cell neoplasm.

DIAGNOSTIC APPROACH TO LYMPHOPROLIFERATIVE DISEASES INVOLVING BODY FLUID

Previous studies have proposed various diagnostic algorithms for lymphocyte-rich effusions. Chen et al. [12] presented an algorithmic approach based on the cell size (large, intermediate, and small) and morphologic features (Reed-Sternberg like and plasmacytoid), along with immunohistochemical panel and genomic assays for proper subtyping of LPDs in body fluid. Gochhait et al. [13] also suggested cell sized based triage using a 3-tier (large, intermediate, and small) system for initial classification, whereas more practical 2-tier (small and large) scheme was recently introduced [5]. We consider that 2-tier scheme would be easier to apply in daily practice, particularly for pathologist other than hematopathologist, therefore, we suggest a modified diagnostic algorithm as depicted in Fig. 1.

First, it is important to acknowledge that non-hematolymphoid malignant cells in body fluid specimens can masquerade as lymphocyte-rich effusions. Specific subtypes of non-hemato-

https://doi.org/10.4132/jptm.2022.05.16

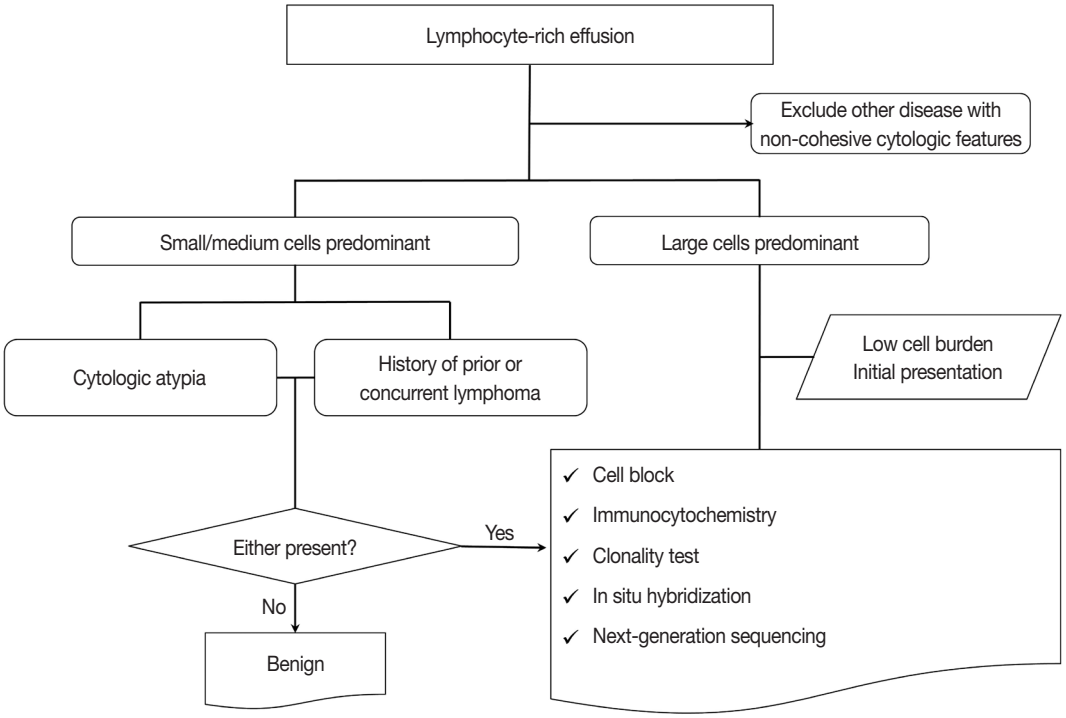

Fig. 1. A practical diagnostic approach toward lymphocyte-rich effusion. Cell sized based initial triage is useful approach when dealing with lymphocyte-rich effusion. Small/medium-sized cell dominant effusions require ancillary testings when either obvious cellular atypia or history of lymphoproliferative disease is present. Large-sized cell dominant effusions usually suggest pathologic fluid accumulation, however, in the settings of initial presentation or low overall cellularity, ancillary studies are helpful for further clarification.

logic cancers often showing discohesive cells include invasive lobular carcinoma of breast [14], small cell lung carcinoma [15], gastric signet ring cell carcinoma [16,17], malignant melanoma [18], and small round cell sarcomas [19] including Ewing sarcoma and rhabdomyosarcoma. Careful review of clinical history and cytomorphology is crucial for differential diagnosis; the cytomorphology of discohesive non-hematolymphoid malignant effusion will not be elaborated in this review. Adjunctive testings including immunocytochemistry (ICC) using cell blocks (CB) could be helpful for differential diagnosis, which will be discussed in detail in ancillary tests section.

After ruling out the possibility of non-hematolymphoid malignant cells in body fluid specimens, we suggest starting with the assessment of the size of the lymphocytes in the effusion fluid and categorize the samples into either small/medium-sized cell dominant or large-sized cell dominant fluid (Table 2, Fig. 1). The criteria for defining cell size are proposed as follows: small/medium-sized cells have diameters less than those of 2 mature lymphocytes or red blood cells (RBCs), while large-sized cells usually have diameters exceeding 3 to 4 times of those of lymphocytes or RBCs.

Representative neoplastic conditions presenting as small/medium-sized cell dominant or large-sized cell dominant fluid are summarized in Table 2 (right column). However, it should be emphasized that classification of hematolymphoid malignancy other than PEL using fluid is beyond the scope of cytologic diagnosis in practice.

Body fluid rich in small/medium-sized lymphoid cells

When dealing with the effusions having predominantly small/medium-sized cells, the distinction between neoplastic conditions from reactive lymphocytosis is often very difficult. Numerous physiologic and pathologic processes can produce reactive lymphocytosis, and commonly encountered causes are described in Table 2 and Fig. 2A–C. Careful review of clinical history should be taken to rule out the possibilities of reactive lymphocytosis; conversely, if the patients have history of previous or suspected concurrent LPD, this warrants further investigation with ancillary studies.

Cytomorphological clues indicating a malignant process in small/medium-sized effusions are suggested in Table 3. Cellular atypia usually refers to the following features: irregular nuclear membrane, nuclear folding or cleavage, coarse chromatin or unusual chromatin patterns (e.g., clotted or soccer-ball-like) [5].

Table 2. Etiology of lymphocyte-rich effusions

Benign lymphocyte-rich effusion	Neoplastic lymphocyte-rich effusion
Infectious cause	Small/medium-sized cells
Tuberculosis	Mantle cell lymphoma
Viral infection	Follicular lymphoma
Fungal infection	Small lymphocytic lymphoma/chronic lymphocytic leukemia
Systemic disease	Lymphoplasmacytic lymphoma
Congestive heart failure	Marginal zone lymphoma
Renal failure	Lymphoblastic lymphoma
Liver cirrhosis	Burkitt lymphoma
Sarcoidosis	Myeloid leukemia
Rheumatoid disease	T/NK-cell lymphoma
Other rare conditions	Large-sized cells
Chylothorax	Diffuse large B-cell lymphoma
Radiotherapy for a malignant disease	Primary effusion lymphoma/effusion-based lymphoma
Dasatinib-induced pleural effusion in patients with leukemia	Multiple myeloma
	Burkitt lymphoma
	Lymphoblastic lymphoma
	Myeloid leukemia
	T/NK-cell lymphoma

NK, natural killer.

However, one should note that these atypical features are hardly recognizable in small/medium-sized lymphocytes in effusion cytology, especially on liquid-based cytology (LBC) specimens [20] where the cells and their nuclei appear smaller than in conventional smears. Nevertheless, when there is significant and obvious cellular atypia in the small/medium-sized cell predominant effusions, further workup including ancillary tests is strongly recommended.

On the other hand, monomorphic appearance of small/medium-sized lymphoid cells with high cellularity usually represents a neoplastic process (Fig. 2D–F), therefore justifying the use of ancillary tests even in the absence of clinical history of LPD. In addition, frequent apoptotic figures also indicate a likelihood of malignant fluid (Fig. 2E).

When small/medium-sized lymphoid cells are dispersed in the polymorphous cellular background, it usually suggests benign reactive process, especially when combined with large centroblasts, immunoblasts, and plasma cells. However, when medium to large plasmacytoid cells are predominant cellular components, outnumbering all other cell types, careful consideration should be taken to rule out the possibility of plasma cell neoplasm. Thorough review of clinical features and assessment of nuclear atypia would aid in the differential diagnosis.

Body fluid rich in large-sized lymphoid cells

Large cell dominant (particularly monomorphic) lymphoid effusions almost always suggest pathologic conditions, therefore diagnostic steps on these fluids are easier to approach. In many cases, large cells show significant cytologic atypia and the background usually exhibit degenerated cell debris, necrosis and apoptosis. DLBCL is the most common cause of secondary large cell predominant lymphoid effusions, and often suggest poor prognosis (Fig. 3A, B) [7]. Less common causes of body fluids rich in large cells include leukemic conditions (Fig. 3C), and T- or natural killer (NK)-cell lineage lymphomas of certain entities which often show twisted, convoluted or multi-lobated nuclei and nuclear folding or grooving (Fig. 3D). In many cases, the diagnosis of large cell predominant lymphoid effusions is followed by ancillary studies for accurate subtyping, if required, and prognostic stratification, which will be further discussed in ancillary tests section.

SPECIFIC DISEASE ENTITIES

Primary effusion lymphoma

PEL is a unique type of large B-cell lymphoma presenting solely as serous effusion in body cavity without tumor masses, lymphadenopathy or organomegaly, usually associated with immunodeficient condition (as represented by human immunodeficiency virus [HIV] infection). PEL is almost always associated with human herpes virus 8 (HHV8) and may be co-infected with Epstein-Barr virus (EBV). It usually confers extremely unfavorable prognosis, with expected median survival of less than 6 months [21].

According to a recent nationwide study, PEL accounts for 0.1% of all malignant lymphoma in Republic of Korea [21,22]. Typically, PEL is composed of large size B-cell with immunoblastic, plasmablastic or anaplastic morphology and shows post-germinal center plasmablastic differentiation. A typical example is shown in the Fig. 4A. A 79-year-old male patient with a history

 https://doi.org/10.4132/jptm.2022.05.16

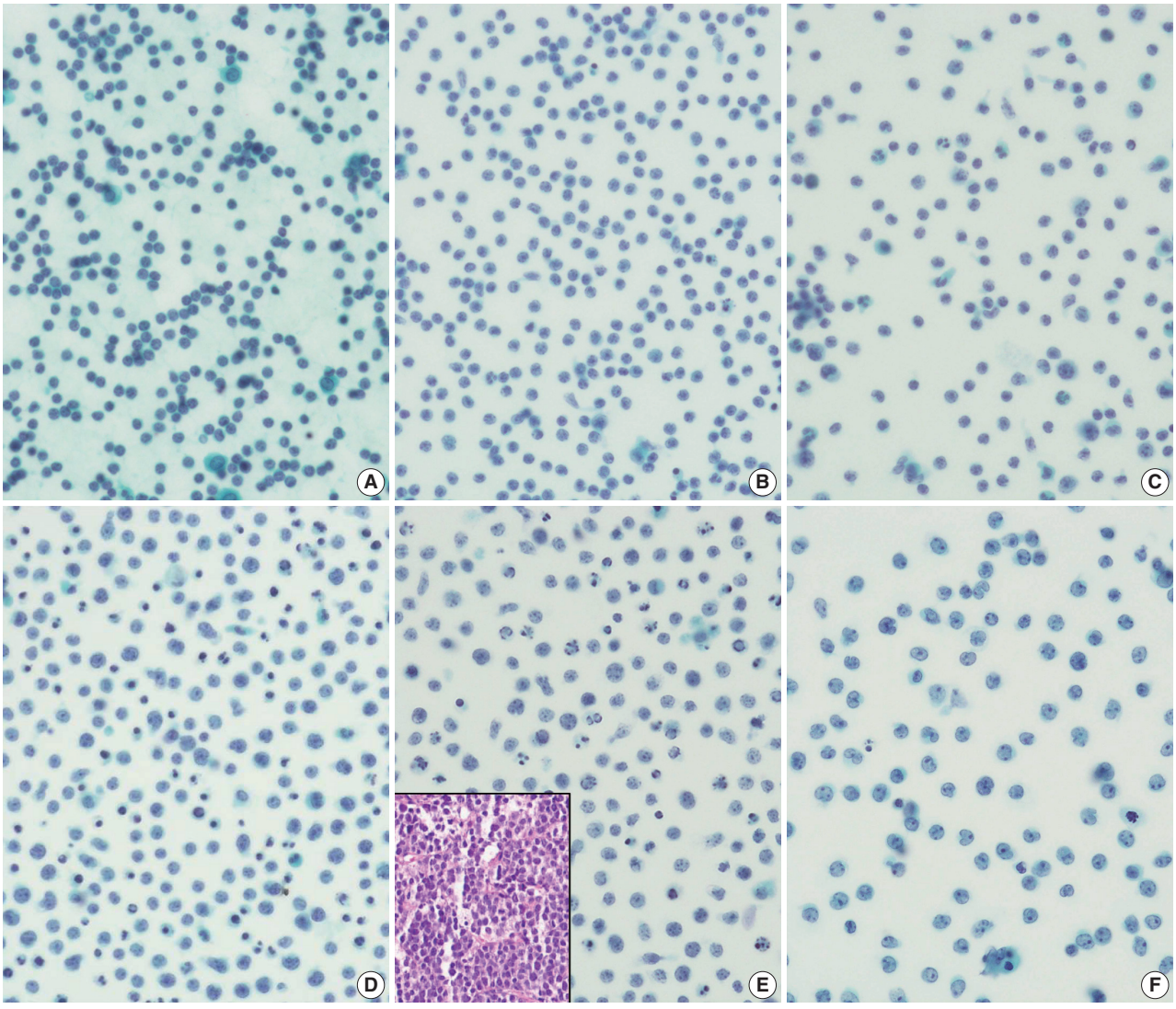

Fig. 2. Differential diagnosis of small/medium-sized cell predominant effusion. Reactive lymphocytosis due to infectious process (A, ascitic fluid from a 64-year-old female with peritoneal tuberculosis) or hemodynamic condition (B, pleural fluid from a 59-year-old male who underwent lung transplantation) result in producing small/medium-sized cells. Chylothorax is another uncommon condition showing small/medium-sized lymphocyte-predominant body fluid (C, pleural fluid from a 50-year-old male). In neoplastic conditions, the overall cellularity of small/medium-sized cells are very high and often accompanied by apoptotic bodies, as shown in the pericardial fluid from a 72-year-old male with known mantle cell lymphoma (D) and ascitic fluid from a 46-year-old male with Burkitt lymphoma (E, inset showing H&E staining of the tumor). The site of fluid accumulation also gives a clue, especially cerebrospinal fluid (CSF) where high cellular composition almost always suggests a pathologic condition (F, CSF from a 42-year-old female with B-acute lymphoblastic leukemia).

of prostate cancer presented with dyspnea on exertion, where large amount of pleural effusion was noted. On systemic work-up, there was no evidence of solid tumor mass or lymphadenopathy. Drained pleural fluid was composed of numerous large lymphoid cells with many apoptotic bodies, and subsequent ICC on CB revealed CD45-positive, CD20-negative, CD38-positive and HHV8-positive immunophenotype, consistent with PEL.

Recently, further subtyping of PEL was suggested, namely PEL type I and type II [23]. In contrast to the classic type I PEL, type II PEL (also called effusion-based lymphoma) is characterized by frequent expression of pan B-cell markers (e.g., CD20 and CD79a) and less plasmablastic differentiation; most importantly, type II is often HHV8-negative and rarely associated with HIV. Clinically, type II PEL is rather associated with medial conditions which lead to fluid overload states, including hepatitis C viral infection. We also experienced a case of HHV8-negative effusion-based large B-cell lymphoma (Fig. 4B). Type II PEL also confers poor prognosis [23-25], despite a little better than the type I.

Dasatinib-induced effusion

Another unique entity presenting as body cavity-based lymphocyte-rich effusion is dasatinib-induced effusion. Dasatinib is the second-generation tyrosine kinase inhibitor used for the treatment of patients with *BCR-ABL* translocation positive chronic myelogenous leukemia (CML) [26]. The abnormal accumulation of body fluid occurs in about 20% to 40% of patients with CML receiving dasatinib, where severe forms develop in 3% to 7% of patients [27,28]. The effusion is composed of clonal proliferation of cytotoxic T- or NK-cells. Although the pathogenesis is unclear, several hypotheses are suggested including increased vascular permeability due to kinase inhibition or immune-mediated reaction [27]. Temporary reduction of dasatinib dosage or short-term steroid therapy usually alleviate the effusion, therefore, it is very important to recognize the lympho-dominant nature of the fluid, thus, not to be confused with the secondary leukemic involve-

Table 3. Cytomorphologic clues for distinction between reactive and neoplastic process in small/medium-sized cell predominant fluids

Favor reactive	Favor neoplastic
Lack of atypia	High cellularity
Polymorphic cells	Cellular atypia/pleomorphism
Predominantly small-sized T cells	Monomorphic cells
	Frequent mitoses and apoptosis

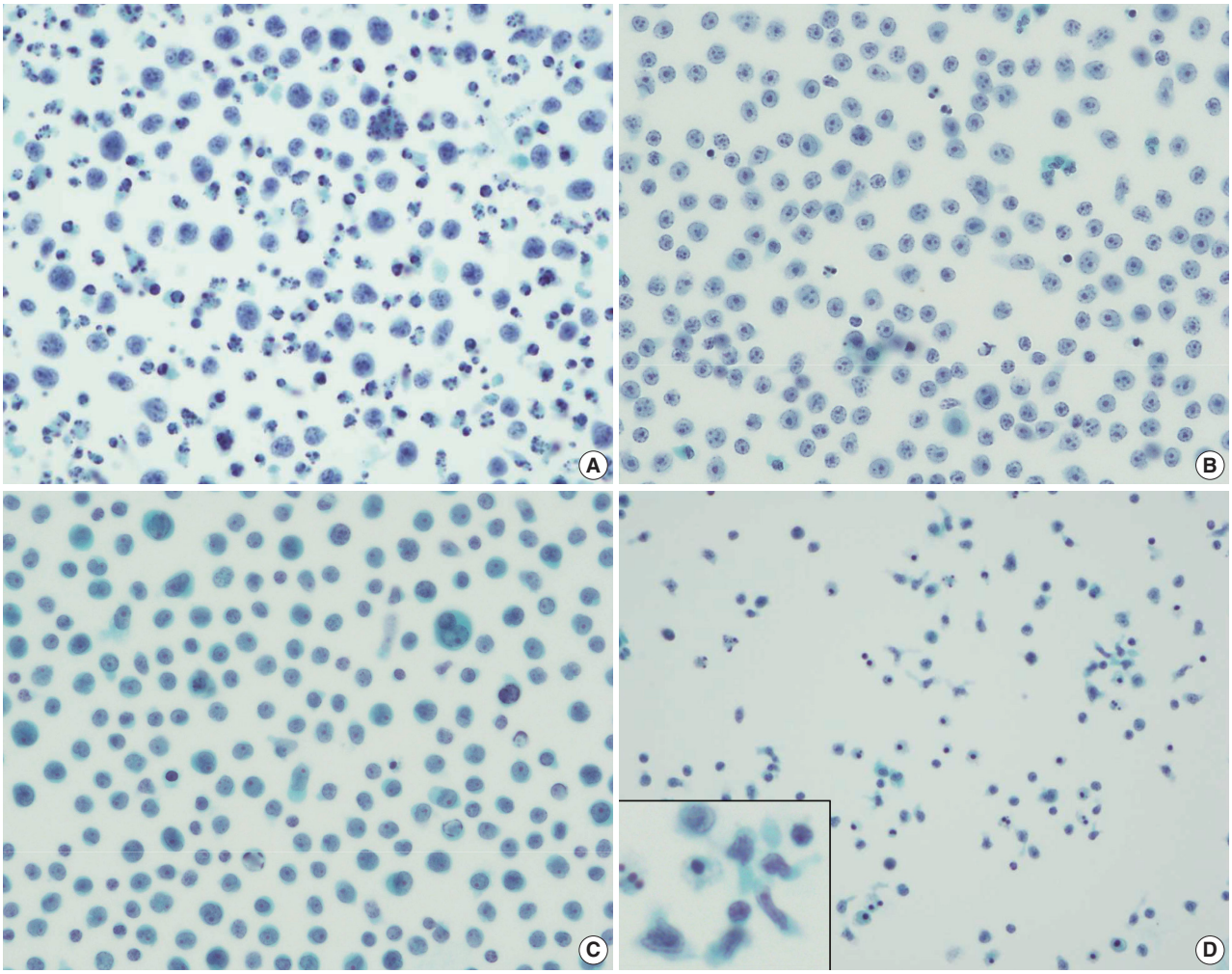

Fig. 3. Differential diagnosis of large-sized cell predominant effusion. Ascitic fluid drained from a 60-year-old male patient with heavily treated diffuse large B-cell lymphoma (DLBCL) has numerous large, atypical cells in the background of apoptotic bodies (A). Another malignant effusion from a DLBCL patient show predominantly immunoblastic morphology, highlighted by central, prominent nucleoli (B). A 42-year-old male with known myeloid sarcoma presented with pleural fluid, where numerous atypical cells were observed, representing a rare cause of malignant effusion (C). Another rare cause of malignant pleural effusion included a 74-year-old female patient with monomorphic epitheliotropic intestinal T-cell lymphoma involving colon and lung (D). Note the peculiar cellular appearance including folded nuclei and cytoplasmic tails (D, inset).

https://doi.org/10.4132/jptm.2022.05.16

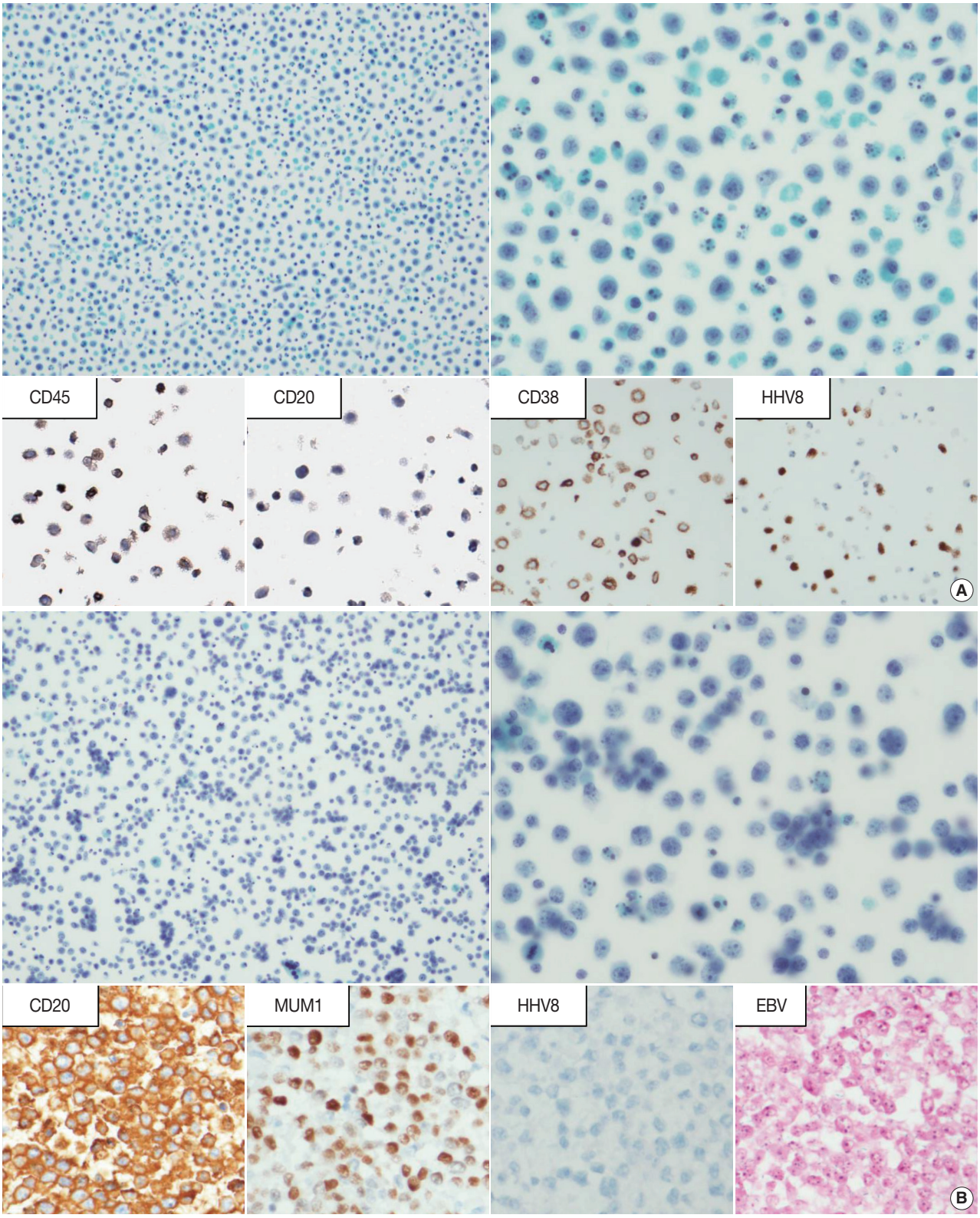

Fig. 4. Primary effusion lymphoma and effusion-based large B-cell lymphoma. For the differential diagnosis of large-sized cell dominant fluid effusion, immunocytochemistry was performed, which revealed immunophenotype consistent with primary effusion lymphoma (A). A case of effusion-based large B-cell lymphoma, also known as type II primary effusion lymphoma, is depicted (B). Note the distinct immunophenotype including negativity for human herpes virus 8 (HHV8) and Epstein-Barr virus (EBV) in situ hybridization.

ment in patients with CML treated with dasatinib.

Breast implant associated anaplastic large cell lymphoma

Breast implant associated anaplastic large cell lymphoma (BI-ALCL) is a rare type of non-Hodgkin T-cell lymphoma occurring in patients who underwent breast augmentation procedure [29-31]. About two thirds of patients present with effusion around the implant, after 9 years from implantation on average [29]. Aspiration fluid cytology evaluation is an effective and minimally invasive method for the diagnosis of BI-ALCL [32].

Aspirated fluid from the patients with BI-ALCL usually shows hypercellular population of large atypical lymphoid cells with lobulated nuclei [33]. Cytoplasmic vacuolizations can be extensive, and necrotic or fibrinoid background can be a distinguishing feature from 'benign seroma' composed of transudate fluid. When BI-ALCL is suspected, CB preparation is recommended for ancillary studies [33].

ANCILLARY TESTS

Concerns regarding the cytology preparation

Body fluid specimen drawn from the patients can be processed for adequate evaluation using variable methods including conventional smears, cytospins, CBs and LBC [34]. Most of the reports comparing the diagnostic performance of variable preparations showed that the newer technology—LBC—is comparable to that of conventional methods [34-37]. Specifically, LBC usually result in better cell yield, provide easier examination since cells are evenly dispersed in a small area, with minimal drying artifact and erythrocytes obscuring examination. However, some technical disadvantages of LBC preparation should be kept in mind. During the process, morphologic alterations including cell/nuclear size shrinkage and architecture disruption can occur [38]. Despite these disadvantages, stored LBC material can be processed for CBs, immunostainings and molecular genetic analyses up to 3 or 4 months [34], therefore, LBC preparation is a preferred method with many additional advantages with comparable diagnostic efficacy.

CB and hematoxylin and eosin stain

When dealing with effusions from patients with known history or clinical suspicion of LPD, or those rich in large-sized lymphoid cells, it is important to preserve a portion of specimen to establish CB with appropriate preparation method. Since the most of procedures in pathology laboratories are based on the use of formalin fixed paraffin embedded (FFPE), CBs can readily be handled with ease. In addition, CB specimens retain the cytomorphologic features and antigenicity for further microscopic examination and ICC studies [39,40].

Immunocytochemistry

ICC is the most commonly used ancillary study for the diagnosis of lymphocyte-rich effusion. The ICC stains retain the cytomorphologic features and expression of certain markers help the confirmatory diagnosis in some entities, i.e., HHV8 expression in PELs. In many cases, panels of multiple items including lineage markers are required for the diagnosis of LPD in effusion cytology.

Fig. 5A shows pleural effusion fluid from a 77-year-old man, where medium-sized lymphoid cells were predominant. CB was prepared and subsequent ICC revealed CD20-positivity, suggesting the possibility of B-cell lymphoma. The cells were negative for cyclin D1 but SOX11 positive, rendering the diagnosis of lymphoma, consistent with MCL. Fig. 5B is another pleural fluid specimen drained from a 46-year-old male, and numerous MUM1 positive plasmacytoid cells having abundant cytoplasm and eccentric nuclei are observed. The cells were diffusely positive for lambda while negative for kappa; this light chain restriction revealed by ICC aids in confirming the neoplastic nature of the fluid and involvement of patient's underlying multiple myeloma.

Flow cytometry

Body fluid effusions are often suitable samples for flow cytometry (FC), given the samples are not fixed by alcohol or formalin. FC-based analysis is an extremely useful method when dealing with differential diagnosis of effusion-based hematolymphoid malignancy, because this technology provides a reproducible, quantitative and sensitive immunophenotyping of cells, using fluorescent-tagged antibodies targeting surface markers [5,41-44]. Similar to ICC, FC analysis using a panel of antibodies can provide diagnostic clues in lymphoid malignancies. One important consideration should be noted; since the reactive lymphocyte-rich effusions are often T-cell predominant, T-cell abundancy shown by FC does not guarantee the diagnosis of T-cell lymphoma [5,41].

Though rarer than lymphoid diseases, FC also serves important roles in leukemic conditions [41,43]. For instance, involvement of chronic lymphocytic leukemia (CLL) on body fluid can be very difficult to distinguish from reactive lymphocytosis. When there is clinical history or suspicion for CLL, FC is strongly recommended, and documentation of CD19+, CD20+ B-cell with CD5 or CD23 expression can qualify the diagnosis of CLL involvement [43].

https://doi.org/10.4132/jptm.2022.05.16

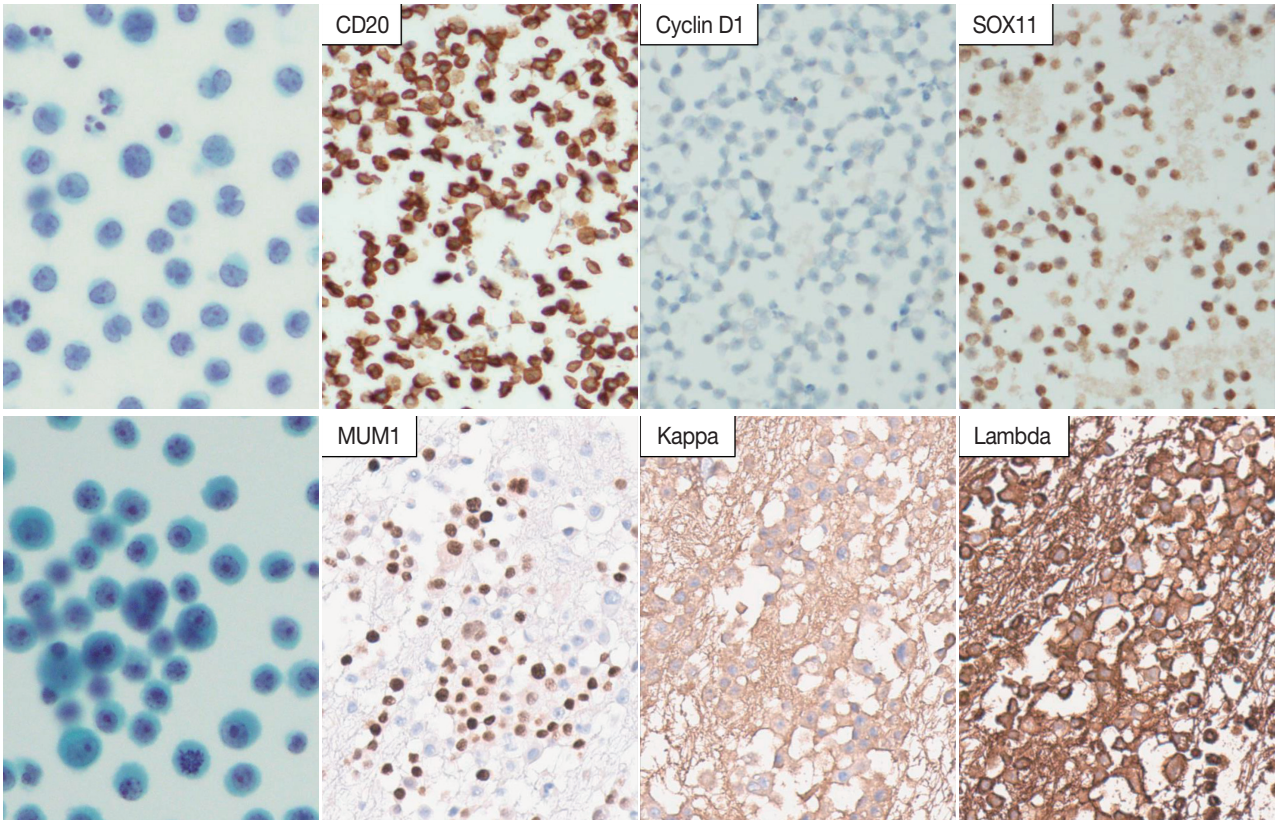

Fig. 5. Use of immunocytochemistry in differential diagnosis of hematolymphoid malignancy involving body fluid. A 77-year-old male patient had a large amount of pleural effusion composed of small/medium-sized atypical lymphoid cells with CD20 and SOX11 expression, consistent with the involvement of mantle cell lymphoma (A). Numerous atypical large plasmacytoid cells with lambda restriction on immunocytochemistry suffices for the diagnosis of myelomatous effusion (B).

Clonality studies

Many studies have shown the efficacy of polymerase chain reaction (PCR) for the assessment of immunoglobulin heavy chain (IgH) gene rearrangements or TCRγ gene rearrangements. Recently, clonality tests in many pathology laboratories are readily performed using BIOMED-2 assay [45,46]. Many studies have reported that detecting clonality is useful for the differential diagnosis between reactive lymphocytosis and lymphomatous fluid [47-51].

Fig. 6A shows a case where clonality testing was very helpful in the diagnosis. A 61-year-old female was diagnosed with primary central nervous system (CNS) DLBCL by stereotactic biopsy, and her CSF contained a few atypical lymphoid cells (Fig. 6A). B-cell monoclonality was found in IgH gene rearrangement study, strongly suggesting the involvement of DLBCL.

Reactive effusions tend to be T-cell predominant, therefore, T-cell clonality test is often required to confirm involvement of T-cell LPD in body fluids [5,52]. T-cell prolymphocytic leukemia (T-PLL) can rarely involve extramedullary sites [53], and nodal involvement was diagnosed in a 63-year-old female patient (Fig. 6B). The patient developed ascites, and leukemic involvement was suspected. Cytomorphologically, some small/medium-sized lymphocytes were observed and the overall cellularity was not remarkable; however, TCRγ gene rearrangement test proved monoclonal T-cell proliferation, supporting the involvement of T-PLL of patient.

One of the practically useful tips for correct interpretation is to consider comparing the clonality testing result from cytology specimen with that from the tissue specimen. If the both results show clonal peaks/bands with approximately same size, the diagnostic power of lymphomatous effusion could be strengthened.

Clonality test could be useful for the diagnosis of CSF cytology in patients with malignant lymphoma. Review of 101 CSF samples from patients with B-cell lymphoma diagnosed in Seoul National University Hospital from 2015 to 2017 showed that monoclonality by IgH gene rearrangement study using BIOMED-2 assay was detected in 42.9% of cytomorphologically atypical/positive CSF and as much as 18.2% of cytomorphologically nega-

tive CSF specimens (Table 4). While clonality tests are very helpful, a specific consideration should be taken when interpreting the test performed on CSF specimen. Since the overall cellularity in CSF specimen is usually very low, high sensitivity of PCR test may result in false positive pseudoclonality due to selective amplification of certain non-neoplastic clones. According to our internal review of CSF cytology from73 patients with B-cell lymphoma and active brain (leptomeningeal and/or parenchymal)

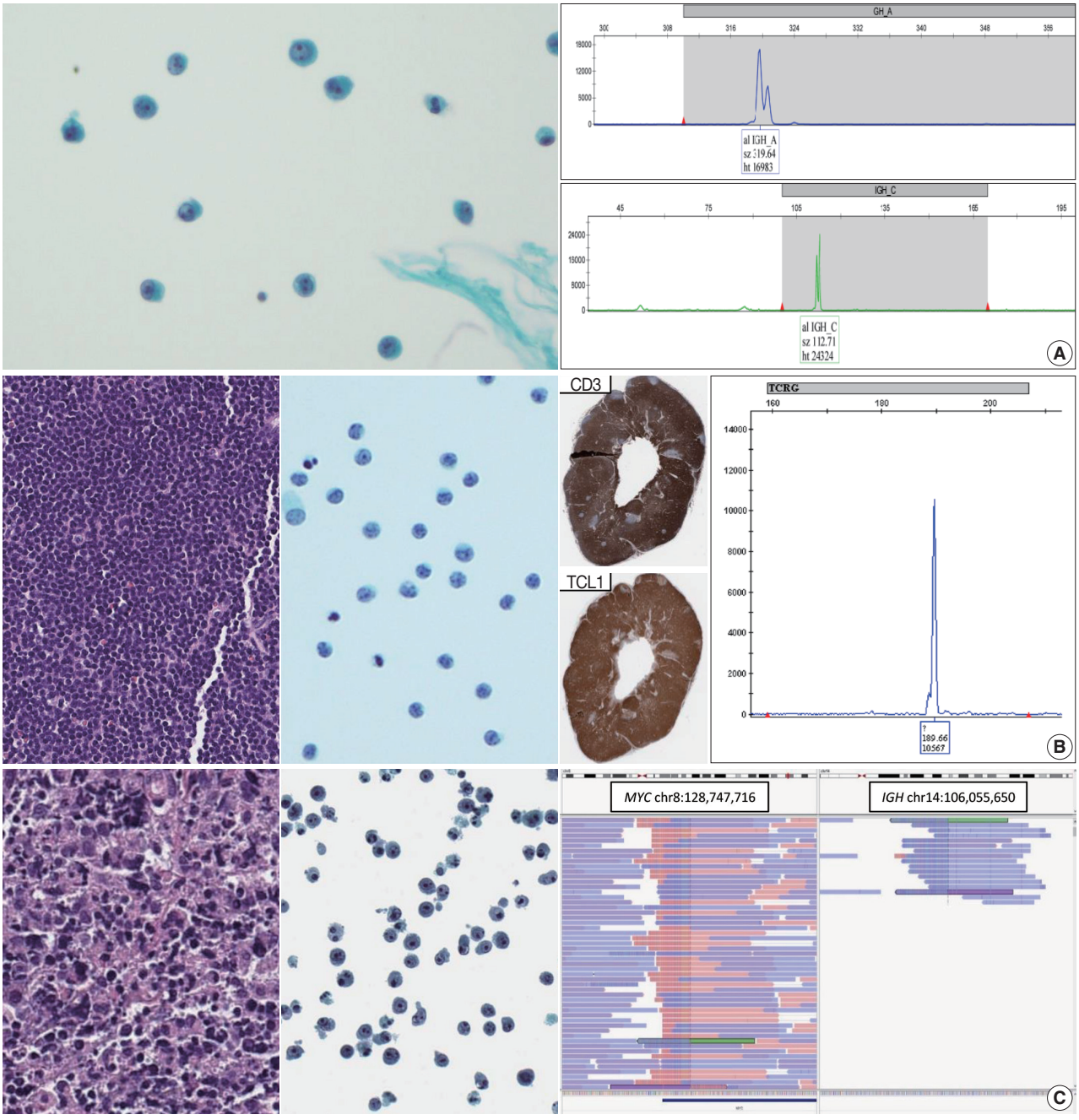

Fig. 6. Use of molecular tests in the diagnosis of lymphocyte-rich effusion. Few atypical large cells were observed in the cerebrospinal fluid from a patient with diffuse large B-cell lymphoma (DLBCL). B-cell monoclonality was documented by polymerase chain reaction (PCR)–based clonality assay, confirming the central nervous system involvement of lymphoma (A). A 63-year-old woman with known T-prolymphocytic leukemia presented with ascitic fluid containing monoclonal T-cell proliferation, suggesting the body cavity involvement (B). A 74-year-old male patient was diagnosed with gastric DLBCL with secondary involvement into ascitic fluid. (C, left) Cytologic preparations are suitable materials for high-throughput genetic analysis, and we found *IGH-MYC* translocation with sufficient supporting reads mapped into chromosomes 8 and 14 (C, right).

https://doi.org/10.4132/jptm.2022.05.16

Table 4. Comparison of CSF cytology and PCR-based clonality assay using BIOMED-2 assay for IgH gene rearrangement in patients with B-cell lymphoma

Cytomorphology	IgH gene PCR		Total
	Polyclonal	Monoclonal	
Negative	54 (81.8)	12 (18.2)	66 (65.3)
Atypical/Positive	20 (57.1)	15 (42.9)	35 (34.7)
Total	74 (73.3)	27 (26.7)	101 (100)

Values are presented as number (%).
PCR, polymerase chain reaction.

disease on neuroimaging (i.e., magnetic resonance imaging), rate of positive/atypical cytology was 35.6% and B-cell monoclonality was detected in 32.9%. The combined interpretation of both cytomorphology and clonality test resulted in a higher concordance up to 50.7% with neuroimaging results. Thus, retrieval of proper clinical and radiological information should accompany the interpretation of molecular study when dealing with CSF cytology.

In situ hybridization

As in histopathologic diagnosis using FFPE specimens, EBV in situ hybridization can readily be performed on cytological preparations including CB [54]. Identification of EBV is extremely valuable in characterization of certain EBV-associated LPDs, for example, EBV-positive DLBCLs, extranodal NK/T-cell lymphomas or PEL.

Fluorescent in situ hybridization (FISH) is another valuable tool for documentation of genetic alterations. Feasibility of FISH on cytologic preparation is well studied in several studies on solid tumors [51,55-65]. Detection of hallmark genomic variations direct leads to final diagnosis, for example, documentation of *BCL2* translocation in follicular lymphoma or *MYC* translocation in Burkitt lymphoma. Prognostic stratification of high-grade B-cell lymphomas can also be achieved by finding *MYC* or *BCL2* translocation. Development of many commercially available diagnostic FISH probes would enable characterization of less common structural variations, for instance, *IRF4*/*DUSP22* or *TP63* translocations.

Mutational analysis and next-generation sequencing

Recent advances in genomic profiling technologies dramatically accelerated precision diagnosis in daily practice. Multiple techniques including direct sequencing, real-time PCR, pyrosequencing have been performed on cytologic preparations, most notably on effusion fluids from the patients with non-small cell lung cancer [65-70]. Clinically meaningful disease-specific genetic alterations have been uncovered in the majority of lymphoma entities [71]. For instance, detection of *MYD88* L265P mutation using allele-specific PCR assay has been proven its efficacy on differentiating lymphoplasmacytic lymphomas [72,73] from other types of low-grade B-cell lymphomas. Recently, genetic classification of DLBCL has been recently introduced, and unique genomic landscape of certain DLBCL entities has been identified. For example, primary CNS lymphoma (PCNSL) and primary vitreoretinal lymphoma are characterized by frequent mutations in *MYD88* and *CD79B*. Thus, clonality test and/or *MYD88* mutation analysis would be helpful to determine the CSF involvement of PCNSL in equivocal cases based on cytomorphology only. In a similar vein, clonality test and/or *MYD88* mutation analysis would be informative in the diagnosis of vitreoretinal lymphoma using cytology specimen (e.g., vitreoretinal fluid) [74-76].

Single gene assays are being gradually replaced by next-generation sequencing (NGS), which enables testing for multiple genetic alterations on a single platform. Accumulating evidences suggest that various types of cytological preparations—smears, cytospins, liquid-based preparations and CBs—can be used for NGS-based assays with equivalent performance [77,78]. Some recommend that a portion of cytology specimens be reserved before CB preparation, for formalin fixation during the process my cause DNA cross-linkage and fragmentation [79-81].

Clinical utility of NGS-based assay on LPDs has been suggested by recent studies, both in diagnostic and prognostic perspectives [82-85]. One example is a report of angioimmunoblastic T-cell lymphoma [86], of which the primary diagnosis was made on pleural effusion fluid by detecting pathognomic *RH0A* G17V mutation by targeted NGS as well as immunophenotyping on CB. Fig. 6C shows another example that NGS-based assay helped in the genomic characterization and prognostic stratification of a patient with lymphoma. A 74-year-old male was diagnosed with gastric DLBCL of non-germinal center B-cell immunophenotype, and the patient developed ascites during the course. Targeted NGS using customized panel encompassing 121 lymphoma-related genes was performed, which revealed *IGH-MYC* translocation. In addition, *TET2* truncating mutations and heterozygous deletions of *CDKN2A* and *CDKN2B* were also found.

In some instances, cytologic specimens may be the only available resource for diagnosis and genomic profiling, therefore, the importance of cytologic preparation in NGS-based practice would be further expanded [81,87].

CONCLUSION

LPDs can frequently involve body cavities, which can pose significant diagnostic challenge to pathologists. Along with proper review of clinical history, cytomorphologic examination is the key process. Triaging the lymphocyte-rich effusions into small/medium-sized cell predominant and large-cell predominant patterns is a useful diagnostic approach. Since the distinction between reactive lymphocytosis and pathologic LPD is seldom possible based on cytologic atypia alone, ancillary tests guided by cytomorphology and clinical information are crucial. In addition to conventional ancillary testings including ICC and clonality assays, recent advances in NGS technology will further aid in retrieval of precious information from cytology specimens.

Ethics Statement

Not applicable.

Availability of Data and Material

The datasets generated or analyzed during the study are available from the corresponding author on reasonable request.

Code Availability

Not applicable.

ORCID

Jiwon Koh https://orcid.org/0000-0002-7687-6477
Sun Ah Shin https://orcid.org/0000-0002-7029-0088
Ji Ae Lee https://orcid.org/0000-0003-1493-6208
Yoon Kyung Jeon https://orcid.org/0000-0001-8466-9681

Author Contributions

Conceptualization: YKJ. Figures and data: SAS, JAL. Writing—original draft: JK. Writing—review & editing: JK, YKJ. Approval of final manuscript: all authors.

Conflicts of Interest

The authors declare that they have no potential conflicts of interest.

Funding Statement

No funding to declare.

References

1. Johnston WW. The malignant pleural effusion. A review of cytopathologic diagnoses of 584 specimens from 472 consecutive patients. Cancer 1985; 56: 905-9.
2. Valdes L, Alvarez D, Valle JM, Pose A, San Jose E. The etiology of pleural effusions in an area with high incidence of tuberculosis. Chest 1996; 109: 158-62.
3. Das DK. Serous effusions in malignant lymphomas: a review. Diagn Cytopathol 2006; 34: 335-47.
4. Tong LC, Ko HM, Saieg MA, Boerner S, Geddie WR, da Cunha Santos G. Subclassification of lymphoproliferative disorders in serous effusions: a 10-year experience. Cancer Cytopathol 2013; 121: 261-70.
5. Liu CY, Chuang SS. A simple and practical guide for triaging lymphocyte-rich effusions for ancillary studies. Adv Anat Pathol 2021; 28: 94-104.
6. Hunter BD, Dhakal S, Voci S, Goldstein NP, Constine LS. Pleural effusions in patients with Hodgkin lymphoma: clinical predictors and associations with outcome. Leuk Lymphoma 2014; 55: 1822-6.
7. Chen YP, Huang HY, Lin KP, Medeiros LJ, Chen TY, Chang KC. Malignant effusions correlate with poorer prognosis in patients with diffuse large B-cell lymphoma. Am J Clin Pathol 2015; 143: 707-15.
8. Yanamandra U, Deo P, Sahu KK, et al. Clinicopathological profile of myelomatous pleural effusion: single-center real-world experience and review of literature. Clin Lymphoma Myeloma Leuk 2019; 19: 183-9.
9. Weick JK, Kiely JM, Harrison EG Jr, Carr DT, Scanlon PW. Pleural effusion in lymphoma. Cancer 1973; 31: 848-53.
10. Alexandrakis MG, Passam FH, Kyriakou DS, Bouros D. Pleural effusions in hematologic malignancies. Chest 2004; 125: 1546-55.
11. Wang RC, Chen YH, Chen BJ, Chuang SS. The cytopathological spectrum of lymphomas in effusions in a tertiary center in Taiwan. Diagn Cytopathol 2021; 49: 232-40.
12. Chen L, Zhang JS, Liu DG, Cui D, Meng ZL. An algorithmic approach to diagnose haematolymphoid neoplasms in effusion by combining morphology, immunohistochemistry and molecular cytogenetics. Cytopathology 2018; 29: 10-21.
13. Gochhait D, Balakrishnan K, Venkatesan D, et al. The cytological evaluation of ascitic fluid led to the diagnosis of mediastinal T-lymphoblastic lymphoma: a simplified algorithmic approach to diagnosis of lymphoid cell-rich effusion. Cytopathology 2020; 31: 359-61.
14. Menet E, Becette V, Briffod M. Cytologic diagnosis of lobular carcinoma of the breast: experience with 555 patients in the Rene Huguenin Cancer Center. Cancer 2008; 114: 111-7.
15. Domagala-Kulawik J, Gornicka B, Krenke R, Mich S, Chazan R. The value of cytological diagnosis of small cell lung carcinoma. Pneumonol Alergol Pol 2010; 78: 203-10.
16. Wang J, Katz RL, Stewart J, Landon G, Guo M, Gong Y. Fine-needle aspiration diagnosis of lymphomas with signet ring cell features: potential pitfalls and solutions. Cancer Cytopathol 2013; 121: 525-32.
17. Ainechi S, Pambuccian SE, Wojcik EM, Barkan GA. Cytomorphologic features and differential diagnosis of neoplasms with small cell features in liquid-based urinary tract cytologic specimens. J Am Soc Cytopathol 2015; 4: 295-306.
18. Murali R, Loughman NT, McKenzie PR, Watson GF, Thompson JF, Scolyer RA. Cytological features of melanoma in exfoliative fluid specimens. J Clin Pathol 2009; 62: 638-43.
19. Wong JW, Pitlik D, Abdul-Karim FW. Cytology of pleural, peritoneal and pericardial fluids in children: a 40-year summary. Acta Cytol 1997; 41: 467-73.
20. Murro D, Slade JM, Gattuso P. Cytologic findings of hematologic malignancies in bronchoalveolar lavage fluid. J Am Soc Cytopathol 2015; 4: 267-75.
21. Kim Y, Park CJ, Roh J, Huh J. Current concepts in primary effusion lymphoma and other effusion-based lymphomas. Korean J Pathol 2014; 48: 81-90.
22. Jung HR, Huh J, Ko YH, et al. Classification of malignant lympho-

ma subtypes in Korean patients: a report of the 4th nationwide study. J Hematopathol 2019; 12: 173-81.
23. Chen BJ, Wang RC, Ho CH, et al. Primary effusion lymphoma in Taiwan shows two distinctive clinicopathological subtypes with rare human immunodeficiency virus association. Histopathology 2018; 72: 930-44.
24. Kim M, An J, Yoon SO, et al. Human herpesvirus 8-negative effusion-based lymphoma with indolent clinical behavior in an elderly patient: a case report and literature review. Oncol Lett 2020; 20: 343.
25. Alexanian S, Said J, Lones M, Pullarkat ST. KSHV/HHV8-negative effusion-based lymphoma, a distinct entity associated with fluid overload states. Am J Surg Pathol 2013; 37: 241-9.
26. Paydas S. Dasatinib, large granular lymphocytosis, and pleural effusion: useful or adverse effect? Crit Rev Oncol Hematol 2014; 89: 242-7.
27. Cortes JE, Jimenez CA, Mauro MJ, Geyer A, Pinilla-Ibarz J, Smith BD. Pleural effusion in dasatinib-treated patients with chronic myeloid leukemia in chronic phase: identification and management. Clin Lymphoma Myeloma Leuk 2017; 17: 78-82.
28. Brixey AG, Light RW. Pleural effusions due to dasatinib. Curr Opin Pulm Med 2010; 16: 351-6.
29. Quesada AE, Medeiros LJ, Clemens MW, Ferrufino-Schmidt MC, Pina-Oviedo S, Miranda RN. Breast implant-associated anaplastic large cell lymphoma: a review. Mod Pathol 2019; 32: 166-88.
30. Leberfinger AN, Behar BJ, Williams NC, et al. Breast implant-associated anaplastic large cell lymphoma: a systematic review. JAMA Surg 2017; 152: 1161-8.
31. Chai SM, Kavangh S, Ooi SS, et al. Anaplastic large-cell lymphoma associated with breast implants: a unique entity within the spectrum of peri-implant effusions. Diagn Cytopathol 2014; 42: 929-38.
32. Granados R, Lumbreras EM, Delgado M, Aramburu JA, Tardio JC. Cytological diagnosis of bilateral breast implant-associated lymphoma of the ALK-negative anaplastic large-cell type: clinical implications of peri-implant breast seroma cytological reporting. Diagn Cytopathol 2016; 44: 623-7.
33. Barbe E, de Boer M, de Jong D. A practical cytological approach to the diagnosis of breast-implant associated anaplastic large cell lymphoma. Cytopathology 2019; 30: 363-9.
34. Gabriel C, Achten R, Drijkoningen M. Use of liquid-based cytology in serous fluids: a comparison with conventional cytopreparatory techniques. Acta Cytol 2004; 48: 825-35.
35. Fetsch PA, Simsir A, Brosky K, Abati A. Comparison of three commonly used cytologic preparations in effusion immunocytochemistry. Diagn Cytopathol 2002; 26: 61-6.
36. Ylagan LR, Zhai J. The value of ThinPrep and cytospin preparation in pleural effusion cytological diagnosis of mesothelioma and adenocarcinoma. Diagn Cytopathol 2005; 32: 137-44.
37. Lee YM, Hwang JY, Son SM, et al. Comparison of diagnostic accuracy between CellprepPlus(R) and ThinPrep(R) liquid-based preparations in effusion cytology. Diagn Cytopathol 2014; 42: 384-90.
38. Hoda RS. Non-gynecologic cytology on liquid-based preparations: a morphologic review of facts and artifacts. Diagn Cytopathol 2007; 35: 621-34.
39. Jain D, Mathur SR, Iyer VK. Cell blocks in cytopathology: a review of preparative methods, utility in diagnosis and role in ancillary studies. Cytopathology 2014; 25: 356-71.
40. Nambirajan A, Jain D. Cell blocks in cytopathology: an update. Cytopathology 2018; 29: 505-24.
41. Gupta P, Pandey T, Gautam U, et al. Lymphoreticular malignancies in serous effusions: cytomorphologic, flow cytometric and immunocytochemical analysis. Diagn Cytopathol 2021; 49: 647-56.
42. Zheng Y, Wan X, Gui X, et al. Value of multi-parameter flow cytometry immunophenotyping in T/NK-cell neoplasms in cytology specimens: a retrospective study in Chinese patients. Pathol Res Pract 2020; 216: 152921.
43. Kaur K, Patel T, Patra S, Trivedi P. Cytomorphology, Immunophenotype, and cytogenetic profile of leukemic serous effusions. Diagn Cytopathol 2021; 49: 948-58.
44. Bhardwaj N, Gupta N, Gupta P, Malhotra P. Flow cytometric immunophenotyping in a liquid-based cytology sample of pleural fluid: connecting the dots. Cytopathology 2022; 33: 269-72.
45. Jeon YK, Yoon SO, Paik JH, et al. Molecular testing of lymphoproliferative disorders: current status and perspectives. J Pathol Transl Med 2017; 51: 224-41.
46. van Dongen JJ, Langerak AW, Bruggemann M, et al. Design and standardization of PCR primers and protocols for detection of clonal immunoglobulin and T-cell receptor gene recombinations in suspect lymphoproliferations: report of the BIOMED-2 Concerted Action BMH4-CT98-3936. Leukemia 2003; 17: 2257-317.
47. Alkan S, Lehman C, Sarago C, Sidawy MK, Karcher DS, Garrett CT. Polymerase chain reaction detection of immunoglobulin gene rearrangement and bcl-2 translocation in archival glass slides of cytologic material. Diagn Mol Pathol 1995; 4: 25-31.
48. Mihaescu A, Gebhard S, Chaubert P, et al. Application of molecular genetics to the diagnosis of lymphoid-rich effusions: study of 95 cases with concomitant immunophenotyping. Diagn Cytopathol 2002; 27: 90-5.
49. Li J, Zhang W, Wang W, et al. Forty-nine cases of acute lymphoblastic leukaemia/lymphoma in pleural and pericardial effusions: a cytological-histological correlation. Cytopathology 2018; 29: 172-8.
50. Murphy M, Signoretti S, Nasser I, Sherburne B, Loda M. Detection of concurrent/recurrent non-Hodgkin's lymphoma in effusions by PCR. Hum Pathol 1999; 30: 1361-6.
51. Pinto D, Schmitt F. Current applications of molecular testing on body cavity fluids. Diagn Cytopathol 2020; 48: 840-51.
52. Bode-Lesniewska B. Flow cytometry and effusions in lymphoproliferative processes and other hematologic neoplasias. Acta Cytol 2016; 60: 354-64.
53. Chen X, Cherian S. Immunophenotypic characterization of T-cell prolymphocytic leukemia. Am J Clin Pathol 2013; 140: 727-35.
54. Garady C, Saieg MA, Ko HM, Geddie WR, Boerner SL, da Cunha Santos G. Epstein-Barr virus encoded RNA detected by in situ hybridization using cytological preparations. Cytopathology 2014; 25: 101-7.
55. Minca EC, Lanigan CP, Reynolds JP, et al. ALK status testing in non-small-cell lung carcinoma by FISH on ThinPrep slides with cytology material. J Thorac Oncol 2014; 9: 464-8.
56. Sundling KE, Cibas ES. Ancillary studies in pleural, pericardial, and peritoneal effusion cytology. Cancer Cytopathol 2018; 126 Suppl 8: 590-8.
57. Walts AE, Hiroshima K, McGregor SM, Wu D, Husain AN, Marchevsky AM. BAP1 immunostain and CDKN2A (p16) FISH analysis: clinical applicability for the diagnosis of malignant mesothelioma in effusions. Diagn Cytopathol 2016; 44: 599-606.
58. Wang W, Tang Y, Li J, Jiang L, Jiang Y, Su X. Detection of ALK rearrangements in malignant pleural effusion cell blocks from patients

with advanced non-small cell lung cancer: a comparison of Ventana immunohistochemistry and fluorescence in situ hybridization. Cancer Cytopathol 2015; 123: 117-22.
59. Chen Z, Wang DD, Peier A, Stone JF, Sandberg AA. FISH in the evaluation of pleural and ascitic fluids. Cancer Genet Cytogenet 1995; 84: 116-9.
60. Savic S, Franco N, Grilli B, et al. Fluorescence in situ hybridization in the definitive diagnosis of malignant mesothelioma in effusion cytology. Chest 2010; 138: 137-44.
61. Matsumoto S, Nabeshima K, Kamei T, et al. Morphology of 9p21 homozygous deletion-positive pleural mesothelioma cells analyzed using fluorescence in situ hybridization and virtual microscope system in effusion cytology. Cancer Cytopathol 2013; 121: 415-22.
62. Betz BL, Dixon CA, Weigelin HC, Knoepp SM, Roh MH. The use of stained cytologic direct smears for *ALK* gene rearrangement analysis of lung adenocarcinoma. Cancer Cytopathol 2013; 121: 489-99.
63. Tsai TH, Wu SG, Hsieh MS, Yu CJ, Yang JC, Shih JY. Clinical and prognostic implications of RET rearrangements in metastatic lung adenocarcinoma patients with malignant pleural effusion. Lung Cancer 2015; 88: 208-14.
64. Jardin F, Jais JP, Molina TJ, et al. Diffuse large B-cell lymphomas with CDKN2A deletion have a distinct gene expression signature and a poor prognosis under R-CHOP treatment: a GELA study. Blood 2010; 116: 1092-104.
65. Cai G, Wong R, Chhieng D, et al. Identification of *EGFR* mutation, *KRAS* mutation, and *ALK* gene rearrangement in cytological specimens of primary and metastatic lung adenocarcinoma. Cancer Cytopathol 2013; 121: 500-7.
66. Lozano MD, Zulueta JJ, Echeveste JI, et al. Assessment of epidermal growth factor receptor and K-ras mutation status in cytological stained smears of non-small cell lung cancer patients: correlation with clinical outcomes. Oncologist 2011; 16: 877-85.
67. Bellevicine C, Malapelle U, Vigliar E, de Luca C, Troncone G. Epidermal growth factor receptor test performed on liquid-based cytology lung samples: experience of an academic referral center. Acta Cytol 2014; 58: 589-94.
68. Scarpa A, Sikora K, Fassan M, et al. Molecular typing of lung adenocarcinoma on cytological samples using a multigene next generation sequencing panel. PLoS One 2013; 8: e80478.
69. Gailey MP, Stence AA, Jensen CS, Ma D. Multiplatform comparison of molecular oncology tests performed on cytology specimens and formalin-fixed, paraffin-embedded tissue. Cancer Cytopathol 2015; 123: 30-9.
70. Lindeman NI, Cagle PT, Aisner DL, et al. Updated molecular testing guideline for the selection of lung cancer patients for treatment with targeted tyrosine kinase inhibitors: guideline from the College of American Pathologists, the International Association for the Study of Lung Cancer, and the Association for Molecular Pathology. Arch Pathol Lab Med 2018; 142: 321-46.
71. Moffitt AB, Dave SS. Clinical Applications of the genomic landscape of aggressive non-Hodgkin lymphoma. J Clin Oncol 2017; 35: 955-62.
72. Pan ST, Wang RC, Kuo CC, Hsieh YC, Su YZ, Chuang SS. MYD88 L265P mutation analysis is a useful diagnostic adjunct for lymphoplasmacytic lymphoma with pleural effusion. Pathol Int 2019; 69: 601-7.
73. Varettoni M, Arcaini L, Zibellini S, et al. Prevalence and clinical significance of the MYD88 (L265P) somatic mutation in Waldenstrom's macroglobulinemia and related lymphoid neoplasms. Blood 2013; 121: 2522-8.
74. Hiemcke-Jiwa LS, Ten Dam-van Loon NH, Leguit RJ, et al. Potential diagnosis of vitreoretinal lymphoma by detection of MYD88 mutation in aqueous humor with ultrasensitive droplet digital polymerase chain reaction. JAMA Ophthalmol 2018; 136: 1098-104.
75. Bonzheim I, Giese S, Deuter C, et al. High frequency of MYD88 mutations in vitreoretinal B-cell lymphoma: a valuable tool to improve diagnostic yield of vitreous aspirates. Blood 2015; 126: 76-9.
76. Tanaka R, Kaburaki T, Taoka K, et al. More accurate diagnosis of vitreoretinal lymphoma using a combination of diagnostic test results: a prospective observational study. Ocul Immunol Inflamm 2021 Apr 1 [Epub]. https://doi.org/10.1080/09273948.2021.1873394.
77. Roy-Chowdhuri S, Goswami RS, Chen H, et al. Factors affecting the success of next-generation sequencing in cytology specimens. Cancer Cytopathol 2015; 123: 659-68.
78. Roy-Chowdhuri S, Chen H, Singh RR, et al. Concurrent fine needle aspirations and core needle biopsies: a comparative study of substrates for next-generation sequencing in solid organ malignancies. Mod Pathol 2017; 30: 499-508.
79. Williams C, Ponten F, Moberg C, et al. A high frequency of sequence alterations is due to formalin fixation of archival specimens. Am J Pathol 1999; 155: 1467-71.
80. Srinivasan M, Sedmak D, Jewell S. Effect of fixatives and tissue processing on the content and integrity of nucleic acids. Am J Pathol 2002; 161: 1961-71.
81. Bellevicine C, Malapelle U, Vigliar E, Pisapia P, Vita G, Troncone G. How to prepare cytological samples for molecular testing. J Clin Pathol 2017; 70: 819-26.
82. Navrkalova V, Plevova K, Hynst J, et al. LYmphoid NeXt-Generation Sequencing (LYNX) panel: a comprehensive capture-based sequencing tool for the analysis of prognostic and predictive markers in lymphoid malignancies. J Mol Diagn 2021; 23: 959-74.
83. Bastos-Oreiro M, Suarez-Gonzalez J, Andres-Zayas C, et al. Incorporation of next-generation sequencing in clinical practice using solid and liquid biopsy for patients with non-Hodgkin's lymphoma. Sci Rep 2021; 11: 22815.
84. Allahyar A, Pieterse M, Swennenhuis J, et al. Robust detection of translocations in lymphoma FFPE samples using targeted locus capture-based sequencing. Nat Commun 2021; 12: 3361.
85. Pillonel V, Juskevicius D, Bihl M, et al. Routine next generation sequencing of lymphoid malignancies: clinical utility and challenges from a 3-year practical experience. Leuk Lymphoma 2020; 61: 2568-83.
86. Tan B, Martin B, Fernandez-Pol S. Angioimmunoblastic T-cell lymphoma diagnosed from pleural fluid by integration of morphologic, immunophenotypic, and molecular findings. Diagn Cytopathol 2021; 49: E462-6.
87. Martini M, Capodimonti S, Cenci T, et al. To obtain more with less: cytologic samples with ancillary molecular techniques: the useful role of liquid-based cytology. Arch Pathol Lab Med 2018; 142: 299-307.

JPTM
Journal of Pathology and Translational Medicine 2022; 56: 187-198
https://doi.org/10.4132/jptm.2022.03.10

ORIGINAL ARTICLE

Clinicopathologic features and survival outcomes of ocular melanoma: a series of 31 cases from a tertiary university hospital

Selin Kestel, Feriha Pınar Uyar Göçün, Betül Öğüt, Özlem Erdem

Department of Pathology, Faculty of Medicine, Gazi University, Ankara, Turkey

Background: We aimed to determine the effect of clinicopathologic features on overall survival among Caucasian ocular melanoma patients in the Central Anatolia region of Turkey. **Methods:** This single-center study included conjunctival (n = 12) and uveal (n = 19) melanoma patients diagnosed between January 2008 and March 2020. Clinicopathologic features and outcomes were reviewed retrospectively. Five cases were tested for *BRAF* V600 mutations with real-time polymerase chain reaction, and one case was tested with next-generation sequencing. Survival was calculated using the Kaplan-Meier method. **Results:** Thirty-one patients had a mean initial age of 58.32 years (median, 61 years; range 25 to 78 years). There were 13 male and 18 female patients. The median follow-up time was 43.5 months (range, 6 to 155 months) for conjunctival melanoma and 35 months (range, 8 to 151 months) for uveal melanoma. When this study ended, eight of the 12 conjunctival melanoma patients (66.7%) and nine of the 19 uveal melanoma patients (47.4%) had died. The presence of tumor-infiltrating lymphocytes was related to improved overall survival in conjunctival melanoma (p = .014), whereas the presence of ulceration (p = .030), lymphovascular invasion (p = .051), tumor in the left eye (p = .012), tumor thickness of >2 mm (p = .012), and mitotic count of >1/mm² (p = .012) reduced the overall survival in conjunctival melanoma. Uveal melanoma tumors with the largest diameter of 9.1–15 mm led to the lowest overall survival among subgroups (p = .035). Involvement of the conjunctiva (p=.005) and lens (p = .003) diminished overall survival in uveal melanoma. *BRAF* V600 mutation was present in one case of conjunctival melanoma, *GNAQ* R183Q mutation was present in one case of uveal melanoma. Patients with uveal melanoma presented with an advanced pathological tumor stage compared to those with conjunctival melanoma (p = .019). **Conclusions:** This study confirmed the presence of tumor-infiltrating lymphocytes as a favorable factor in conjunctival melanoma and conjunctival and lens involvement as unfavorable prognostic factors in uveal melanoma for overall survival, respectively.

Key Words: Uveal melanoma; Conjunctival melanoma; Ocular melanoma; Overall survival; Histopathology

Received: November 17, 2021 **Revised:** February 28, 2022 **Accepted:** March 10, 2022
Corresponding Author: Selin Kestel, MD, Department of Pathology, Faculty of Medicine, Gazi University, Mevlana Ave, No: 29, 06560, Ankara, Turkey
Tel: +90-5078415588, E-mail: selinkestel@gmail.com

Two types of ocular melanoma exist: uveal melanoma (UM) and conjunctival melanoma (CM) [1]. UM represents 79%–91% of all ocular melanomas [2], whereas CM represents < 10% [3]. The incidence of CM in the white population is 0.2–0.8 cases/million [3]. The incidence of UM in the American and European populations is 5–6 cases/million, while it is 7 cases/million in Australia [4]. UM is most commonly seen in Caucasians, followed by Hispanics, Asians, and Blacks, with decreasing frequency [5]. UM's incidence has been relatively stable over the years [6]; however, CM's incidence has shown a rising trend similar to that of cutaneous melanoma [3,7-11]. Although CM is rare, it has the potential to metastasize not only to the eye, eyelid, orbit, and surrounding lymphatics but also to distant sites like the lungs, skin, liver, and brain [12]. The 10-year mortality rate for UM is 50% in the U.S. and higher than other melanoma subtypes [2,13]. Although ocular melanoma is rare, its morbidity is also high, leading to vision loss even in surviving patients. Thus, this study aimed to evaluate the effects of clinicopathologic features on overall survival (OS) among ocular melanoma patients and discuss the relevant literature to highlight some aspects of these deadly diseases.

MATERIALS AND METHODS

This single-center study included CM (n = 12) and UM (n = 19) patients diagnosed between January 2008 and March 2020.

pISSN 2383-7837
eISSN 2383-7845

The final follow-up was conducted by April 2021. Clinicopathologic and outcome data from electronic medical records were reviewed retrospectively.

Baseline clinical variables assessed included age, sex, location and laterality of the tumor, primary surgical treatment, known comorbidities. Pathologic features of each tumor were reviewed primarily from archival slides stained with hematoxylin and eosin and pathology reports. Any histochemical, immunohistochemical, and molecular studies performed at the time of diagnosis were recorded. Real-time polymerase chain reaction (RT-PCR) for *BRAF* V600 mutation was tested using either the AmoyDx BRAF V600 mutations detection kit (Amoy Diagnostics Co., Xiamen, China) or Cobas BRAF V600 mutation kit (Roche, Pleasanton, CA, USA). Next-generation sequencing (NGS) with Qiagen GeneReader workflows (Qiagen, Hilden, Germany) was performed according to the manufacturer's protocol by isolating DNA from the enucleation specimen for UM. Pathological tumor (pT) staging was performed according to the eighth edition of the American Joint Committee on Cancer (AJCC) staging system for UM and CM [14]. Microscopic satellitosis was evaluated as a separated tumor nest from the primary tumor by a normal stroma as described previously by Esmaeli et al. [15]. Infiltration of the iris, ciliary body, anterior chamber, Schlemm canal, lens, posterior chamber, choroid, retina, vitreous, sclera, optic disc, and conjunctiva was evaluated in UM patients [16]. Growth pattern (solid mass, dome shape, mushroom shape [17], or diffuse [18]) was classified as previously described for UM cases [16]. Tumor diameter [16], histologic type and grade [19], and nucleolar prominence were additionally assessed as histopathologic parameters in UM cases.

OS time was calculated as the time from diagnosis to death from any cause or to last follow-up (for surviving patients) within each group (CM and UM) separately. Kaplan-Meier survival analyses and log-rank tests were conducted to identify statistically significant univariable predictors of OS using the SPSS ver. 23 (IBM Corp., Armonk, NY, USA). The statistically significant difference between groups was determined as $p < .05$. The frequencies of common categorical variables for UM and CM were compared using the 2-tailed Fisher exact test.

RESULTS

Ocular melanoma patient demographics and clinical history

Thirty-one patients had a mean initial age of 58.32 ± 0.50 years (median, 61 years; range, 25 to 78 years). There were 13 male and 18 female patients. In terms of tumor site, the tumor was located at the uvea for 19 patients (61%) (choroidal, n = 16; ciliary body, n = 2; iris, n = 1), conjunctiva for nine patients (29%) (bulbar, n = 5; palpebral, n = 3; unknown, n = 1), and eyelid for three patients (10%). Primary treatment most commonly included enucleation (n = 3 for CM, n = 17 for UM), followed by local excision (n = 6 for CM, n = 2 for UM), and exenteration (n = 3 for CM).

Conjunctival melanoma

Table 1 represents the main clinicopathologic characteristics of CM cases and their relationship to OS. At diagnosis, the mean age was 56.08 ± 11.21 years (median, 57.5 years; range, 35 to 74 years). The median follow-up time was 43.5 months and ranged from 6–155 months. When this study ended, eight of the 12 patients (66.7%) had died (Fig. 1A). Three patients with left-sided CM had a reduced OS compared to right-sided patients ($p = .012$) (Fig. 1B).

Histopathologically, three cases with CM were identical to superficial spreading melanoma, suggesting a role of cumulative sun damage similar to pathway I of the skin melanoma classification [1]. One CM showed histologically nodular melanoma features (Fig. 2A). The epithelioid type was the most common cell type (n = 9/12, 75%). Ulceration was present in two cases and related to poor outcomes ($p = .030$) (Fig. 1C). The majority of CM tumors were mildly pigmented. The presence of tumor-infiltrating lymphocytes (TILs) was associated with improved OS ($p = .014$) in CM (Figs. 1D, 2B, C).

Necrosis was present in four of the CM cases. No mortality occurred in tumors with a thickness of ≤ 2 mm ($p = .012$). A mitotic count of ≤ 1/mm^2 was significantly related to improved OS ($p = .012$). A lower mitotic count and tumor thickness were shared between three identical cases; expectedly, their effects on OS were similar. Lymphovascular invasion (LVI) was identified in eight of the CM cases and associated with reduced OS ($p = .051$) (Fig. 1E). Although microscopic satellitosis and surgical margin positivity reduced the OS, they did not statistically significantly affect it. Based on the eighth edition of AJCC staging for CM [14], the tumors were staged as pT1a in one (8.3%), pT1b in four (33.3%), pT2a in two (16.7%), pT2b in one (8.3%), pT3b in one (8.3%), pT3c in two (16.7%), and pT3d in one (8.3%) case (s), respectively. No case presented with central nervous system involvement (pT4). Tumors of any size with local invasion (pT3) were linked to a decreased OS, although this relationship did not exactly reach statistical significance ($p = .056$) (Fig. 1F). Regional lymph node metastasis occurred in four (33%) of CM patients; one also had parotid gland metastasis, and another had additional lung metastasis. Three cases underwent *BRAF* V600 mu-

https://doi.org/10.4132/jptm.2022.03.10

Table 1. Univariate analysis of predictors for overall survival time (mo) in conjunctival melanoma, calculated from Kaplan-Meier analysis with comparisons performed with the log-rank test

	No.	Deaths	Mean ± SE (95% CI)	p-value
Overall survival	12	8	71.45 ± 16.73 (38.66–104.25)	N/A
Sex				.575
Male	6	4	45.92 ± 9.36 (27.58–64.26)	
Female	6	4	80.17 ± 24.09 (32.96–127.37)	
Laterality				.012
Right	8	4	95.06 ± 20.43 (55.01–135.10)	
Left	3	3	24.33 ± 6.06 (12.45–36.22)	
Cell type				.399
Epithelioid	9	6	66.97 ± 19.24 (29.27–104.68)	
Spindle	2	1	100.5 ± 27.22 (47.14–153.86)	
Epithelioid+spindle	1	1	24.0 ± 0.0 (24.0–24.0)	
Ulceration				.030
Negative	10	6	81.94 ± 18.35 (45.99–117.90)	
Positive	2	2	19.0 ± 5.0 (9.2–28.8)	
Pigmentation				.420
Low	9	6	77.96 ± 19.06 (40.61–115.32)	
High	3	2	28.33 ± 3.54 (21.40–35.27)	
TIL				.014
Absent	4	4	26.0 ± 9.06 (8.25–43.75)	
Present	8	4	95.63 ± 20.39 (55.65–135.60)	
Necrosis				.343
Absent	8	5	81.21 ± 20.88 (40.29–122.13)	
Present	4	3	40.50 ± 13.34 (14.35–66.65)	
Tumor thickness (mm)				.012
≤2	3	0	N/A	
>2	9	8	N/A	
Lymphovascular invasion				.051
Negative	4	1	122.25 ± 28.36 (66.66–177.84)	
Positive	8	7	43.71 ± 11.01 (22.14–65.28)	
Microscopic satellitosis				.590
Negative	8	5	72.09 ± 17.03 (38.72–105.47)	
Positive	4	3	59.25 ± 29.64 (1.15–117.35)	
Surgical margin				.376
Negative	9	5	83.97 ± 21.09 (42.63–125.31)	
Positive	3	3	49.00 ± 24.54 (0.90–97.10)	
Mitotic count (/mm^2)				.012
≤1	3	0	N/A	
>1	9	8	N/A	
pT				.056
pT1	5	3	85.93 ± 22.98 (40.90–130.97)	
pT2	3	1	100.67 ± 31.30 (39.32–162.01)	
pT3	4	4	26.50 ± 12.39 (2.21–50.79)	

SE, standard error; CI, confidence interval; N/A, not applicable; TIL, tumor-infiltrating lymphocyte.

tation analysis with RT-PCR. One patient with lymph node metastasis had *BRAF* V600 mutations (Fig. 2); others, including the patient with parotid gland metastasis, were wild-type for *BRAF* V600 mutation.

Uveal melanoma

Table 2 represents some of the clinicopathologic features of UM cases investigated in this study and their relationship to OS (Fig. 3). More patients were female (n = 12/19, 63.2%). The mean age at diagnosis was 59.74 ± 15.25 years (median, 63 years; range, 25 to 78 years). Follow-up time ranged from 8–151 months with a median of 35 months. When this study ended, nine of the 19 patients (47.4%) had died (Fig. 3A)

Two UM tumors arose from the iris and ciliary body and were

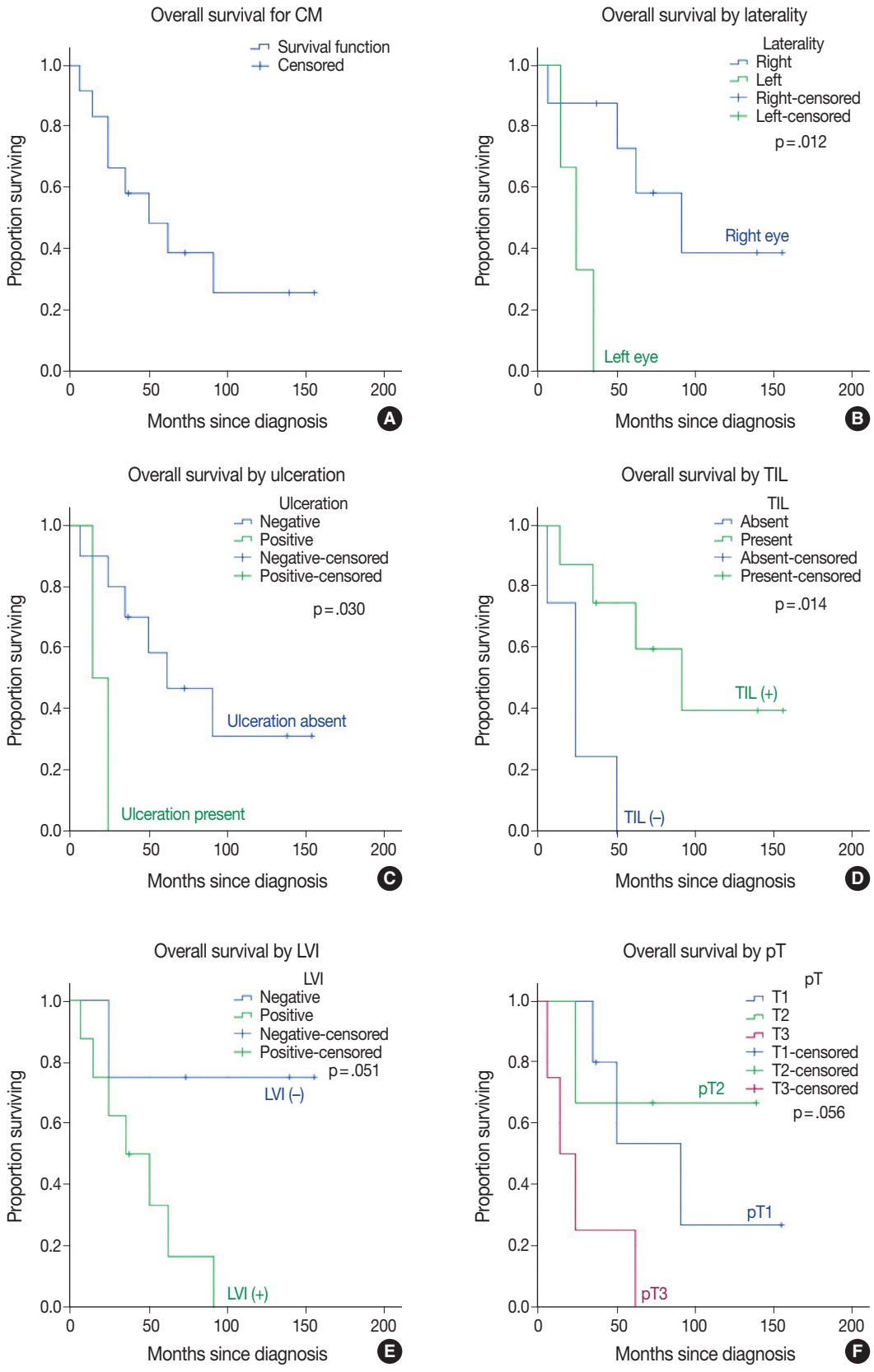

Fig. 1. Kaplan-Meier overall survival curves in conjunctival melanoma (CM) (A) patients are compared for tumor variables by laterality (B), ulceration (C), tumor-infiltrating lymphocytes (TILs) (D), lymphovascular invasion (LVI) (E), and pathological tumor (pT) staging (F).

https://doi.org/10.4132/jptm.2022.03.10

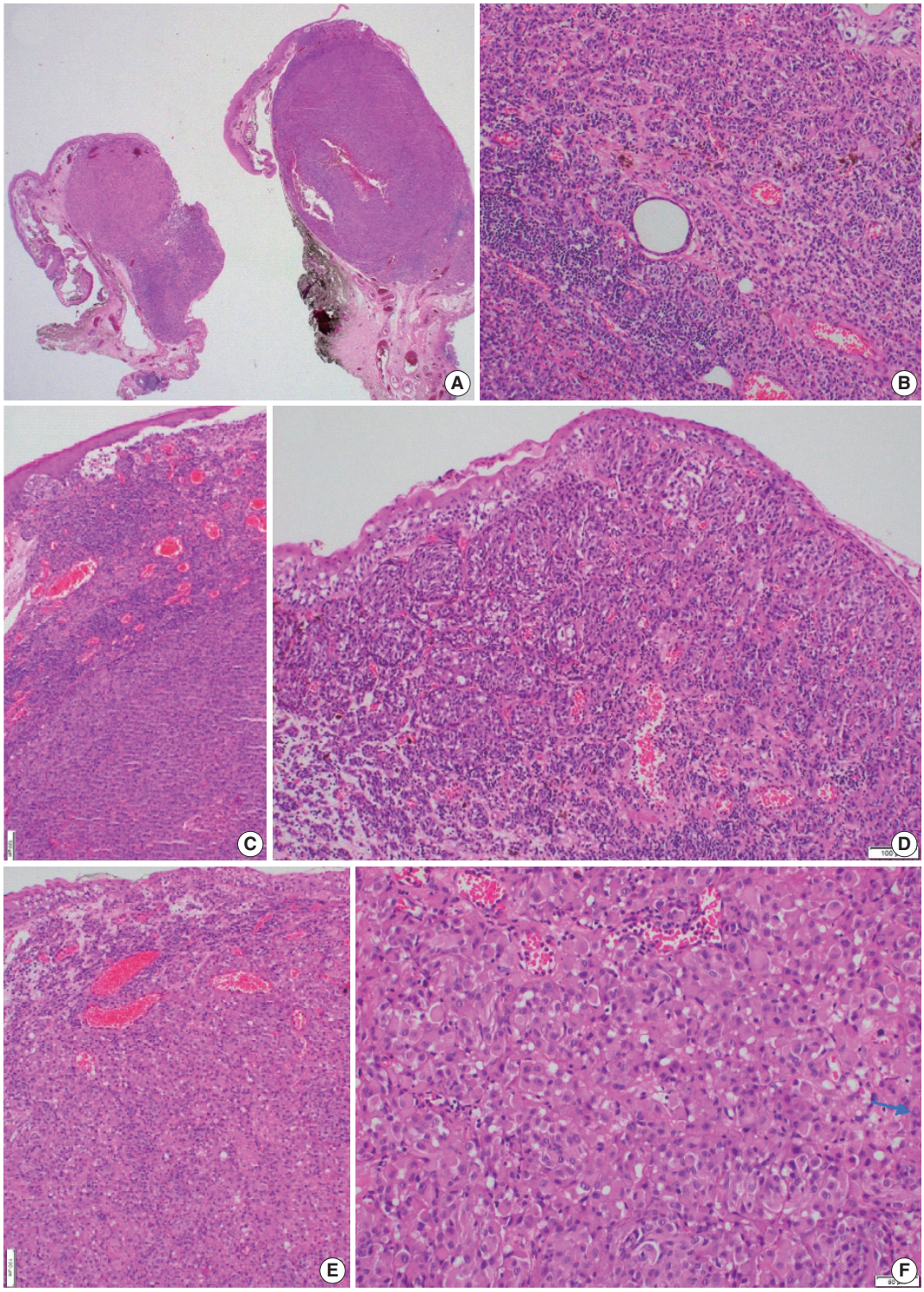

Fig. 2. (A) A conjunctival melanoma with nodular and well-circumscribed appearance is located in the left-eye nasal side bulbar conjunctiva in a 73-year-old male patient. (B, C) A subepithelial portion of melanoma nodule shows increased vascularization and a moderate amount of tumor-infiltrating lymphocytes. In addition, junctional involvement of the conjunctival epithelium (C, D) and prominent pagetoid spreading (D) are present at the nodule periphery. (D) Monotonous-appearing melanocytes have invaded the stroma in a nested growth pattern and exhibit slight, scattered pigmentation. (E) Beneath the intraepithelial melanocytic proliferation, the conjunctival stroma is invaded by epithelioid melanocytes with large eosinophilic cytoplasm (F) with rare intranuclear eosinophilic pseudo-inclusion (arrow), and prominent nucleoli dominate in this *BRAF* V600 mutant conjunctival melanoma.

treated with local excision, whereas the remaining patients (n = 17/19, 89.5%) underwent enucleation. The mean largest tumor diameter was 13.68 mm (median, 14 mm; range, 4 to 21 mm). The UM tumor with the largest diameter interval of 9.1–15 mm led to the lowest OS among subgroups (p = .035) (Fig. 3B). Conjunctiva involvement was present in 1 UM case and

Table 2. Univariate analysis of predictors for overall survival time (mo) in uveal melanoma, calculated from Kaplan-Meier analysis with comparisons performed with the log-rank test

	No.	Deaths	Mean ± SE (95% CI)	p-value
Overall survival	19	9	86.05 ± 15.50 (55.68–116.42)	N/A
Gender				.109
Male	7	5	57.86 ± 22.51 (13.74–101.97)	
Female	12	4	100.67 ± 18.30 (64.80–136.54)	
Surgical treatment				.252
Local excision	2	0	N/A	
Enucleation	17	9	79.45 ± 16.10 (47.89–111.01)	
Laterality				.083
Right	12	4	105.48 ± 18.50 (69.21–141.75)	
Left	7	5	36.86 ± 10.69 (15.91–57.81)	
Largest tumor diameter (mm)				.035
0–9	4	1	113.33 ± 30.76 (53.05–173.61)[ab]	
9.1–15	7	5	43.14 ± 16.06 (11.66–74.63)[a]	
> 15	8	3	99.63 ± 21.00 (58.47–140.78)[b]	
Scleral involvement				.226
None	10	4	80.93 ± 15.06 (51.41–110.46)	
Intrascleral	5	2	96.20 ± 30.06 (37.28–155.12)	
Extrascleral (largest diameter ≤ 5 mm)	2	2	21.0 ± 8.0 (5.32–36.68)	
Extrascleral (largest diameter > 5 mm)	2	1	91.00 ± 38.89 (14.77–167.23)	
Conjunctiva involvement				.005
Negative	18	8	90.11 ± 15.82 (59.11–121.11)	
Positive	1	1	13.00 ± 0.00 (13.00–13.00)	
Anterior chamber involvement				.134
Negative	15	6	97.26 ± 16.89 (64.16–130.37)	
Positive	4	3	26.50 ± 6.07 (14.60–38.40)	
Ciliary body involvement				.199
Negative	11	4	102.81 ± 19.19 (65.19–140.42)	
Positive	8	5	46.88 ± 16.08 (15.37–78.39)	
Iris involvement				.134
Negative	15	6	97.26 ± 16.89 (64.16–130.37)	
Positive	4	3	26.50 ± 6.07 (14.60–38.40)	
Schlemm canal involvement				.134
Negative	15	6	97.26 ± 16.89 (64.16–130.37)	
Positive	4	3	26.50 ± 6.07 (14.60–38.40)	
Posterior chamber involvement				.098
Negative	12	4	105.48 ± 18.50 (69.21–141.75)	
Positive	7	5	43.14 ± 14.96 (13.82–72.47)	
Lens involvement				.003
Negative	14	4	111.26 ± 16.74 (78.44–144.08)	
Positive	5	5	23.80 ± 3.97 (16.02–31.58)	
Optic disc involvement				.085
Negative	17	7	93.77 ± 16.39 (61.64–125.89)	
Positive	2	2	24.50 ± 4.50 (15.68–33.32)	
Necrosis				.166
Negative	8	2	113.35 ± 22.61 (69.04–157.66)	
Positive	10	6	69.95 ± 19.47 (31.80–108.10)	

SE, standard error; CI, confidence interval; N/A, not applicable.
[a,b]The same letters between groups define no significant difference between them statistically.

https://doi.org/10.4132/jptm.2022.03.10

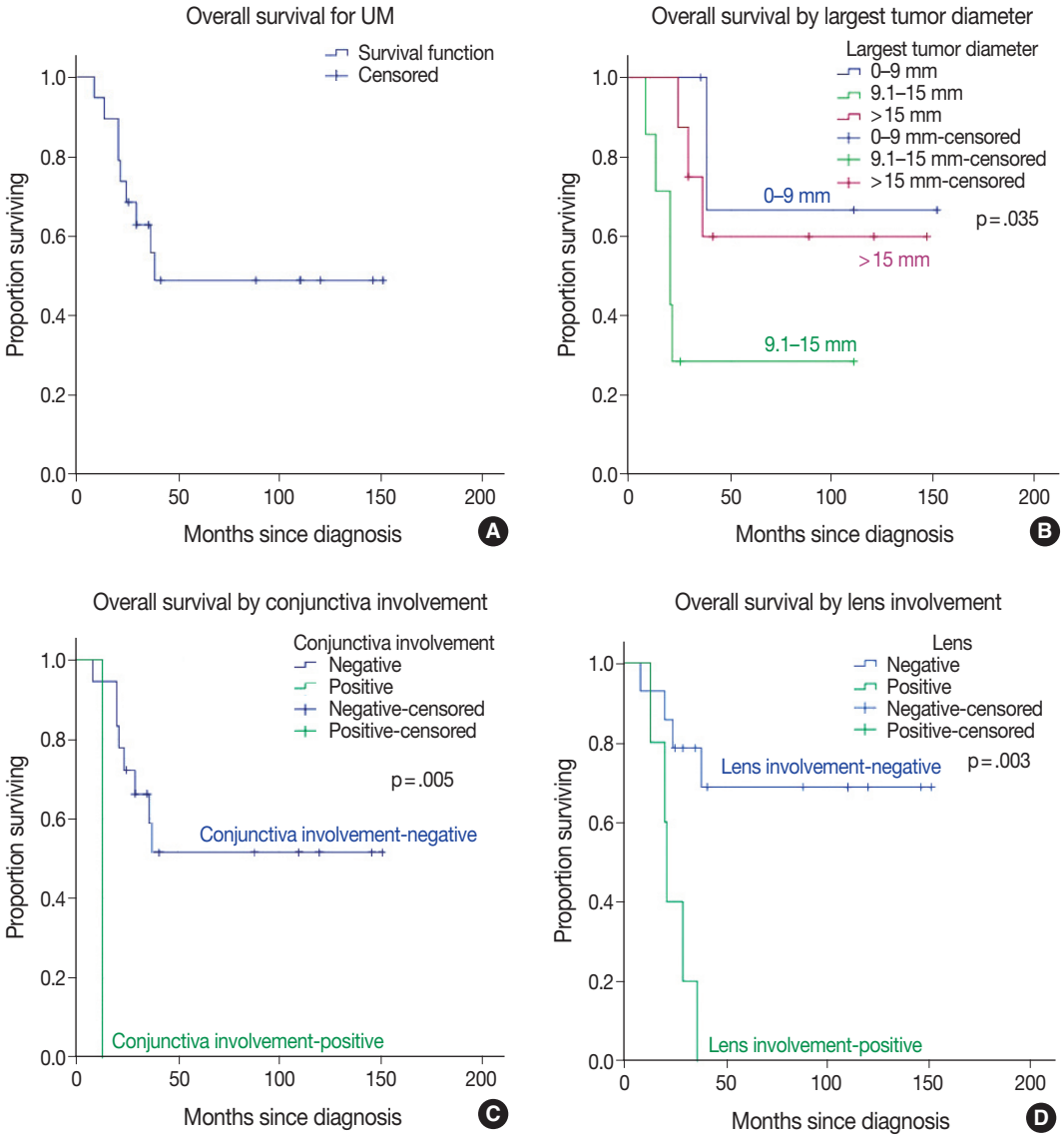

Fig. 3. Kaplan-Meier overall survival curves in uveal melanoma (UM) patients (A) compared by largest tumor diameter (B), conjunctival involvement (C), and lens involvement (D).

inversely associated with OS (p=.005) (Fig. 3C). The other involved ocular structures in UM patients were the sclera in nine (47.4%), anterior chamber in four (21.1%), ciliary body in eight (42.1%), iris in four (21.1%), Schlemm canal in four (21.1%), posterior chamber in seven (36.8%), lens in five (26.3%), vitreous in 18 (94.7%), choroid in 17 (89.5%), retina in five (26.3%), and optic disc in two (10.5%) patients, respectively. Even though the involvement of each ocular structure diminished the OS time and probability in UM patients, lens involvement had particular importance statistically (p = .003) (Fig. 3D). Scleral involvement of tumors was confined to the intrascleral area in five (26.3%) UM cases and extended to < 5 mm of extrascleral area in two (10.5%) UM cases or ≥ 5 mm of the extrascleral area in two (10.5%) UM cases (p = .226).

The most frequent growth pattern was a dome shape (n = 8/19, 42.1%) (Fig. 4A), followed by a mushroom shape (n = 6/19, 31.6%), diffuse shape (n = 3/19, 15.8%), and a solid mass (n = 2/19, 10.5%). Epithelioid cell melanoma (Fig. 4) was present in 12 cases (63.2%). Based on the eighth edition of AJCC staging for iris [14], ciliary body, and choroid [14] melanomas, pathological tumor stages of cases were pT1b in one (5.3%), pT2b in three (15.8%), pT3 in one (5.3%), pT3a in five (26.3%), pT3b in one (5.3%), pT3d in one (5.3%), pT4a in four (21.1%), pT4d in one (5.3%), and pT4e in two (10.5%), respectively. Pigmen-

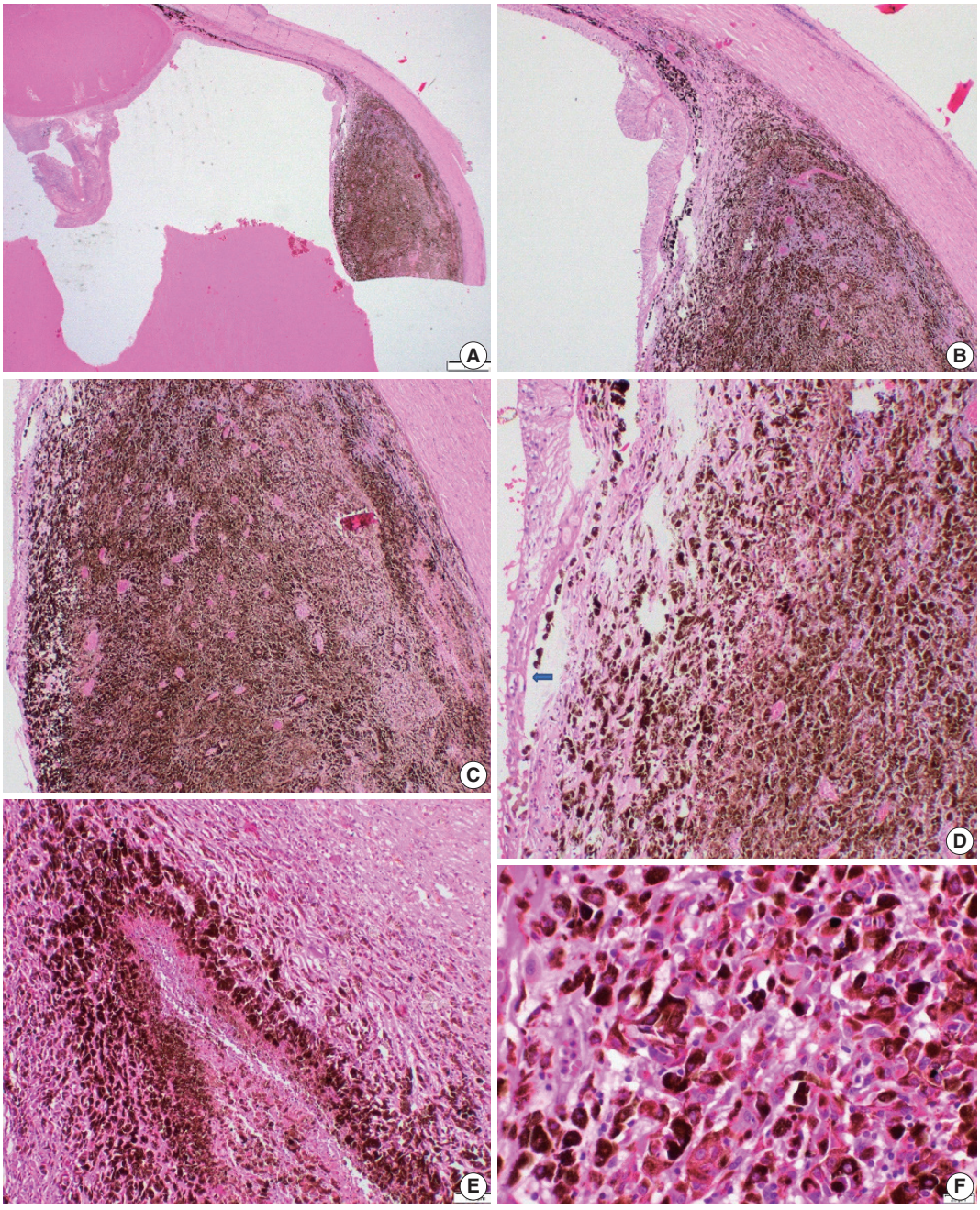

Fig. 4. Right enucleation from a 25-year-old female patient revealed a densely pigmented, dome-shaped posterior choroidal melanoma with a basal diameter of 16 mm and a tumor thickness of 3.3 mm (A–C). Effacement of the overlying retinal layer by infiltrating melanocytes (D) (arrow). Densely pigmented atypical melanocytes are arranged around the necrosis reminiscent of pseudo-palisading necrosis (E). A closer look highlights the atypical epithelioid melanocytes with large nuclei and prominent nucleoli (F). This case is wild-type for *BRAF* V600 mutation.

tation was dense and covered > 75% of the UM (Fig. 4) in eight (42.1%) tumors (p = .296). Necrosis was evident in 10 (55.6%) UM cases (p = .166). TILs were present in six UM cases (33.3%) (p = .233). The mitotic count was > 1/mm^2 in seven UM cases (36.8%) (p = .448). Inconspicuous, prominent, and prominent and large nucleoli were present in two (11.1%), eight (44.4%), and eight (44.4%) UM cases, respectively. *BRAF* V600 mutations were absent in three UM cases tested with RT-PCR (n = 2) and NGS (n = 1). NGS data from the enucleation specimen revealed a mutation in *GNAQ* (guanine nucleotide–binding protein G(q) subunit alpha) exon 4 codon 183 that resulted in a substitution of arginine with glutamine. Additionally, this case

https://doi.org/10.4132/jptm.2022.03.10

was immunohistochemically intact for mismatch repair proteins (MLH1, PMS2, MSH2, and MSH6).

Comparisons between CM and UM cases revealed that pT staging was the only significant difference between them. The variations resulted specifically from the pT1 and pT4 categories when the comparison were broken down further. UM patients presented with an advanced pT category compared to CM patients (p = .019) (Supplementary Table S1).

DISCUSSION

CM is most common in middle-aged (55–65 years) patients [20], mainly similar to our study. In this study, female and male patients were equal in number. Berta-Antalics et al. [21] reported 80 CM cases among 42 female patients and 38 male patients. Similar to our research, others reported that the most frequently involved site was the bulbar conjunctiva in 60% [21] to 75% [22] of patients.

In this study, UM patients totaled 61.3% of all ocular melanomas, which was a lower percentage than that in previously published reports [2,13]. The 5- and 10-year OS rates for UM were the same and 48.8% (Fig. 3A). Although there was no mortality at 5–10 years, OS probabilities were lower than previously documented [2,23,24]. At the end of this study, all deceased patients (n = 9/19, 47.4%) were within their first five years after diagnosis. In a very long-term (≥ 20 years) follow-up study including 289 UM patients, 239 participants (83%) were deceased at the study's end, and 145 (61%) of these deaths were due to UM [24]. Their 5- and 10-year audited melanoma-specific Kaplan-Meier survival estimates were 68% and 57%, respectively [24]. The differences between our study and the mentioned article could be due to the small sample size in this study.

In our study, female patients (n = 12, 63%) were dominant for UM, consistent with previously published reports [25]. We did not find statistical significance for gender-related OS differences. Shields et al. [26] also reported no association between gender and metastasis or mortality in a comprehensive study for UM. Kaliki et al. [27] divided 122 UM patients into three groups regarding diagnosis age. They reported that patients who were diagnosed at ≤ 20 years had lower metastasis rates than patients who were diagnosed at middle (21–60 years) or elderly (> 60) ages [27]. In our study, there were no patients aged < 20 years old. Besides, we identified no significant difference in OS between age groups by decade.

This study established that a tumor thickness of > 2 mm (p = .012) and ulceration (p = .030) reduced the OS of CM patients. Esmaeli et al. [15] also determined that a tumor thickness of > 2 mm was significantly correlated with regional lymph node metastasis (p = .033), regional lymph node or distant metastasis (p = .005), and death from disease (p = .004). Additionally, ulceration was related to an increased risk for nodal metastasis, distant metastasis, and death from disease in CM [15,28]. In our study, a mitotic count of > 1/mm^2 and LVI diminished the OS probability for CM patients. Tuomaala et al. [29] suggested an increasing mitotic count was related to a shorter time to recurrence (p = .042). Esmaeli et al. [15] reported that mitotic count ≥ 1 mm^2 and vascular invasion were significantly correlated with regional lymph node metastasis and death from the disease.

Tumor diameter (largest basal diameter and tumor thickness) is one of the most important prognostic factors for UM [26,30,31]. In this study, when we compared the UM tumors according to the largest tumor diameter, 5-year OS rates were 66.7%, 28.6%, and 60% for UM tumors of small (≤ 9 mm), middle (9.1–15 mm), and large (> 15 mm) sizes, respectively. OS rates differed significantly between middle- and large-sized subgroups (p = .035) (Table 2, Fig. 3B). Middle-sized UM tumors had the worst prognosis in our study. This could be due to features other than tumor size; however, the rarity of cases prevented us from performing a multivariate analysis for further comparisons.

In this study, the presence of TILs had a favorable effect on OS (p = .014) for CM patients. Cao et al. [32] studied programmed cell death 1/programmed cell death-ligand 1 (PD-L1) proteins and TILs in CM. Although TIL density was not directly associated with survival or tumoral/stromal PD-L1 expression (p > .05), these investigators determined that smaller tumors had higher TILs than larger tumors. Correspondingly, thicker tumors had a lower number of CD3$^+$ CD8$^+$ T-cells (p = .030) and tumor-infiltrating M2 macrophages (p = .020) [32]. Another study revealed that tumors with neural cell-adhesion molecule expression had a 6.4-fold higher risk of dying from CM (p = .020) and had no or only weak CD3$^+$ infiltration (p = .030) [33]. In a recent review by Brouwer et al. [34], the earliest report indicating that the presence of TILs, detected by hematoxylin and eosin, led to better survival was published in 1980 by Crawford [35] and contained 19 cases. Two other studies [36,37] with different approaches followed this publication and reported that the presence of TILs was associated with better survival in CM. Therefore, although our study contained a small sample size, the presence of TILs with improved OS in CM might be regarded as a valuable factor to conclude or support the role of TILs for OS in CM in the area of a few research reports.

Vodencarevic et al. [38] published 32 UM cases, and choroi-

dal involvement was the most common site, affecting 27 (84%) patients, followed by ciliary body involvement in four (13%) and iris involvement in one (3%) patient(s), respectively. We also found that the choroid was the most common site of involvement. Ciliary body melanoma can extend to the lens and result in cataract [39]. Various changes in the lens were reported in ciliary body melanoma [40]. This study determined that lens and conjunctival involvement negatively affected OS (Table 2, Fig. 3C, D). To the best of our knowledge, these features have not been reported previously for UM. However, a chance factor could not be excluded for the significance of conjunctival involvement with worse OS since only one patient with UM infiltrating the conjunctiva was present.

Jain et al. [11] stated that their CM patients were diagnosed with early-stage disease, and staging for them was as follows: pTis in 43 (14.9%), pT1 in 169 (58.7%), pT2 in 33 (11.5%), pT3 in 12 (4.2%), and pTx in 31 (10.8%). Wolf et al. [22] also confirmed pT1 disease in 83.3% of CM patients. Pathological tumor staging was reported to be associated with cumulative mortality rates and survival in CM patients [11]. Even though the result did not reach statistical significance, CM patients with pT3 had increased mortality and reduced OS compared to those with pT1 in our study (Table 1, Fig. 1F).

In large-scale studies, the 10-year mortality rate for CM has been reported as approximately 30%–40% [41,42]. However, in this study, OS ratios were lower than previous estimates [10,11, 41,42], and OS rates for CM at 1, 2, 3, 5, and 10 year(s) were 91.7%, 66.7%, 58.3%, 48.6%, and 25.9%, respectively (Fig. 1A). However, the small sample size is the main limitation of the generalizability of this study's results.

GNAQ/guanine nucleotide-binding protein subunit alpha 11 (*GNA11*) mutations are the most common (90%) mutations in UM patients [43]. One UM patient had a single-nucleotide variation at codon 183 on exon 4 of the *GNAQ* gene, which triggered a substitution of arginine with glutamine. This particular mutation is rarely reported in UM [44]. *GNAQ*/*GNA11* mutations induce abnormal activation of the mitogen-activated protein kinase (MAPK) pathway, making MAPK/MEK (MAPK kinase) signaling pathway inhibitors an impressive target for therapy [45].

In conclusion, OS data with a detailed histopathological evaluation of ocular melanoma patients suggested some previously known and not well-identified features for OS. The presence of TILs is currently not well defined and is a controversial prognostic feature for CM. However, this study suggests TILs as a favorable factor for OS in CM. The current study also confirmed the poor prognostic effect on OS for ulceration, a tumor thickness of > 2 mm, and a mitotic count of > 1/mm^2; those features were previously determined and suggested to be included in future tumor classification guidelines [15,28]. For UM, conjunctival and lens involvement have not previously been reported as unfavorable prognostic factors for OS to the best of our knowledge. Future studies may verify the relationship between survival and detailed clinicopathologic features of CM and UM. Next, these features may benefit initial patient management, treatment, and surveillance.

Supplementary Information

The Data Supplement is available with this article at https://doi.org/10.4132/jptm.2022.03.10.

Ethics Statement

Approval from the institutional research ethics board (2020-357) was obtained in accordance with the 1964 Declaration of Helsinki and its later amendments. The need for informed consent was waived due to the retrospective nature of the study.

Availability of Data and Material

The datasets generated or analyzed during the study are available from the corresponding author on reasonable request.

Code Availability

Not applicable.

ORCID

Selin Kestel https://orcid.org/0000-0003-1625-8447
Feriha Pınar Uyar Göçün https://orcid.org/0000-0003-0037-4435
Betül Öğüt https://orcid.org/0000-0002-1385-7324
Özlem Erdem https://orcid.org/0000-0002-5981-4856

Author Contributions

Conceptualization: SK, FPUG, BÖ. Data curation: SK, FPUG, BÖ, ÖE. Investigation: SK, FPUG. Methodology: SK, FPUG. Supervision: FPUG, ÖE. Writing—original draft: SK. Writing—review & editing: SK, FPUG, BÖ, ÖE. Approval of final manuscript: SK, FPUG, BÖ, ÖE.

Conflicts of Interest

The authors declare that they have no potential conflicts of interest.

Funding Statement

No funding to declare.

References

1. Elder DE, Massi D, Scolyer RA, Willemze R. WHO classification of skin tumours. 4th ed. Lyon: IARC Press, 2018.
2. Singh AD, Turell ME, Topham AK. Uveal melanoma: trends in incidence, treatment, and survival. Ophthalmology 2011; 118: 1881-5.
3. Kastelan S, Gverovic Antunica A, Beketic Oreskovic L, Salopek Rabatic J, Kasun B, Bakija I. Conjunctival melanoma: epidemiological trends and features. Pathol Oncol Res 2018; 24: 787-96.
4. Kastelan S, Antunica AG, Oreskovic LB, Pelcic G, Kasun E, Hat K. Immunotherapy for uveal melanoma: current knowledge and per-

spectives. Curr Med Chem 2020; 27: 1350-66.
5. Shields CL, Kaliki S, Cohen MN, Shields PW, Furuta M, Shields JA. Prognosis of uveal melanoma based on race in 8100 patients: The 2015 Doyne Lecture. Eye (Lond) 2015; 29: 1027-35.
6. Jovanovic P, Mihajlovic M, Djordjevic-Jocic J, Vlajkovic S, Cekic S, Stefanovic V. Ocular melanoma: an overview of the current status. Int J Clin Exp Pathol 2013; 6: 1230-44.
7. Li Y, Fan X, Jia R. Conjunctival melanoma: update on management. Int Ophthalmol Clin 2019; 59: 27-35.
8. Yu GP, Hu DN, McCormick S, Finger PT. Conjunctival melanoma: is it increasing in the United States? Am J Ophthalmol 2003; 135: 800-6.
9. Vora GK, Demirci H, Marr B, Mruthyunjaya P. Advances in the management of conjunctival melanoma. Surv Ophthalmol 2017; 62: 26-42.
10. Tan LLY, Hong J, Goh WL, et al. Clinical features and survival outcomes of ocular melanoma in a multi-ethnic Asian cohort. Sci Rep 2020; 10: 16367.
11. Jain P, Finger PT, Damato B, et al. Multicenter, international assessment of the eighth edition of the American Joint Committee on Cancer cancer staging manual for conjunctival melanoma. JAMA Ophthalmol 2019; 137: 905-11.
12. Sagiv O, Thakar SD, Kandl TJ, et al. Immunotherapy with programmed cell death 1 inhibitors for 5 patients with conjunctival melanoma. JAMA Ophthalmol 2018; 136: 1236-41.
13. Kaliki S, Shields CL. Uveal melanoma: relatively rare but deadly cancer. Eye (Lond) 2017; 31: 241-57.
14. Amin MB, Edge S, Greene FL, et al. AJCC cancer staging manual. 8th ed. New York: Springer, 2017.
15. Esmaeli B, Roberts D, Ross M, et al. Histologic features of conjunctival melanoma predictive of metastasis and death (an American Ophthalmological thesis). Trans Am Ophthalmol Soc 2012; 110: 64-73.
16. Protocol for the examination of specimens from patients with uveal melanoma [Internet]. Northfield: College of American Pathologists, 2017 [cited 2021 May 10]. Available from: https://documents.cap.org/protocols/cp-uveal-melanoma-17protocol-4000.pdf.
17. Jager MJ, Shields CL, Cebulla CM, et al. Uveal melanoma. Nat Rev Dis Primers 2020; 6: 24.
18. Shields CL, Shields JA, De Potter P, Cater J, Tardio D, Barrett J. Diffuse choroidal melanoma: clinical features predictive of metastasis. Arch Ophthalmol 1996; 114: 956-63.
19. McLean IW, Foster WD, Zimmerman LE, Gamel JW. Modifications of Callender's classification of uveal melanoma at the Armed Forces Institute of Pathology. Am J Ophthalmol 1983; 96: 502-9.
20. Koc I, Kiratli H. Current management of conjunctival melanoma part 1: clinical features, diagnosis and histopathology. Turk J Ophthalmol 2020; 50: 293-303.
21. Berta-Antalics AI, Kruse FE, Holbach L. Pathology and prognostic factors of conjunctival melanoma. Ophthalmologe 2015; 112: 892, 894-8.
22. Wolf J, Auw-Haedrich C, Schlecht A, et al. Transcriptional characterization of conjunctival melanoma identifies the cellular tumor microenvironment and prognostic gene signatures. Sci Rep 2020; 10: 17022.
23. Tarlan B, Kiratli H. Uveal melanoma: current trends in diagnosis and management. Turk J Ophthalmol 2016; 46: 123-37.
24. Kujala E, Makitie T, Kivela T. Very long-term prognosis of patients with malignant uveal melanoma. Invest Ophthalmol Vis Sci 2003; 44: 4651-9.
25. Alkatan HM, Al Qahtani AA, Maktabi AM. Enucleated globes with choroidal melanoma: a retrospective histopathological study and correlation with cytogenetic profile in 2 eye centers. Ann Med Surg (Lond) 2020; 55: 227-33.
26. Shields CL, Kaliki S, Furuta M, Mashayekhi A, Shields JA. Clinical spectrum and prognosis of uveal melanoma based on age at presentation in 8,033 cases. Retina 2012; 32: 1363-72.
27. Kaliki S, Shields CL, Mashayekhi A, Ganesh A, Furuta M, Shields JA. Influence of age on prognosis of young patients with uveal melanoma: a matched retrospective cohort study. Eur J Ophthalmol 2013; 23: 208-16.
28. Esmaeli B, Rubin ML, Xu S, et al. Greater tumor thickness, ulceration, and positive sentinel lymph node are associated with worse prognosis in patients with conjunctival melanoma: implications for future AJCC classifications. Am J Surg Pathol 2019; 43: 1701-10.
29. Tuomaala S, Toivonen P, Al-Jamal R, Kivela T. Prognostic significance of histopathology of primary conjunctival melanoma in Caucasians. Curr Eye Res 2007; 32: 939-52.
30. Damato B, Coupland SE. A reappraisal of the significance of largest basal diameter of posterior uveal melanoma. Eye (Lond) 2009; 23: 2152-60.
31. Kaliki S, Shields CL, Shields JA. Uveal melanoma: estimating prognosis. Indian J Ophthalmol 2015; 63: 93-102.
32. Cao J, Brouwer NJ, Richards KE, et al. PD-L1/PD-1 expression and tumor-infiltrating lymphocytes in conjunctival melanoma. Oncotarget 2017; 8: 54722-34.
33. Anastassiou G, Esser M, Bader E, Steuhl KP, Bornfeld N. Expression of cell adhesion molecules and tumour infiltrating leucocytes in conjunctival melanoma. Melanoma Res 2004; 14: 381-5.
34. Brouwer NJ, Verdijk RM, Heegaard S, Marinkovic M, Esmaeli B, Jager MJ. Conjunctival melanoma: New insights in tumour genetics and immunology, leading to new therapeutic options. Prog Retin Eye Res 2022; 86: 100971.
35. Crawford JB. Conjunctival melanomas: prognostic factors a review and an analysis of a series. Trans Am Ophthalmol Soc 1980; 78: 467-502.
36. Folberg R, McLean IW, Zimmerman LE. Malignant melanoma of the conjunctiva. Hum Pathol 1985; 16: 136-43.
37. Bobic-Radovanovic A, Latkovic Z, Marinkovic J, Radovanovic Z. Predictors of survival in malignant melanoma of the conjunctiva: a clinico-pathological and follow-up study. Eur J Ophthalmol 1998; 8: 4-7.
38. Vodencarevic AN, Jusufovic V, Terzic S, Burgic M, Halibasic M, Sinanovic M. Epidemiological analysis of ocular melanoma in university clinic center in Tuzla, Bosnia and Herzegovina. Mater Sociomed 2016; 28: 314-5.
39. Papastefanou VP, Cohen VM. Uveal melanoma. J Skin Cancer 2011; 2011: 573974.
40. Demirci H, Shields CL, Shields JA, Honavar SG, Eagle RC Jr. Ring melanoma of the ciliary body: report on twenty-three patients. Retina 2002; 22: 698-706.
41. Shildkrot Y, Wilson MW. Conjunctival melanoma: pitfalls and dilemmas in management. Curr Opin Ophthalmol 2010; 21: 380-6.
42. Missotten GS, Keijser S, De Keizer RJ, De Wolff-Rouendaal D. Conjunctival melanoma in the Netherlands: a nationwide study. Invest Ophthalmol Vis Sci 2005; 46: 75-82.
43. Ortega MA, Fraile-Martinez O, Garcia-Honduvilla N, et al. Update on uveal melanoma: translational research from biology to clinical

practice (Review). Int J Oncol 2020; 57: 1262-79.
44. Toomey CB, Fraser K, Thorson JA, Goldbaum MH, Lin JH. *GNAQ* and *PMS1* mutations associated with uveal melanoma, ocular surface melanosis, and nevus of ota. Ocul Oncol Pathol 2019; 5: 267-72.
45. Rodriguez A, Duenas-Gonzalez A, Delgado-Pelayo S. Clinical presentation and management of uveal melanoma. Mol Clin Oncol 2016; 5: 675-7.

https://doi.org/10.4132/jptm.2022.03.10

JPTM
Journal of Pathology and Translational Medicine 2022; 56: 199-204
https://doi.org/10.4132/jptm.2022.03.19

ORIGINAL ARTICLE

Correlation between myoferlin expression and lymph node metastasis in papillary thyroid carcinoma

Ji Min Na[1], Dong Chul Kim[1,2,3], Dae Hyun Song[2,3,4], Hyo Jung An[4], Hyun Min Koh[5], Jeong-Hee Lee[1,2,3], Jong Sil Lee[1,2,3], Jung Wook Yang[1,2,3], Min Hye Kim[1]

[1]Department of Pathology, Gyeongsang National University Hospital, Jinju;
[2]Department of Pathology, Gyeongsang National University School of Medicine, Jinju;
[3]Gyeongsang Institute of Health Science, Jinju;
[4]Department of Pathology, Changwon Gyeongsang National University Hospital, Changwon;
[5]Department of Pathology, Jeju National University Hospital, Jeju, Korea

Background: Myoferlin is a multifunctional protein expressed in various normal and cancer cells, with novel oncogenic roles being newly discovered. Recently, correlations have been found between myoferlin expression and unfavorable prognosis in various carcinomas. This study investigated the prognostic role of myoferlin expression in papillary thyroid carcinoma (PTC), specifically that associated with nodal metastasis. **Methods:** We collected clinicopathological data and PTC tissues from 116 patients who had been admitted to Gyeongsang National University Hospital in 2010. Immunohistochemical analysis was performed on surgical specimen-derived tissue microarray blocks. Myoferlin expression was graded, and the relationship between expression level and pathological features of tumors based on the American Joint Committee on Cancer staging system was evaluated. **Results:** Of the 116 patient samples, 100 cases exhibited positive myoferlin expression. Higher grade of myoferlin expression was correlated with lower T category group ($p = .010$). Presence of lymph node metastasis was determined to be significantly correlated with low-grade myoferlin expression ($p = .019$), with no significant difference between pN1a and pN1b tumors. **Conclusions:** Our study revealed an adverse correlation between myoferlin expression and pathological features of PTC, evidence of the potential prognostic role of myoferlin in PTC lymph node metastasis.

Key Words: Myoferlin; Papillary thyroid carcinoma; Lymph node metastasis; Tumor staging

Received: January 27, 2022 **Revised:** March 11, 2022 **Accepted:** March 19, 2022
Corresponding Author: Dong Chul Kim, MD, PhD, Department of Pathology, Gyeongsang National University School of Medicine, 15 Jinju-daero 816beon-gil, Jinju 52727, Korea
Tel: +82-55-772-8060, Fax: +82-55-759-7952, E-mail: kdcjes@gnu.ac.kr

In general, papillary thyroid carcinoma (PTC) has an excellent prognosis, with survival rates of 96% at 5 years and 93% at 10 years [1]. Unlike most other malignant tumors, the presence of lymph node metastasis has not been considered an independent risk factor for survival and has traditionally not been included in the criteria for survival risk stratification of papillary and follicular thyroid carcinoma. The current tumor, nodes, and metastasis (TNM) classification by the American Joint Committee on Cancer (AJCC) staging system categorizes the N category of PTC into N0 or N1 based on the existence of regional lymph node metastasis [2]. In patients younger than 55 years, determination of the AJCC prognostic stage. group for patient survival is not affected by the N category. Recent studies have suggested that nodal metastases in differentiated thyroid cancer are prognostic of not only an increased risk of recurrence, but also of poorer survival, particularly among older patients [3-6]. Additional variable features are also considered prognostic, including the size, number, and existence of metastatic nodal extracapsular extensions [7-10].

Myoferlin is a membrane-anchored protein of the ferlin family and is expressed in various cells such as myoblasts and endothelial cells. Myoferlin is involved in many cell functions such as cell fusion, cell growth and repair, and vesicle trafficking [11,12]. It also plays a role in oncogenesis through the regulation of cell proliferation and homeostasis and induces the epithelial-mesenchymal transition, leading to tumor metastasis [13-15]. The expression of this protein is found in various cancers including non-small cell lung cancer, breast cancer, pancreatic adenocarcinoma, clear cell renal cell carcinoma, hepatocellular carcinoma, and endo-

pISSN 2383-7837
eISSN 2383-7845

metrioid carcinoma [14-20]. In studies that have investigated the associations between myoferlin expression and disease survival, studies of non–small cell lung cancer, pancreatic adenocarcinoma, and clear cell renal cell carcinoma found significant correlation of higher tumor cell myoferlin expression with unfavorable prognosis [16-18].

According to the Human Protein Atlas, in normal thyroid glandular cells, myoferlin is expressed at a medium expression level [21]. To the best of our knowledge, no previous study has investigated PTC-specific patterns of myoferlin expression. Therefore, in this study, we describe evidence for an association between tumoral myoferlin expression and nodal metastatic status in PTC.

MATERIALS AND METHODS

Case selection

We collected clinicopathological data from the electronic medical records of PTC patients who underwent either total thyroidectomy or lobectomy in 2010 at Gyeongsang National University Hospital, Jinju, Korea. Cases with morphologic variants other than conventional (classic) PTC were excluded. The TNM stages of the tumors were assessed according to the *American Joint Committee on Cancer staging manual, 8th edition* [2]. All gross photographs and hematoxylin and eosin-stained slides of the surgical specimens were reviewed by two pathologists.

Tissue microarray

Tumor specimens from the selected cases were fixed overnight in buffered neutral formalin (10%) and embedded in paraffin blocks. Representative cores 2 mm in diameter were selected and obtained from each paraffin block after microscopic examination. They were then arranged onto new recipient tissue microarray (TMA) blocks.

Immunohistochemical analysis

To investigate protein expression, immunohistochemical staining was performed on 4 μm sections from the TMA blocks. The sections were deparaffinized, rehydrated, and incubated in 3% hydrogen peroxide. After heating in 10 mM citrate buffer (pH 6.0), the slides were incubated with a mouse monoclonal primary myoferlin antibody (1:100, 7D2, ab76746, Abcam, Cambridge, UK). 3,3'-Diaminobenzidine staining and counterstaining of hematoxylin were carried out for visualization. The expression of myoferlin in the tumor cells was graded from negative to weak (+1), moderate (+2), and strong (+3) positivity by two experienced pathologists. Normal thyroid follicular cells were used as the internal control. If tumor cells exhibited equivalent intensity of myoferlin expression compared to normal follicular cells, they were graded as moderate positive. Similarly, tumor cells that exhibited stronger or weaker expression were graded as strong and weak positive, respectively.

Statistical analysis

Pearson's chi square test and Fisher's exact test were used to evaluate correlations between myoferlin expression level and a range of clinicopathological features including age and sex of patients and the size, extension, lymph node metastasis, and pathologic T category and N category in AJCC staging of the tumors. For all statistical analyses, differences were considered statistically significant at $p < .05$. IBM SPSS Statistics for Windows, ver. 21.0 (IBM Corp., Armonk, NY, USA) was used for the statistical analysis.

RESULTS

Clinicopathological features

Table 1 summarizes the clinical data and pathological features

Table 1. Clinical and pathological information of the 116 papillary thyroid carcinoma patients

Variable	No. of patients (%)
Age (yr), mean (range)	49.5 (25–88)
Sex	
Male	20 (17.2)
Female	96 (82.8)
Size (cm), mean (range)	1.1 (0.1–6.0)
Gross extrathyroidal extension	
Absent	105 (90.5)
Present	11 (9.5)
T category	
T1a	73 (62.9)
T1b	23 (19.8)
T2	7 (6.0)
T3a	2 (1.7)
T3b	6 (5.2)
T4a	5 (4.3)
N category	
NX	65 (56.0)
N0	27 (23.3)
N1	24 (20.7)
N1a	17 (14.7)
N1b	7 (6.0)
Myoferlin	
Negative	16 (13.8)
Weak (+1)	35 (30.2)
Moderate (+2)	53 (45.7)
Strong (+3)	12 (10.3)

https://doi.org/10.4132/jptm.2022.03.19

of the patients enrolled in this study. Of the 116 PTC patients enrolled, the mean age was 49.5 years (range, 25 to 88 years), with 20 male (17.2%) and 96 female (82.8%) patients. The largest diameter tumor sizes ranged from 0.1–6.0 cm (mean, 1.12 cm). Notably, in 11 (9.5%) of these cases, gross tumor extension beyond the thyroid gland was observed. Most patients (96/116, 82.7%) had pT1 carcinomas, whereas seven (6%), eight (6.9%), and five (4.3%) were observed for pT2, pT3, and pT4 tumors, respectively. Lymph node dissection was performed in 51 (44.0%) patients, of whom 24 (20.7%) were found to have lymph node PTC metastasis. There were 17 (14.7%) pN1a tumors and seven (6.0%) pN1b tumors. No distant metastasis was observed in any of the cases.

Myoferlin expression in PTC

Normal thyroid follicular cells exhibited myoferlin expression in the cell cytoplasm and membrane (Fig. 1A). Myoferlin expression in PTC cells was observed in 100 cases (86.2%), showing a even expression pattern involving the cytoplasm and membrane (Fig. 1B–E). Myoferlin expression level was graded as weak (+1) in 35 cases (30.2%), moderate (+2) in 53 cases (45.75%), and strong (+3) in 12 cases (10.3%) (Table 1). To facilitate reproducibility, these grading categories were further simplified into two categories: low (negative or only weakly positive, +1) and high (moderate, +2 to strong, +3) expression levels. Of all patients, 51 (44.0%) exhibited negative or weak myoferlin expression level, whereas 65 (56.0%) showed moderate to strong expression.

Correlation of myoferlin expression with T category and N category of PTC

Table 2 summarizes the associations between myoferlin expression level and the clinicopathological features of patients. Patient age and sex, tumor size, and presence of gross extrathyroidal extensions did not demonstrate a significant correlation with myoferlin expression of tumors. In pT1 tumors, a larger number exhibited a high (moderate or strong) level of myoferlin expression (n = 60, 51.7%) compared to low (negative or weak) expression (n = 36, 31.0%). In pT4 tumors, it was the opposite, as the number of tumors with a low level of expression (n = 4, 3.4%) outnumbered those with a high level of expression (n = 1, 0.9%). Overall, the T category and myoferlin expression level of tumors exhibited the

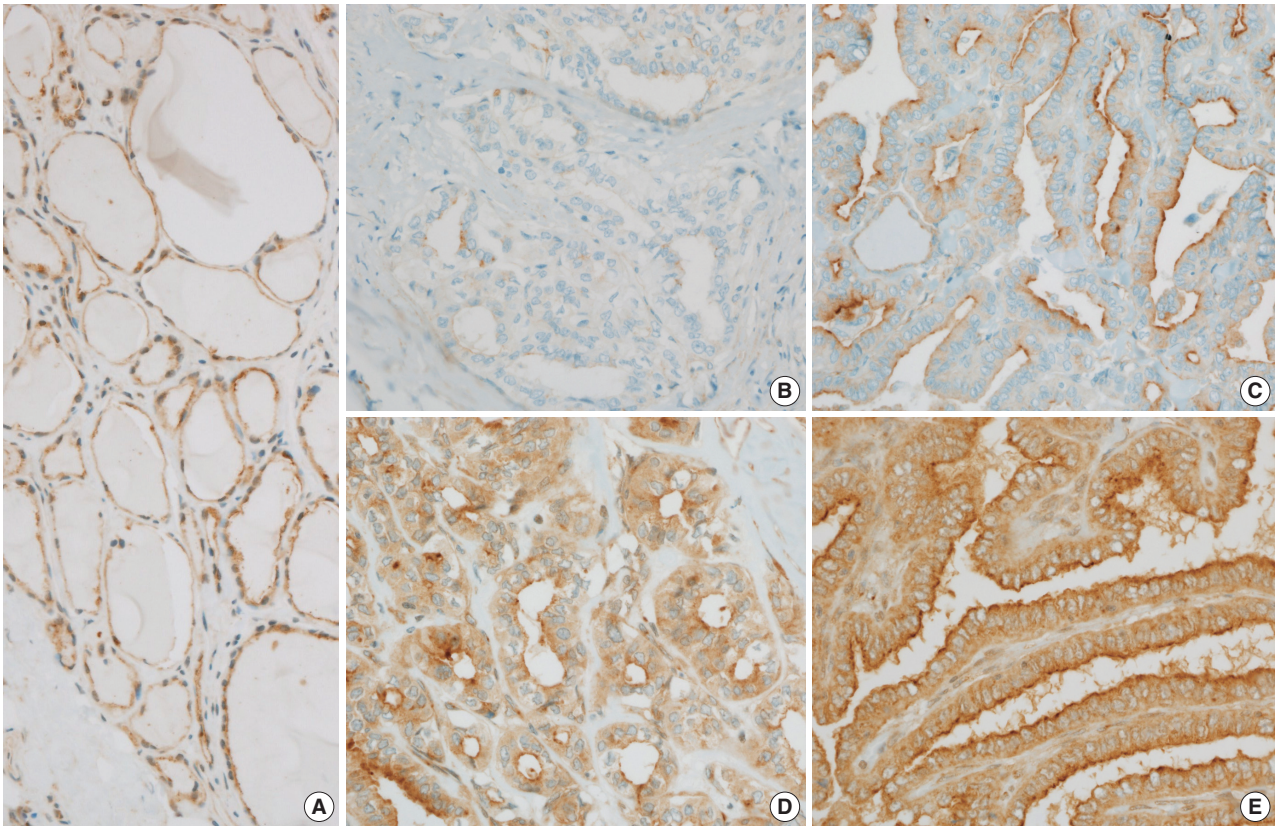

Fig. 1. (A) Myoferlin expression observed in the cytoplasm and membrane of normal thyroid follicular cells. (B–E) Myoferlin expression observed in papillary thyroid carcinoma. Negative (B), weak (+1) (C), moderate (+2) (D), and strong (+3) (E) myoferlin expression in tumor cells.

Table 2. Correlations between myoferlin expression and clinicopathological features of the patients

	Myoferlin expression		Total (n = 116)	p-value
	Low	High		
Age (yr)	50.8 ± 13.3	48.5 ± 12.1		.343
Sex				
Male	11 (9.5)	9 (7.8)	20 (17.2)	.274
Female	40 (34.5)	56 (48.3)	96 (82.8)	
Size (cm)	1.25 ± 1.12	1.02 ± 0.65		.194
Gross extrathyroidal extension				
Absent	43 (37.0)	62 (53.4)	105 (90.5)	.057
Present	8 (6.9)	3 (2.6)	11 (9.5)	
T category				
1	36 (31.0)	60 (51.7)	96 (82.8)	.010
2	6 (5.2)	1 (0.9)	7 (6.0)	
3	5 (4.3)	3 (2.6)	8 (6.9)	
4	4 (3.4)	1 (0.9)	5 (4.3)	
N category				
X	32 (27.6)	33 (28.4)	65 (56.0)	.019
0	6 (5.2)	21 (18.1)	27 (23.3)	
1	13 (11.2)	11 (9.5)	24 (20.7)	
1a	8 (6.9)	9 (7.8)		.386
1b	5 (4.3)	2 (1.7)		
Total	51 (44.0)	65 (56.0)	116	

Values are presented as mean ± SD or number (%).
SD, standard deviation.

following tendency: tumors of the higher T category group showed a correlation with a lower level of myoferlin expression (p = .010).

Among the cases that underwent lymph node dissection, in lymph node metastasis-free (pN0) tumors, six (5.2%) exhibited low myoferlin expression level, whereas high levels were observed in 21 (18.1%). Among lymph node metastatic tumors (pN1), 13 (11.2%) indicated low myoferlin expression levels, whereas 11 (9.5%) cases revealed high levels. Statistically, pN1 tumors with lymph node metastasis were significantly correlated with low myoferlin expression levels (p = .019). Whether the tumor of the pN1 category was pN1a or pN1b showed no significant association with myoferlin expression (p = .386).

DISCUSSION

This study confirmed that myoferlin is expressed in PTC cells. In previous studies, myoferlin overexpression was indicative of poor disease survival in various types of carcinomas including non-small cell lung carcinoma [16], pancreatic adenocarcinoma [17], and clear cell renal cell carcinoma [18]. However, our retrospective study data showed a statistically significant correlation of loss of myoferlin expression with a higher T category of tumor and lymph node PTC metastasis. With both features being risk factors for poor survival and disease recurrence, this correlation counters the majority of recent research observations that have reported an evident correlation between higher myoferlin level and unfavorable prognosis.

In a study from our institution on endometrioid carcinoma, loss of myoferlin expression level correlated with high histologic grade [20]. This result also counters the previously described correlation of high myoferlin expression with poor prognosis in some carcinomas. The continuous cyclic regeneration of normal endometrial tissue was suggested as a possible cause of this correlation. Myoferlin is a multifunctional protein in normal cells, although its role in various cancer cells is unknown. Research findings suggest that myoferlin expression has different tendencies due to its various roles in different types of carcinomas.

No previous myoferlin studies were performed on endocrine cell–derived tumors. Myoferlin is expressed in normal thyroid follicular cells, but its specific roles in normal cells or oncogenic roles have yet to be studied. Therefore, one plausible hypothesis is that the endocrine activity of thyroid follicular cells influences the distinctive pattern of myoferlin expression in the thyroid. The difference in key functions of myoferlin could possibly be the cause of its expression tendency differing in PTC from lung and pancreatic epithelial tumors. Further molecular studies on the role of myoferlin in different types of tumor cells are needed to clarify the specific function of this protein.

https://doi.org/10.4132/jptm.2022.03.19

Of the 116 patients enrolled, there were only four cases with recurrent disease and no patient death during follow-up. With regard to these findings, owing to the limited sample size in the present study, an analysis of a larger cohort is necessary to confirm correlations with survival rates.

In differentiated papillary carcinoma, therapeutic neck dissection is strongly recommended and routinely performed in clinically palpable or biopsy-proven nodal disease, as it is well established that nodal metastasis is associated with disease recurrence [6]. However, the use of prophylactic neck dissection for clinically node-negative PTC is controversial. If prediction of occult lymph node metastatic status is determinable by pre-surgical cytology or biopsy specimens, a justification could be made for more individualized disease management, which could include determining whether to perform neck dissection or to closely follow-up on the case. The correlation proposed in the present study points to a potential prognostic role of myoferlin in lymph node PTC metastasis.

Conclusively, our study demonstrated correlation of myoferlin expression with pathological features in papillary thyroid carcinoma. Loss of expression of myoferlin was correlated with a higher T category of tumor and the presence of lymph node metastasis in PTC. This result shows the potential prognostic role of myoferlin in PTC as a helpful biomarker in therapeutic management.

Ethics Statement

This study was approved by the Institutional Review Board of Gyeongsang National University Hospital, and the need for informed consent was waived (GNUH-10-026).

Availability of Data and Material

The datasets generated or analyzed during the study are available from the corresponding author on reasonable request.

Code Availability

Not applicable.

ORCID

Ji Min Na	https://orcid.org/0000-0003-4330-6598
Dong Chul Kim	https://orcid.org/0000-0002-9484-7792
Dae Hyun Song	https://orcid.org/0000-0001-7163-0403
Hyo Jung An	https://orcid.org/0000-0002-2068-8370
Hyun Min Koh	https://orcid.org/0000-0002-7457-7174
Jeong-Hee Lee	https://orcid.org/0000-0001-5833-4773
Jong Sil Lee	https://orcid.org/0000-0001-9159-7575
Jung Wook Yang	https://orcid.org/0000-0002-9698-3667
Min Hye Kim	https://orcid.org/0000-0002-8631-5104

Author Contributions

Conceptualization: DCK, DHS. Data curation: JMN, DCK, JHL, JSL, JWY, HJA, MHK. Investigation: DCK, DHS, JHL, JSL, JWY, MHK. Methodology: JMN, DCK. Project administration: DCK, DHS. Resources: DHS. Supervision: DHS, MHK, JWY. Validation: DCK, HJA, HMK. Visualization: JMN. Writing—original draft: JMN, DCK. Writing—review & editing: JMN, DCK, JWY. Approval of final manuscript: all authors.

Conflicts of Interest

The authors declare that they have no potential conflicts of interest.

Funding Statement

This work was supported by the fund of research promotion program, Gyeongsang National University, 2015.

References

1. Hundahl SA, Fleming ID, Fremgen AM, Menck HR. A National Cancer Data Base report on 53,856 cases of thyroid carcinoma treated in the U.S., 1985-1995 [see commetns]. Cancer 1998; 83: 2638-48.
2. Amin MB, Edge S, Greene FL, et al. AJCC cancer staging manual. 8th ed. New York: Spinger, 2017; 873-90.
3. Harwood J, Clark OH, Dunphy JE. Significance of lymph node metastasis in differentiated thyroid cancer. Am J Surg 1978; 136: 107-12.
4. Zaydfudim V, Feurer ID, Griffin MR, Phay JE. The impact of lymph node involvement on survival in patients with papillary and follicular thyroid carcinoma. Surgery 2008; 144: 1070-7.
5. Nixon IJ, Wang LY, Palmer FL, et al. The impact of nodal status on outcome in older patients with papillary thyroid cancer. Surgery 2014; 156: 137-46.
6. Haugen BR, Alexander EK, Bible KC, et al. 2015 American Thyroid Association management guidelines for adult patients with thyroid nodules and differentiated thyroid cancer: the American Thyroid Association Guidelines Task Force on Thyroid Nodules and Differentiated Thyroid Cancer. Thyroid 2016; 26: 1-133.
7. Sugitani I, Kasai N, Fujimoto Y, Yanagisawa A. A novel classification system for patients with PTC: addition of the new variables of large (3 cm or greater) nodal metastases and reclassification during the follow-up period. Surgery 2004; 135: 139-48.
8. Wang LY, Palmer FL, Nixon IJ, et al. Central lymph node characteristics predictive of outcome in patients with differentiated thyroid cancer. Thyroid 2014; 24: 1790-5.
9. Jeon MJ, Yoon JH, Han JM, et al. The prognostic value of the metastatic lymph node ratio and maximal metastatic tumor size in pathological N1a papillary thyroid carcinoma. Eur J Endocrinol 2013; 168: 219-25.
10. Lee J, Song Y, Soh EY. Prognostic significance of the number of metastatic lymph nodes to stratify the risk of recurrence. World J Surg 2014; 38: 858-62.
11. Doherty KR, Cave A, Davis DB, et al. Normal myoblast fusion requires myoferlin. Development 2005; 132: 5565-75.
12. Demonbreun AR, Posey AD, Heretis K, et al. Myoferlin is required for insulin-like growth factor response and muscle growth. FASEB J 2010; 24: 1284-95.
13. Leung C, Yu C, Lin MI, Tognon C, Bernatchez P. Expression of myoferlin in human and murine carcinoma tumors: role in membrane repair, cell proliferation, and tumorigenesis. Am J Pathol 2013; 182: 1900-9.
14. Volakis LI, Li R, Ackerman WEt, et al. Loss of myoferlin redirects breast cancer cell motility towards collective migration. PLoS One 2014; 9: e86110.
15. Li R, Ackerman WEt, Mihai C, Volakis LI, Ghadiali S, Kniss DA.

Myoferlin depletion in breast cancer cells promotes mesenchymal to epithelial shape change and stalls invasion. PLoS One 2012; 7: e39766.
16. Song DH, Ko GH, Lee JH, et al. Myoferlin expression in non-small cell lung cancer: Prognostic role and correlation with VEGFR-2 expression. Oncol Lett 2016; 11: 998-1006.
17. Wang WS, Liu XH, Liu LX, et al. iTRAQ-based quantitative proteomics reveals myoferlin as a novel prognostic predictor in pancreatic adenocarcinoma. J Proteomics 2013; 91: 453-65.
18. Song DH, Ko GH, Lee JH, et al. Prognostic role of myoferlin expression in patients with clear cell renal cell carcinoma. Oncotarget 2017; 8: 89033-9.
19. Hermanns C, Hampl V, Holzer K, et al. The novel MKL target gene myoferlin modulates expansion and senescence of hepatocellular carcinoma. Oncogene 2017; 36: 3464-76.
20. Kim MH, Song DH, Ko GH, et al. Myoferlin expression and its correlation with FIGO histologic grading in early-stage endometrioid carcinoma. J Pathol Transl Med 2018; 52: 93-7.
21. Uhlen M, Fagerberg L, Hallstrom BM, et al. Proteomics: tissue-based map of the human proteome. Science 2015; 347: 1260419.

https://doi.org/10.4132/jptm.2022.03.19

JPTM
Journal of Pathology and Translational Medicine 2022; 56: 205-211
https://doi.org/10.4132/jptm.2022.04.22

ORIGINAL ARTICLE

EGFL7 expression profile in IDH-wildtype glioblastomas is associated with poor patient outcome

Bruno Henrique Bressan da Costa[1,2], Aline Paixão Becker[3], Luciano Neder[1,4], Paola Gyuliane Gonçalves[1,5], Cristiane de Oliveira[1,5], Allan Dias Polverini[6], Carlos Afonso Clara[6], Gustavo Ramos Teixeira[2,7], Rui Manuel Reis[1,8,9], Lucas Tadeu Bidinotto[1,2,5]

[1]Molecular Oncology Research Center, Barretos Cancer Hospital, Barretos, São Paulo;
[2]Barretos School of Health Sciences, Dr. Paulo Prata – FACISB, Barretos, São Paulo, Brazil;
[3]The Ohio State University, Department of Radiation Oncology, Columbus, OH, USA;
[4]Department of Pathology, School of Medicine of Ribeirao Preto, University of Sao Paulo, Ribeirão Preto, Sao Paulo;
[5]UNESP – Univ. Estadual Paulista, School of Medicine, Department of Pathology, Botucatu, São Paulo;
[6]Department of Neurosurgery, Barretos Cancer Hospital, Barretos, São Paulo;
[7]Department of Pathology, Barretos Cancer Hospital, Barretos, São Paulo, Brazil;
[8]Life and Health Sciences Research Institute (ICVS), School of Medicine, University of Minho, Braga;
[9]ICVS/3B's – PT Government Associate Laboratory, Braga/Guimarães, Portugal

Background: Despite the advances in glioblastoma (GBM) treatment, the average life span of patients is 14 months. Therefore, it is urgent to identity biomarkers of prognosis, treatment response, or development of novel treatment strategies. We previously described the association of high epidermal growth factor-like domain multiple 7 (EGFL7) expression and unfavorable outcome of pilocytic astrocytoma patients. The present study aims to analyze the prognostic potential of EGFL7 in GBM isocitrate dehydrogenase (IDH)-wildtype, using immunohistochemistry and in silico approaches. **Methods:** Spearman's correlation analysis of The Cancer Genome Atlas RNA sequencing data was performed. The genes strongly correlated to EGFL7 expression were submitted to enrichment gene ontology and Kyoto Encyclopedia of Genes and Genomes (KEGG) analysis. Additionally, EGFL7 expression was associated with patient overall survival. The expression of EGFL7 was analyzed through immunohistochemistry in 74 GBM IDH-wildtype patients' samples, and was associated with clinicopathological data and overall survival. **Results:** In silico analysis found 78 genes strongly correlated to EGFL7 expression. These genes were enriched in 40 biological processes and eight KEGG pathways, including angiogenesis/vasculogenesis, cell adhesion, and phosphoinositide 3-kinase–Akt, Notch, and Rap1 signaling pathways. The immunostaining showed high EGFL7 expression in 39 cases (52.7%). High immunolabelling was significantly associated with low Karnofsky Performance Status and poor overall survival. Cox analysis showed that GBMs IDH-wildtype with high EGFL7 expression presented a higher risk of death compared to low expression (hazard ratio, 1.645; 95% confidence interval, 1.021 to 2.650; p = .041). **Conclusions:** This study gives insights regarding the genes that are correlated with EGFL7, as well as biological processes and signaling pathways, which should be further investigated in order to elucidate their role in glioblastoma biology.

Key Words: EGFL7; Glioblastoma IDH-wildtype; PI3K-Akt pathway; Notch pathway; Rap1 pathway

Received: January 28, 2022 **Revised:** April 7, 2022 **Accepted:** April 22, 2022
Corresponding Author: Lucas Tadeu Bidinotto, PhD, Molecular Oncology Research Center, Barretos Cancer Hospital, Rua Antenor Duarte Villela, 1331, Barretos, São Paulo 14784 400, Brazil
Tel: +55-1733216600 (ext. 7350), Fax: +55-1733216600, E-mail: lucasbidinotto@gmail.com

Gliomas are responsible for 70% of brain tumors [1]. Although rare (correspond to less than 2% of tumors), these are the second leading cause of death of cancer in patients of pediatric age [2] making this cancer an important public health problem. Glioblastomas correspond to almost half of the cases of malignant brain tumors [1]. They usually affect adults, with a peak incidence between 45 and 75 years [1,3]. Glioblastomas (GBMs) are lethal tumors, and less than 10% of patients live 2 years after diagnosis [4,5]. They are highly infiltrative; thus, the complete surgical resection usually is not possible [3]. In addition to surgery, standard therapy was proposed by Stupp and collaborators, through radiotherapy with concurrent chemotherapy using temozolomide, however the average life span of patients is 14 months [6].

Epidermal growth factor-like domain multiple 7 (EGFL7) is

pISSN 2383-7837
eISSN 2383-7845

a pro-angiogenic factor, largely restricted to the endothelium [7]. This protein plays a specific role in vascular tubulogenesis, regulates angiogenesis [8] and acts in vascular development of the placenta and embryonic growth in mammals [9]. Evidence suggests that EGFL7 expression plays a role in tumor progression through mediation of metastasis, proliferation, and angiogenesis [10,11]. Moreover, EGFL7 overexpression is associated with poor prognosis events on different tumor types such as gliomas [12-14] and colorectal cancer [10,15]. Also, interaction of EGFL7 with epidermal growth factor receptor (EGFR), a key oncogene, is directly related to the development, growth, and metastasis of several tumor types, such as gliomas [13].

In our previous studies, we found recurrent chr7q34 gain in gliomas, encompassing *EGFL7* gene [16], and high EGFL7 expression associated with an unfavorable outcome of pilocytic astrocytoma patients [14]. Therefore, we extended the investigation of the potential prognostic of EGFL7 expression in GBM isocitrate dehydrogenase (IDH)-wildtype through in silico and immunohistochemistry approaches, and also proposed signaling pathways that EGFL7 can be contributing to gliomagenesis.

MATERIALS AND METHODS

In silico analysis

We performed in silico analysis in R software, using the TCGA2STAT package [17] and the tools of cBio [18] and DAVID [19] portals.

In order to evaluate potential pathways related to EGFL7 expression, correlation analysis was performed in cBio portal. RNA sequencing (RNASeq) data of GBM was obtained from The Cancer Genome Atlas (TCGA) (n = 152 patients), and the genes with Spearman's correlation ≥ |0.6| were considered strongly correlated to EGFL7 expression. Those were submitted to gene ontology (GO) and Kyoto Encyclopedia of Genes and Genomes (KEGG) pathway analysis in DAVID portal, and GO/KEGG terms with $p \leq 0.05$ were considered as statistically significant.

Additionally, RSEM-normalized data of expression (RNASeq) of GBM IDH-wildtype of the TCGA was obtained, together with the clinical data (n = 138). The number of reads of all genes were log10-transformed. Further, Z score was calculated for EGFL7, and patients with Z score ≥ 1.0 were classified with high EGFL7 expression. In order to evaluate the prognostic value of EGFL7, overall survival of the patients was analyzed in Kaplan Meier curves using log-rank statistical test.

Patients

Glioblastoma IDH-wildtype tissues were obtained from a series of 74 patients who had undergone surgery at Barretos Cancer Hospital. Formalin-fixed, paraffin embedded slides were reviewed by expert neuropathologists (A.P.B., L.N., and G.R.T.), who confirmed glioblastoma IDH-wildtype diagnosis according to 2021 World Health Organization central nervous system classification [1,20] and selected areas for tissue microarray construction. Overall, the age ranged from 26 to 75 years (median of 57 years), who were stratified in 20–59 years old (45 patients) and > 59 years old (29 patients). The average overall survival was 7.61 months (ranging from 0.13 to 45.50 months). All patients were deceased.

EGFL7 immunohistochemistry

The EGFL7 immunohistochemistry reactions were performed according to Brunhara et al. (2021) [14]. Briefly, slides with sections of 4 μm were deparaffinized and rehydrated. Then, antigenic retrieval was performed in tris(hydroxymethyl)aminomethane (Tris)–ethylenediaminetetraacetic acid buffer for 20 minutes at 98ºC. Inhibition of endogenous peroxidases and non-specific proteins was performed with the Novolink Polymer Detection System immunohistochemistry kit (Leica Biosystems, Wetzlar, Germany). The rabbit anti-EGFL7 antibody (cat. No. ab115786, Abcam, Cambridge, MA, USA) was applied at a 1:100 dilution on the slide, for 90 minutes at room temperature. Further, immunoreaction product complexes were treated by Novolink Polymer Detection System (30 minutes of post-primary antibody and 30 minutes of polymer at room temperature). Staining was performed using 3,3'-diaminobenzidine and counterstaining was performed with Gill-2 hematoxylin.

The reactions were analyzed by an expert neuropathologist (L.N.) using intensity (0, negative; 1, weak; 2, medium; and 3, strong) and extension (0, negative; 1, ~25% of mark; 2, between 25% and 50%; and 3, more than 50% of mark) scores. The scores were summed, and the expression was considered low (sum between 0 and 3) or high (sum between 4 and 6) [14]. Endothelial cells were used as positive internal control.

Statistical analysis

Immunohistochemistry staining was associated with clinicopathological data (location, age, sex, and Karnofsky Performance Status [KPS]). Finally, overall survival was analyzed using Kaplan Meier curves. Statistical analysis was performed using chi-square tests or Fisher exact test (clinicopathological), log-rank (overall survival), or univariate Cox proportional hazards. Contrasts with

https://doi.org/10.4132/jptm.2022.04.22

a p≤.05 were considered statistically significant.

RESULTS

Through in silico analysis, we found 78 genes significantly associated with EGFL7 expression profile in GBM patients of TCGA database (Supplementary Table S1). These genes were found in 40 enriched GO terms, most of them related to angiogenesis/vasculogenesis, Notch pathway, and cell adhesion (shown in Fig. 1, Supplementary Table S2). Furthermore, pathway analysis using KEGG showed eight enriched terms, mainly related to adhesion, blood cells or blood vessel events, and phosphoinositide 3-kinase (PI3K)–Akt, Notch, and Rap1 signaling pathways (shown in Fig. 1, Supplementary Table S3). Survival analysis of

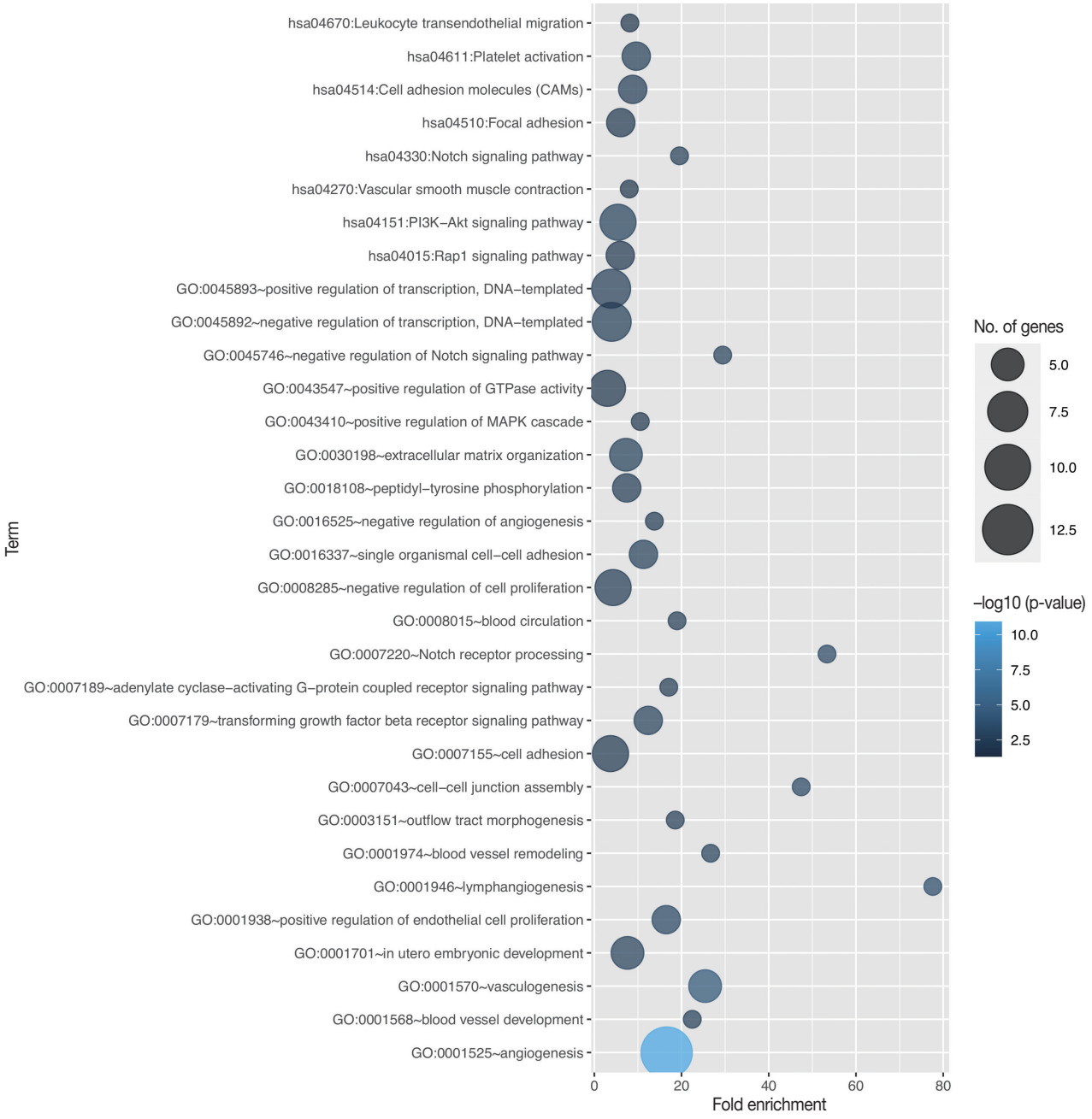

Fig. 1. Kyoto Encyclopedia of Genes and Genomes pathway and gene ontology (GO, biological processes) enrichment analysis of the genes highly correlated to EGFL7 expression. The sizes and color of the bubbles indicate the number of genes per term and significance level. EGFL7, epidermal growth factor-like domain multiple 7.

TCGA data showed no difference in overall survival regarding *EGFL7* gene expression (p = .182, shown in Fig. 2A).

We further performed analysis of EGFL7 expression by immunohistochemistry in a series of 74 glioblastomas IDH-wild-type. We found high cytoplasmatic EGFL7 expression in 39 cases (52.7%) (shown in Fig. 3). We further associated EGFL7 immu-

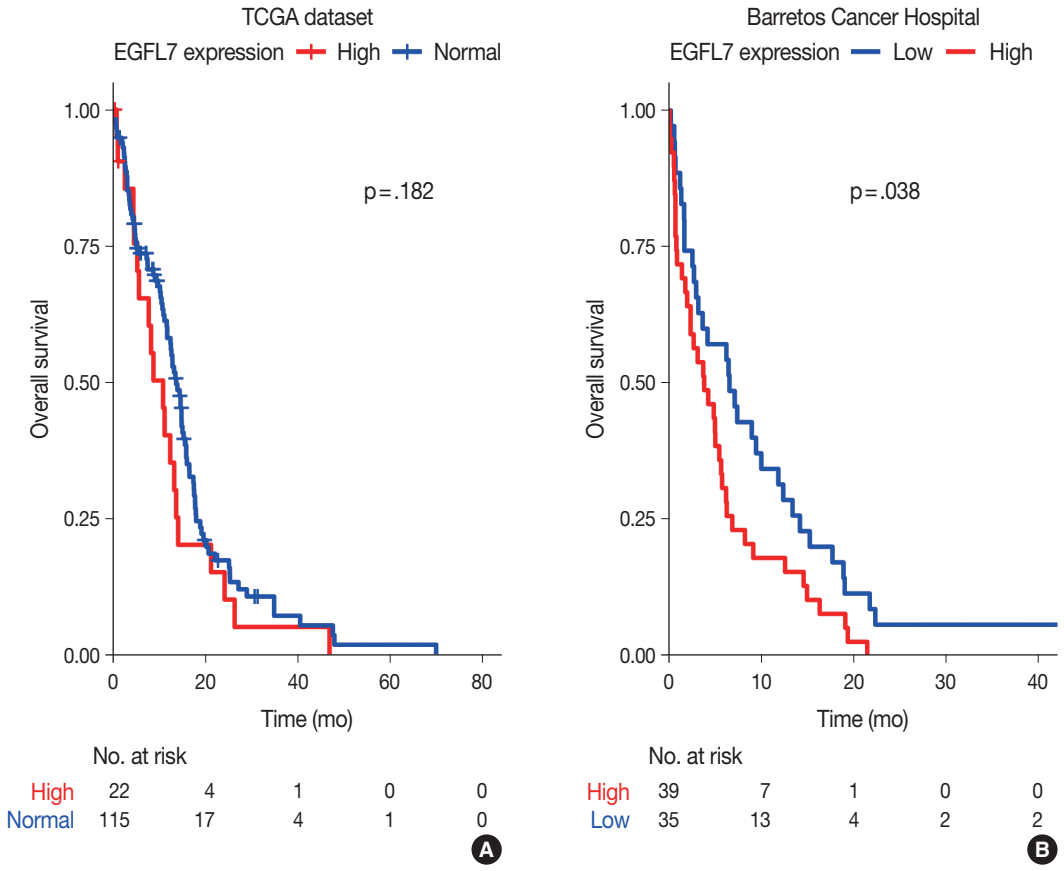

Fig. 2. Overall survival curves of glioblastoma patients. (A) *In silico* data of The Cancer Genome Atlas (TCGA) RNA sequencing. (B) Data of protein expression from 74 patients detected through immunohistochemistry. p-values were calculated using log-rank analysis. EGFL7, epidermal growth factor-like domain multiple 7.

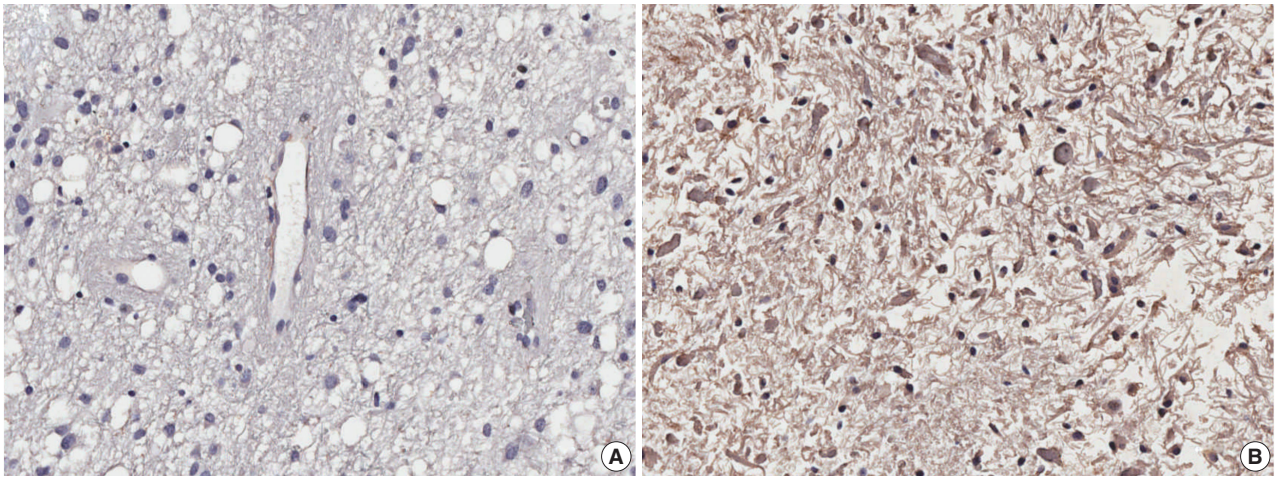

Fig. 3. Microphotographs of resected specimens of glioblastomas immunostained for EGFL7. (A) Absence of immunoreactivity, although vascular endothelial cells serve as a positive internal control for EGFL7. (B) Diffuse and strong EGFL7 immunoreactivity. EGFL7, epidermal growth factor-like domain multiple 7.

https://doi.org/10.4132/jptm.2022.04.22

Table 1. EGFL7 expression and its association with clinicopathological data

	No.	EGFL7 expression		p-value
		Low	High	
Sex				
Female	29	16 (45.7)	13 (33.3)	0.276
Male	45	19 (54.3)	26 (66.7)	
Location				
Frontal	21	12 (34.3)	9 (23.1)	0.466
Parietal	13	8 (22.9)	5 (12.8)	
Temporal	12	4 (11.4)	8 (20.5)	
Occipital	3	1 (2.9)	2 (5.1)	
Other	25	10 (28.6)	15 (38.5)	
Age group (yr)				
20–59	45	24 (68.6)	21 (53.8)	0.195
>59	29	11 (31.4)	18 (46.2)	
KPS				
≤70	43	16 (45.7)	27 (69.2)	0.041
>70	31	19 (54.3)	12 (30.8)	

Values are presented as number (%).
EGFL7, epidermal growth factor-like domain multiple 7; KPS, Karnofsky Performance Status.

nostaining with patients clinicopathological features (Table 1). High EGFL7 immunolabelling was significantly associated with patients presenting KPS lower or equal to 70 (69.2% of the patients with high EGFL7 expression presented KPS ≤70 vs. 45.7% of the patients with low EGFL7 expression, p = .041) (Table 1). EGFL7 expression was not associated with the other clinical features analyzed (sex, location, or age group) (Table 1). Importantly, there was found a poorer overall survival of the patients with high EGFL7 expression (mean of 5.69 months) compared to low EGFL7 expression (mean of 9.95 months, p = 0.038, in log-rank analysis, shown in Fig. 2B). Univariate Cox regression showed that patients with high EGFL7 expression have a 1.645-fold risk of death (95% confidence interval, 1.021 to 2.650; p = .041) compared to patients with low EGFL7 expression.

DISCUSSION

In the present study, we analyzed the TCGA database in order to infer genes that may participate in the regulation of EGFL7 expression, as well as evaluated whether EGFL7 expression had a prognostic role in glioblastomas. Our analysis found that patients with high EGFL7 expression generally have low KPS and poor survival. Additionally, our findings give insights of the role and regulation of EGFL7 in this tumor type.

EGFL7, a downstream target of BMP9-SMAD1/5-mediated signaling, is a secreted angiogenic factor and promotes endothelial expansion through the interference of Notch signaling, ERK activation, and extracellular matrix remodeling [7]. Data of the literature points to the relation of high expression of EGFL7 and poor prognosis in acute myeloid leukemia (AML) [21,22], hepatocellular carcinoma [23], colorectal cancer [10], pancreatic carcinoma [11], and ovarian epithelial cancer [24]. Wang and colleagues additionally found a poor survival of patients with high EGFL7 expression who were EGFRwt [13] mainly by improving the activity of the β-catenin/TCF complex. Li et al. [25] described that EGFL7 expression promotes the proliferation of hepatocellular carcinoma by increasing CKS2. Corroborating these data, EGFR activation (p-EGFR) was found correlated with EGFL7 overexpression in hormone-producing pituitary adenomas [26].

Our in silico results showed the genes co-expressed with EGFL7 participating mainly in events such as angiogenesis, vasculogenesis, leukocyte transendothelial migration, corroborating the data present in the literature [7,27]. Data also shows enriched genes of Notch pathway (NOTCH4, DLL4, and JAG2). These genes may be subject of further studies to help elucidating the role of this gene in Notch pathway and angiogenesis. In fact, the relation between EGFL7 and Notch pathway remains with conflicting results in the literature. In AML, studies indicate that EGFL7 antagonizes Notch signaling through antagonism to the canonical Notch ligand [28]. On the other hand, silencing of *EGFL7* in cutaneous melanoma inactivated Notch pathway, increasing apoptosis and suppressing cell proliferation [29]. Either way, EGFL7 provides its own microenvironment for the migration of endothelial cells, facilitating the budding that leads to angiogenesis [30]. It is known that angiogenesis is one of the hallmarks of cancer, and allows a better supply of blood to the tumor tissue, preventing its cells from having hypoxia/anoxia and/or nutrient deficiency [31].

Parsatuzumab, a humanized anti-EGFL7 antibody, selectively blocks the interaction between EGFL7 and endothelial cells. There is rationale of using this antibody in the inhibition of vascular growth and, used in combination to anti–vascular endothelial growth factor therapy, inhibition of vascular regrowth after vessel damage, which could reduce tumor vascularization [32]. Given the interesting results of the prognostic role of EGFL7, randomized phase II studies used parsatuzumab in combination with FOLFOX or bevacizumab in the treatment of metastatic colorectal cancer [33] and parsatuzumab in combination with carboplatin, paclitaxel, and bevacizumab for first-line nonsquamous non–small cell lung cancer [34] were performed. The authors found no evidence of the effectiveness of combining parsatuzumab with the proposed treatments, but stress the importance of future studies regarding the mechanisms of EGFL7 and de-

velopment.

EGFL7 expression should be considered beyond vascular background since its expression was found in neuronal components in addition to endothelium [35]. Our immunohistochemistry analysis showed that the patients presenting high EGFL7 expression in tumor cells generally have lower KPS and poorer survival. In line, we have previously shown in pilocytic astrocytoma that high EGFL7 expression was associated with unfavorable outcome [14]. Our in silico analysis pointed to the enrichment of PI3K-Akt and Rap1 signaling pathways. In fact, PI3K-Akt pathway has been extensively described in carcinogenesis, including gliomagenesis. Together with mTOR, this pathway regulates several biological processes that are important in growth, metabolism, angiogenesis, autophagy, and chemotherapy resistance in GBM [36]. Importantly, these pathways have been considered for drug design [36]. On the other hand, Rap1 signaling pathway has been less studied in GBM. Rap1 belongs to Ras-related protein family and is involved in cell adhesion and cell junction formation [37] through ERK/mitogen-activated protein kinase signaling and integrin activation [38]. In vitro, Rap1 was activated by integrin through phospholipase D, enhancing cell adhesion and cell proliferation whereas in vivo Rap1 knockdown profoundly altered U373MG glioblastoma growth in xenograft model [39].

Altogether, our data point to biological functions and pathways related to the increase of tumor vasculature, tumor growth, metabolism, chemotherapy resistance, and changes in cell adhesion and/or cell junction formation. These alterations may be influencing tumor behavior, leading to lower KPS at diagnosis and consequent poor overall survival. However, more molecular studies are warranted in order to elucidate EGFL7 participation in glioblastoma biology.

Supplementary Information

The Data Supplement is available with this article at https://doi.org/10.4132/jptm.2022.04.22.

Ethics Statement

Written informed consent was obtained from each patient and this study was approved by the ethics committee of Barretos Cancer Hospital (Barretos, Brazil, process CEP 408/2010).

Availability of Data and Material

The datasets generated or analyzed during the current study are available in TCGA repository (https://www.cancer.gov/tcga).

Code Availability

Not applicable.

ORCID

Bruno Henrique Bressan da Costa https://orcid.org/0000-0003-4044-9745
Aline Paixão Becker https://orcid.org/0000-0002-8695-810X
Luciano Neder https://orcid.org/0000-0003-3790-3476
Paola Gyuliane Gonçalves https://orcid.org/0000-0001-6515-3102
Cristiane de Oliveira https://orcid.org/0000-0002-3729-6904
Allan Dias Polverini https://orcid.org/0000-0001-6363-6290
Carlos Afonso Clara https://orcid.org/0000-0002-9908-507X
Gustavo Ramos Teixeira https://orcid.org/0000-0001-8363-3513
Rui Manuel Reis https://orcid.org/0000-0002-9639-7940
Lucas Tadeu Bidinotto https://orcid.org/0000-0002-6909-8347

Author Contributions

Conceptualization: RMR, LTB. Data curation: LTB. Formal analysis: APB, LN, GRT, LTB. Funding acquisition: LTB. Investigation: BHBC, PGG, CO, LTB. Methodology: BHBC, APB, LN, PGG, CO, ADP, CAC. Project administration: RMR, LTB. Resources: RMR, LTB. Supervision: LTB. Validation: RMR, LTB. Visualization: BHBC, APB, LN, GRT, LTB. Writing—original draft: BHBC, LTB. Writing—review & editing: BHBC, PGG, CO, GRT, RMR, LTB.

Conflicts of Interest

The authors declare that they have no potential conflicts of interest.

Funding Statement

This work was supported by The São Paulo Research Foundation (fellowship number 2018/20737-1 to Costa BHB, fellowship number 2017/09749-5 to Gonçalves PG, grant number 2016/21727-4 to Bidinotto LT); Coordenação de Aperfeiçoamento de Pessoal de Nível Superior (CAPES) fellowship to Oliveira C; CNPq (productivity fellowship to Reis RM and Universal grant number 472447/2013-0 to Bidinotto LT).

References

1. WHO Classification of Tumours Editorial Board. Central nervous system tumours. 5th ed. Lyon: International Agency for Research on Cancer, 2021.
2. Broniscer A, Gajjar A. Supratentorial high-grade astrocytoma and diffuse brainstem glioma: two challenges for the pediatric oncologist. Oncologist 2004; 9: 197-206.
3. Hadjipanayis CG, Van Meir EG. Brain cancer propagating cells: biology, genetics and targeted therapies. Trends Mol Med 2009; 15: 519-30.
4. Paugh BS, Qu C, Jones C, et al. Integrated molecular genetic profiling of pediatric high-grade gliomas reveals key differences with the adult disease. J Clin Oncol 2010; 28: 3061-8.
5. Ohgaki H. Epidemiology of brain tumors. Methods Mol Biol 2009; 472: 323-42.
6. Stupp R, Mason WP, van den Bent MJ, et al. Radiotherapy plus concomitant and adjuvant temozolomide for glioblastoma. N Engl J Med 2005; 352: 987-96.
7. Richter A, Alexdottir MS, Magnus SH, et al. EGFL7 mediates BMP9-induced sprouting angiogenesis of endothelial cells derived from human embryonic stem cells. Stem Cell Reports 2019; 12: 1250-9.
8. Parker LH, Schmidt M, Jin SW, et al. The endothelial-cell-derived secreted factor Egfl7 regulates vascular tube formation. Nature 2004; 428: 754-8.
9. Fitch MJ, Campagnolo L, Kuhnert F, Stuhlmann H. Egfl7, a novel

epidermal growth factor-domain gene expressed in endothelial cells. Dev Dyn 2004; 230: 316-24.
10. Hansen TF, Andersen RF, Olsen DA, Sorensen FB, Jakobsen A. Prognostic importance of circulating epidermal growth factor-like domain 7 in patients with metastatic colorectal cancer treated with chemotherapy and bevacizumab. Sci Rep 2017; 7: 2388.
11. Shen X, Han Y, Xue X, et al. Epidermal growth factor-like domain 7 promotes cell invasion and angiogenesis in pancreatic carcinoma. Biomed Pharmacother 2016; 77: 167-75.
12. Huang CH, Li XJ, Zhou YZ, Luo Y, Li C, Yuan XR. Expression and clinical significance of EGFL7 in malignant glioma. J Cancer Res Clin Oncol 2010; 136: 1737-43.
13. Wang FY, Kang CS, Wang-Gou SY, Huang CH, Feng CY, Li XJ. EGFL7 is an intercellular EGFR signal messenger that plays an oncogenic role in glioma. Cancer Lett 2017; 384: 9-18.
14. Brunhara BB, Becker AP, Neder L, et al. Evaluation of the prognostic potential of EGFL7 in pilocytic astrocytomas. Neuropathology 2021; 41: 21-8.
15. Fan C, Yang LY, Wu F, et al. The expression of Egfl7 in human normal tissues and epithelial tumors. Int J Biol Markers 2013; 28: 71-83.
16. Bidinotto LT, Torrieri R, Mackay A, et al. Copy number profiling of Brazilian astrocytomas. G3 (Bethesda) 2016; 6: 1867-78.
17. Wan YW, Allen GI, Liu Z. TCGA2STAT: simple TCGA data access for integrated statistical analysis in R. Bioinformatics 2016; 32: 952-4.
18. Cerami E, Gao J, Dogrusoz U, et al. The cBio cancer genomics portal: an open platform for exploring multidimensional cancer genomics data. Cancer Discov 2012; 2: 401-4.
19. Huang da W, Sherman BT, Lempicki RA. Bioinformatics enrichment tools: paths toward the comprehensive functional analysis of large gene lists. Nucleic Acids Res 2009; 37: 1-13.
20. Louis DN, Perry A, Wesseling P, et al. The 2021 WHO classification of tumors of the central nervous system: a summary. Neuro Oncol 2021; 23: 1231-51.
21. Cheng Z, Dai Y, Pang Y, et al. High EGFL7 expression may predict poor prognosis in acute myeloid leukemia patients undergoing allogeneic hematopoietic stem cell transplantation. Cancer Biol Ther 2019; 20: 1314-8.
22. Papaioannou D, Shen C, Nicolet D, et al. Prognostic and biological significance of the proangiogenic factor EGFL7 in acute myeloid leukemia. Proc Natl Acad Sci U S A 2017; 114: E4641-7.
23. Yang C, Wang YL, Sun D, Zhu XL, Li Z, Ni CF. Increased expression of epidermal growth factor-like domain-containing protein 7 is predictive of poor prognosis in patients with hepatocellular carcinoma. J Cancer Res Ther 2018; 14: 867-72.
24. Oh J, Park SH, Lee TS, Oh HK, Choi JH, Choi YS. High expression of epidermal growth factor-like domain 7 is correlated with poor differentiation and poor prognosis in patients with epithelial ovarian cancer. J Gynecol Oncol 2014; 25: 334-41.
25. Li Z, Xue TQ, Yang C, Wang YL, Zhu XL, Ni CF. EGFL7 promotes hepatocellular carcinoma cell proliferation and inhibits cell apoptosis through increasing CKS2 expression by activating Wnt/beta-catenin signaling. J Cell Biochem 2018; 119: 10327-37.
26. Liu Q, Zhang J, Gao H, et al. Role of EGFL7/EGFR-signaling pathway in migration and invasion of growth hormone-producing pituitary adenomas. Sci China Life Sci 2018; 61: 893-901.
27. Nichol D, Shawber C, Fitch MJ, et al. Impaired angiogenesis and altered Notch signaling in mice overexpressing endothelial Egfl7. Blood 2010; 116: 6133-43.
28. Bill M, Pathmanathan A, Karunasiri M, et al. EGFL7 antagonizes NOTCH signaling and represents a novel therapeutic target in acute myeloid leukemia. Clin Cancer Res 2020; 26: 669-78.
29. Tang H, Xiao WR, Liao YY, et al. EGFL7 silencing inactivates the Notch signaling pathway; enhancing cell apoptosis and suppressing cell proliferation in human cutaneous melanoma. Neoplasma 2019; 66: 187-96.
30. Schmidt M, De Maziere A, Smyczek T, et al. The role of Egfl7 in vascular morphogenesis. Novartis Found Symp 2007; 283: 18-28.
31. Hanahan D, Weinberg RA. Hallmarks of cancer: the next generation. Cell 2011; 144: 646-74.
32. Yeung S, Smyczek T, Cheng J, et al. Abstract 3295: inhibiting vascular morphogenesis in tumors: EGFL7 as a novel therapeutic target. Cancer Res 2011; 71: 3295.
33. Garcia-Carbonero R, van Cutsem E, Rivera F, et al. Randomized phase II trial of parsatuzumab (anti-EGFL7) or placebo in combination with FOLFOX and bevacizumab for first-line metastatic colorectal cancer. Oncologist 2017; 22: 375.
34. von Pawel J, Spigel DR, Ervin T, et al. Randomized phase II trial of parsatuzumab (anti-EGFL7) or placebo in combination with carboplatin, paclitaxel, and bevacizumab for first-line nonsquamous non-small cell lung cancer. Oncologist 2018; 23: 654.
35. Bicker F, Schmidt MH. EGFL7: a new player in homeostasis of the nervous system. Cell Cycle 2010; 9: 1263-9.
36. Shahcheraghi SH, Tchokonte-Nana V, Lotfi M, Lotfi M, Ghorbani A, Sadeghnia HR. Wnt/beta-catenin and PI3K/Akt/mTOR signaling pathways in glioblastoma: two main targets for drug design: a review. Curr Pharm Des 2020; 26: 1729-41.
37. Bos JL, de Rooij J, Reedquist KA. Rap1 signalling: adhering to new models. Nat Rev Mol Cell Biol 2001; 2: 369-77.
38. Han J, Lim CJ, Watanabe N, et al. Reconstructing and deconstructing agonist-induced activation of integrin alphaIIbbeta3. Curr Biol 2006; 16: 1796-806.
39. Sayyah J, Bartakova A, Nogal N, Quilliam LA, Stupack DG, Brown JH. The Ras-related protein, Rap1A, mediates thrombin-stimulated, integrin-dependent glioblastoma cell proliferation and tumor growth. J Biol Chem 2014; 289: 17689-98.

JPTM
Journal of Pathology and Translational Medicine 2022; 56: 212-216
https://doi.org/10.4132/jptm.2022.05.02

ORIGINAL ARTICLE

Founder *BRCA1* mutations in Nepalese population

Anurag Mehta[1], Himanshi Diwan[1], Garima Gupta[2], Shrinidhi Nathany[1], Shalini Agnihotri[3], Surender Dhanda[1]

[1]Department of Laboratory, Molecular and Transfusion Services, Rajiv Gandhi Cancer Institute and Research Centre (RGCIRC), New Delhi; [2]Research Department, Indian Institute of Technology, New Delhi; [3]Department of Research, Rajiv Gandhi Cancer Institute and Research Centre (RGCIRC), New Delhi, India

Background: Founder mutation is a heritable genetic alteration observed with high frequency in a geographically and culturally isolated population where one or more ancestors becomes the forebearer of the altered gene. The current study reports two founder mutations in the *BRCA1* gene in the Nepalese people. **Methods:** Germline *BRCA* testing in all surface epithelial ovarian cancers and the selected case of breast, prostate, and pancreatic cancers has been the standard practice from 2016 to 2021. One thousand one hundred thirty-three probands were screened for germline *BRCA* variants by next generation sequencing. The variants were classified as per the American Society of Medical Genetics and Genomics recommendations. Pathogenic (class V) and likely pathogenic (class IV) were considered clinically relevant and utilized for cascade screening. **Results:** Nepalese population made up a subcohort of 5.12% (58/1,133) of probands tested for germline *BRCA1/2* variants. Twenty-seven of these 58 tested harbored pathogenic genetic alterations in *BRCA1/2* genes, with 23 being *BRCA1* mutant. Sixteen of 23 *BRCA1* mutant cases shared one common pathogenic mutation c.2214_2215insT (p.Lys739Ter) (NM_007294.4). Additionally, a second highly recurrent mutation in *BRCA1* gene c.5068A>T (p.Lys1690Ter) (NM_007294.4) was noted in six patients from this population. **Conclusions:** The overwhelming abundance of the above two variants in a geographically confined population confers these two genetic alterations a status of founder mutations amongst the people of Nepal. A more extensive population-based study to reaffirm these findings will help establish a dual site-specific germline testing similar to the "Multisite-3-assay" in Ashkenazi Jews as the primary screening tool, especially in a resource-constrained environment.

Key Words: *BRCA1*; *BRCA2*; Founder mutation; Nepal

Received: January 10, 2022 **Revised:** March 27, 2022 **Accepted:** May 2, 2022

Corresponding Author: Himanshi Diwan, MD, Department of Laboratory, Molecular and Transfusion Services, Rajiv Gandhi Cancer Institute and Research Centre, New Delhi 110085, India
Tel: +91-9413542252, Fax: +91-11-27051037, E-mail: himanshidiwan89@gmail.com

The founder effect amplifies a particular genotypic alteration' in a geographically or culturally confined population caused by several generations of interbreeding. Deleterious germline alterations of the *BRCA1* (OMIM *113705) and *BRCA2* (OMIM *600185) gene result in breast and ovarian cancer susceptibility. The lifetime risk of breast cancer is 55%–72% and 45%–69% in mutation carriers of *BRCA1* and *BRCA2* deleterious germline alterations, respectively [1-4]. Likewise, the risk of ovarian cancer is 39%–44% and 11%–17% in the *BRCA1* and *BRCA2* germline variants [1-4].

Germline alterations of *BRCA2* variants and, to a lesser extent, *BRCA1* variants in males predispose them to the breast [5] and prostate carcinoma [6-8]. The inherited pathogenic *BRCA1*/*BRCA2* variants also increase the risk of pancreatic cancers, albeit to a lower extent [9]. The prevalence of *BRCA1* or *BRCA2* mutations varies considerably between ethnic groups and geographical areas [10,11]. Founder *BRCA* mutations that are population-specific mutation(s) have been described in Iceland, Netherlands, Sweden, Norway, Germany, France, Spain, countries of central and eastern Europe, and Ashkenazi Jews [10,11]. The prevalence of *BRCA* mutation carriers in the general population is estimated at 1/800 to 1/1,000; however, the rate of occurrence of *BRCA* mutation increases several-fold in the population carrying founder mutation, for instance, the rate of a founder mutation in Ashkenazi Jews goes up to 1 in 40 [12,13]. Nepal is a Himalayan country with limited groupings of Tibeto-Burman and Indo-Aryan stock [14]. The geographically confined existence and restricted interaction with the outside world due to rugged terrain and the land-locked nature of the country provided an appropriate milieu for a deleterious mutation to breed, dominate and produce the founder effect. The current study reports the concentration of two particular *BRCA1*-specific vari-

pISSN 2383-7837
eISSN 2383-7845

ants in the Nepalese population tested for *BRCA1* and *BRCA2* deleterious mutations.

MATERIALS AND METHODS

Research setting and subjects

One thousand one hundred thirty-three patients diagnosed with breast/ovarian/prostate/pancreatic cancer and who fulfilled the *BRCA* testing criteria recommended by National Comprehensive Cancer Network (NCCN) were included in the study [15]. Each eligible subject was explicitly explained and counseled about the pros and cons of undergoing *BRCA* testing by the institutional genetic counselor, and informed written consent was obtained for testing and using the information for research. The included participants were screened for the mutations in the *BRCA* genes by next generation sequencing (NGS), and the large genomic rearrangements (Big Indels) were examined through Multiplex Ligation-dependent Probe Amplification (MLPA).

Isolation of DNA from blood, NGS, and data analysis

Genomic DNA was isolated from 2 mL of peripheral blood of the index case using the commercially available DNA isolation kit (Qiagen DNeasy Blood and Tissue kit, Qiagen NV, Hilden, Germany), following the manufacturer's instructions. Isolated DNA was quantified by Qubit 3.0 Fluorometric quantitation (Thermo Fisher Scientific, Waltham, MA, USA). NGS library was prepared manually with 10 ng of the isolated DNA using Oncomine BRCA assay – A328400 (Thermo Fisher Scientific) as detailed elsewhere [16]. Data generated from the runs was assessed for quality metrics on Torrent Suite Viewer (Ion Torrent Suite 5.10, Thermo Fisher Scientific) for parameters like the number of mapped reads, average base coverage depth, uniformity of coverage, coverage at 1×, 20×, and 100×, strand bias, end to end amplicon reads. Thresholds were employed as enunciated in The National Cancer Institute-Molecular Analysis for Therapy Choice (NCI-MATCH) trial [17]. Mapped reads of > 1,00,000 with 90% uniformity, average base coverage depth ≥ 100, and > 90% coverage at 100x were considered optimal for reporting though the base coverage and mapped reads were usually far more. The variants were classified according to the American Society of Medical Genetics and Genomics recommendations for standards of interpretation and reporting of sequence variations [18].

Cases tested negative for *BRCA1/BRCA2* mutations were further investigated for possible large genomic rearrangements (Big Indels) by MLPA assay described previously elsewhere [16].

Statistical analysis

Descriptive statistics were used to summarize the data. The data were analyzed statistically using SPSS ver. 23.0 (IBM Corp., Armonk, NY, USA). The statistical analysis comprised of calculating means and proportions. Appropriate tests of significance were applied, and a p-value of < .05 was considered significant.

RESULTS

One thousand one hundred thirty-three comprehensive *BRCA1* and *BRCA2* testing for different ethnic populations, comprising the Indian, Nepalese, Bangladeshi, Afghani, Kenyan, Iraqi, and the Myanmarese, were performed at the Molecular Diagnostic laboratory of a tertiary cancer care hospital in India. Of the 1,133 patients tested, 58 were Nepalese descent (5.1%) with a mean age of 47.3 years. Twenty-seven of the 58 Nepalese patients harbored pathogenic *BRCA1/BRCA2* genetic alteration, 16 breast, and 11 ovarian carcinoma cases. The mean age was 46.5 years in the Nepalese against 46.8 years in the rest of the cohort (95% confidence interval, –4.288 to 5.088; p = .867). Strikingly 23 of these 27 affected probands carried *BRCA1* mutation and, far more significantly, just two recurrent nonsense mutations, as shown in Table 1 below. Only one proband out of 23 with *BRCA1* inactivating alteration had a frameshift mutation outside these two genetic alterations. The two recurrent *BRCA1* alterations (c.2214_2215insT and c.5068A>T) were not found in any other ethnic population in the study (Fig. 1).

A *BRCA* mutation is seen in 27 Nepalese patients (27/58), ac-

Table 1. *BRCA1/BRCA2* variants encountered in 27 Nepalese patients in our study

Gene	Variant	NM transcript	No. of patients with the variant
BRCA1	c.2214_2215insT (p.Lys739Ter)	NM_007294.4	16
BRCA1	c.5131A>T(p.Lys1690Ter)	NM_007294.4	6
BRCA1	c.2157_2158insA (p.Glu720ArgfsTer6)	NM_007294.4	1
BRCA2	c.1303_1304insA(p.Arg435fs)	NM_000059.4	1
BRCA2	c.2808_2811 del ACAA (p.Ala938fs)	NM_000059.4	1
BRCA2	c.6270_6271delTA(p.His2090glnfsTer9)	NM_000059.4	1
BRCA2	c.7030delA(p.Ile2344TyrfsTer23	NM_000059.4	1

counting for 46.5% of tested patients. In comparison, *BRCA* mutation is observed in 227 non-Nepalese patients (227/1,075), accounting for 21.1%. The preceding emphasizes that *BRCA* mutation is significantly higher in the Nepalese population than in the non-Nepalese population (Fisher exact test, statistical value is <0.001). Also, *BRCA1* mutation was more common in Nepalese subcohort (23/58) than non-Nepalese subcohort (167/1,075) (Fisher exact test, statistical value is <0.001).

Of the total *BRCA* mutant cases, c.2214_2215insT is the most frequently observed *BRCA1* variant in the Nepalese population (16/27), constituting 59.2% of the total *BRCA* mutant cases followed by c.5068A>T (6/27) (22.2%). Thirty three point three three percentage of these 27 *BRCA* mutant cases constituted triple-negative breast carcinoma with 29.6% luminal type breast cancer and 25.9% high-grade serous ovarian carcinoma, as summarized in Table 2. Only 11 (11/27) *BRCA* mutant cases had a family history of breast/ovarian cancer.

One of the probands was tested for somatic alteration in the *BRCA1* gene in ovarian carcinoma, and p.Lys1690Ter was detected in the *BRCA1* gene at a high variant allele frequency (VAF). Combined with our observation of this variant being highly repetitive in the Nepalese people and the high VAF, a peripheral blood testing was done by an orthogonal method (site-specific Sanger sequencing) and confirmed as germline.

DISCUSSION

BRCA1 and *BRCA2* mutations show variable prevalence in different ethnic populations. The prevalence of *BRCA1/2* mutation in the general population is estimated to be around 1/800 to 1/1,000 or at the rate of 0.125 to 0.1%. In contrast, the prevalence increases several-fold in the geographically confined ethnic groups with founder mutation as in Ashkenazi Jews, where *BRCA* mutation is observed at a frequency of 2.5% [12,13]. The present study highlighted a similarly high incidence of *BRCA* mutation in the Nepalese patient cohort (46.5%), with the *BRCA1* gene altered in 39.6% and the *BRCA2* in 7%.

The discovery of a founder mutation in Ashkenazi Jews population paved the way to the "Multisite 3 assay" testing for *BRCA1* 185delAG, *BRCA1* 5382insC, and *BRCA2* 6174delT. The present study identifies two founder mutations in the *BRCA1* gene (c.2214_2215insT and c.5068A>T) in the Nepalese population. Significantly, none from the non-Nepalese cohort of the 1,075 probands tested positive for these two mutations. This exclusiveness and high frequency of just two variants in an ethnic group support the founder nature of these variants.

These two alterations account for 85.2% of all cases detected with germline *BRCA* mutation in the Nepalese subcohort, which is far higher than the three mutations that make up 73.2% of all germline *BRCA* mutations amongst Ashkenazi Jews [21].

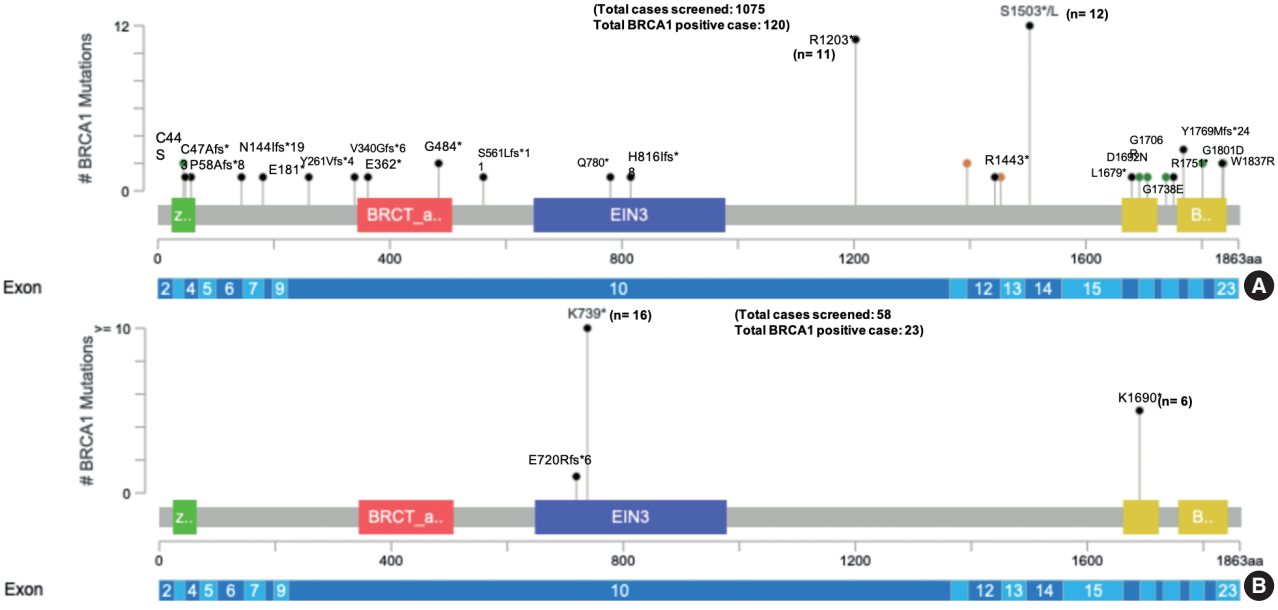

Fig. 1. The commonly encountered *BRCA1* mutations in the non-Nepalese population (A) and the Nepalese population (B) in the present study [19,20]. Note the dominance of just two genetic alterations in the Nepalese people and contrast to the widespread distribution of pathogenic mutation in the full-length *BRCA1* gene in the non-Nepalese population.

https://doi.org/10.4132/jptm.2020.05.02

Table 2. Clinical and morphological profile of *BRCA* mutant and *BRCA* wild-type cases in Nepalese and Non-Nepalese subcohorts

	BRCA mutant Nepalese cohort (n=27)	*BRCA* wild Nepalese cohort (n=31)	*BRCA* mutant non-Nepalese subcohort (n=227)	*BRCA* wild non-Nepalese cohort (n=848)
Age (yr)				
Mean[a]	46.5	51.6	46.8	51.6
Median (range)	44.5 (32–76)	52 (27–72)	44.5 (29–66)	52 (29–86)
Ovarian carcinoma with the morphology of HGSC	7 (25.9)	10 (32.5)	90 (39.6)	160 (18.8)
TNBC cases	9 (33.3)	11 (35.5)	96 (42.3)	300 (35.4)
Luminal type breast carcinoma cases	8 (29.6)	6 (19.3)	23 (10.1)	207 (24.4)
HER-2 enriched breast carcinoma	1 (3.7)	1 (3.2)	2 (0.1)	26 (3.1)
Cases with ovarian HGSC and TNBC	1 (3.7)	0	10 (4.4)	2 (0.02)
Cases with endometrioid ovarian carcinoma and TNBC	0	0	0	2 (0.02)
Cases with mixed ovarian carcinoma	0	0	2 (0.1)	0
Cases with ovarian low-grade serous carcinoma	0	0	0	2 (0.02)
Cases with ovarian endometrioid carcinoma	0	2 (6.4)	0	5 (0.6)
Prostate carcinoma cases	0	1 (3.2)	2 (0.1)	62 (7.3)
Pancreatic carcinoma cases	0	0	2 (0.1)	82 (9.7)
Cases with positive family history	11 (40.71)	4 (12.9)	54 (23.8)	43 (5.1)

Values are presented as number (%) unless otherwise indicated.
HGSC, high-grade serous carcinoma; TNBC, triple-negative breast carcinoma; HER-2, human epidermal growth factor receptor 2.
[a]p=.867; 95% confidence interval, –4.288 to 5.088 (Nepalese vs. non-Nepalese *BRCA* mutant population).

Such high occurrence of just two mutations opens up the possibility that, like in Ashkenazi Jews, the first tier of testing can be reduced to dual site-specific testing for *BRCA1* c.2214_2215insT and *BRCA1* c.5068A>T for the Nepalese people. Failing to identify one of the two nonsense mutations shall prompt further testing by a more extensive NGS-based assay.

One of the index cases of ovarian carcinoma screened for somatic *BRCA* testing had c. 5068A>T mutation in *BRCA1* gene at a high VAF and confirmed as germline mutation on orthogonal testing by site-specific Sanger sequencing on peripheral blood. Further, even when detected in tumor tissue, these two mutations shall get full consideration of germline origin, and germline testing should follow.

A positive family history of breast/ovarian carcinoma was found in 40.71% of BRCA mutant cases in the Nepalese subcohort, clearly far more common than non-Nepalese subcohort (23.8%). The observation of a significantly high *BRCA* mutant population sans a family history of cancer predisposition thus mandates testing all patients for *BRCA* irrespective of the family history as emphasized by the NCCN guidelines [15].

c.2214_2215insT is located at chr17:41245334; exon 10 of 24 results in a frameshift that generates a new stop codon in place of Lysine, either causing the formation of a truncated BRCA1 protein or lack of it due to Nonsense-mediated mRNA decay [22,23]. Likewise, c.5068A>T is located at chr17:41219631; exon 17 of 23; position 57 of 78 (on assembly GRCh37) [22] also forms a premature stop codon in place of Lysine with similar effects as for the other founder mutation. These mutations were reported by the first author in the LOVD Database [24]. The variants above are not reported in the population databases (ExAC) [25]. The Clinvar has annotated these variants to be pathogenic [26].

The present hospital-based study on cancer patients acting as probands reveals founder mutations in the Nepalese people. A more extensive population-based study confirming their high-frequency and lack of other randomly distributed deleterious mutations in *BRCA* genes shall permit the development of a dual site-specific *BRCA1* testing as the first-line screen for probands and kindred. Such a strategy shall prevent the need for NGS, drastically reduce the cost of *BRCA* testing, allow deeper reach, especially in a resource-constrained setting. This strategy shall also provide a fillip to a preventive approach towards cancer.

BRCA1 c.2214_2215insT and *BRCA1* c. 5068A>T are the two germline alterations in the Nepalese population with founder effect and incidence of 85.2%. Further confirmation of our findings by a more extensive population-based study shall allow developing a limited dual site-specific germline test as a first-line screening tool, especially in a resource-restricted environment with limited accessibility to NGS. Additionally, Founder mutations can help conclude or rule out an anthropological hypothesis and has immense research potential in that field.

Ethics Statement

This study was approved by the institutional review board (Rajiv Gandhi

Cancer Institute and Research Center), vide the ethical approval letter number RGCIRC/IRB-BHR/41/2020. The study was conducted per the Declaration of Helsinki. Informed written consent was obtained for testing and using the information for research.

Availability of Data and Material

The datasets generated or analyzed during the study are available from the corresponding author on reasonable request.

Code Availability

Not applicable.

ORCID

Anurag Mehta	https://orcid.org/0000-0001-6517-3664
Himanshi Diwan	https://orcid.org/0000-0002-4305-0951
Garima Gupta	https://orcid.org/0000-0001-7867-1072
Shrinidhi Nathany	https://orcid.org/0000-0001-6006-6309
Shalini Agnihotri	https://orcid.org/0000-0003-0762-6463
Surender Dhanda	https://orcid.org/0000-0003-2388-7452

Author Contributions

Conceptualization: AM. Data curation: GG, HD, SA, SN. Formal analysis: AM, GG, HD, SN. Investigation: AM, HD, GG, SN, SA, SD. Methodology: AM. Project administration: AM. Resources: SD. Supervision: AM. Visualization: HD, SN. Writing—original draft: GG, HD. Writing—review & editing: AM.

Conflicts of Interest

The authors declare that they have no potential conflicts of interest.

Funding Statement

No funding to declare.

References

1. Kuchenbaecker KB, Hopper JL, Barnes DR, et al. Risks of breast, ovarian, and contralateral breast cancer for *BRCA1* and *BRCA2* mutation carriers. JAMA 2017; 317: 2402-16.
2. Antoniou A, Pharoah PD, Narod S, et al. Average risks of breast and ovarian cancer associated with *BRCA1* or *BRCA2* mutations detected in case Series unselected for family history: a combined analysis of 22 studies. Am J Hum Genet 2003; 72: 1117-30.
3. Chen S, Parmigiani G. Meta-analysis of BRCA1 and BRCA2 penetrance. J Clin Oncol 2007; 25: 1329-33.
4. Mehta A. *BRCA1* and *BRCA2* mutations in ovarian cancer. J Curr Oncol 2018; 1: 1-4.
5. Tai YC, Domchek S, Parmigiani G, Chen S. Breast cancer risk among male *BRCA1* and *BRCA2* mutation carriers. J Natl Cancer Inst 2007; 99: 1811-4.
6. Levy-Lahad E, Friedman E. Cancer risks among *BRCA1* and *BRCA2* mutation carriers. Br J Cancer 2007; 96: 11-5.
7. Oh M, Alkhushaym N, Fallatah S, et al. The association of *BRCA1* and *BRCA2* mutations with prostate cancer risk, frequency, and mortality: a meta-analysis. Prostate 2019; 79: 880-95.
8. Nyberg T, Frost D, Barrowdale D, et al. Prostate cancer risks for male *BRCA1* and *BRCA2* mutation carriers: a prospective cohort study. Eur Urol 2020; 77: 24-35.
9. Hu C, Hart SN, Polley EC, et al. Association between inherited germline mutations in cancer predisposition genes and risk of pancreatic cancer. JAMA 2018; 319: 2401-9.
10. Nelson HD, Fu R, Goddard K, et al. Risk assessment, genetic counseling, and genetic testing for *BRCA*-related cancer: systematic review to update the U.S. Preventive Services Task Force Recommendation. Report AHRQ Publication No. 12-05164-EF-1. Portland: Oregon Health and Science University, 2013.
11. Hall MJ, Reid JE, Burbidge LA, et al. *BRCA1* and *BRCA2* mutations in women of different ethnicities undergoing testing for hereditary breast-ovarian cancer. Cancer 2009; 115: 2222-33.
12. Balmana J, Diez O, Rubio IT, Cardoso F; ESMO Guidelines Working Group. BRCA in breast cancer: ESMO clinical practice guidelines. Ann Oncol 2011; 22 Suppl 6: vi31-4.
13. Rosenthal E, Moyes K, Arnell C, Evans B, Wenstrup RJ. Incidence of *BRCA1* and *BRCA2* non-founder mutations in patients of Ashkenazi Jewish ancestry. Breast Cancer Res Treat 2015; 149: 223-7.
14. Yadava YP. Linguistic diversity in Nepal: perspectives on language policy. In: International Seminar on Constitutionalism and Diversity in Nepal; 2007 Aug 22-24; Kathmandu, Nepal.
15. Daly MB, Pilarski R, Yurgelun MB, et al. NCCN guidelines insights: genetic/familial high-risk assessment: breast, ovarian, and pancreatic, version 1.2020. J Natl Compr Canc Netw 2020; 18: 380-91.
16. Mehta A, Vasudevan S, Sharma SK, et al. Germline *BRCA1* and *BRCA2* deleterious mutations and variants of unknown clinical significance associated with breast/ovarian cancer: a report from North India. Cancer Manag Res 2018; 10: 6505-16.
17. Lih CJ, Harrington RD, Sims DJ, et al. Analytical validation of the next-generation sequencing assay for a nationwide signal-finding clinical trial: molecular analysis for therapy choice clinical trial. J Mol Diagn 2017; 19: 313-27.
18. Richards S, Aziz N, Bale S, et al. Standards and guidelines for the interpretation of sequence variants: a joint consensus recommendation of the American College of Medical Genetics and Genomics and the Association for Molecular Pathology. Genet Med 2015; 17: 405-24.
19. Gao J, Aksoy BA, Dogrusoz U, et al. Integrative analysis of complex cancer genomics and clinical profiles using the cBioPortal. Sci Signal 2013; 6: pl1.
20. Cerami E, Gao J, Dogrusoz U, et al. The cBio cancer genomics portal: an open platform for exploring multidimensional cancer genomics data. Cancer Discov 2012; 2: 401-4.
21. Tonin P, Weber B, Offit K, et al. Frequency of recurrent *BRCA1* and *BRCA2* mutations in Ashkenazi Jewish breast cancer families. Nat Med 1996; 2: 1179-83.
22. Kopanos C, Tsiolkas V, Kouris A, et al. VarSome: the human genomic variant search engine. Bioinformatics 2019; 35: 1978-80.
23. Schwarz JM, Cooper DN, Schuelke M, Seelow D. MutationTaster2: mutation prediction for the deep-sequencing age. Nat Methods 2014; 11: 361-2.
24. Fokkema IF, Taschner PE, Schaafsma GC, Celli J, Laros JF, den Dunnen JT. LOVD v.2.0: the next generation in gene variant databases. Hum Mutat 2011; 32: 557-63.
25. Karczewski KJ, Francioli LC, Tiao G, et al. The mutational constraint spectrum quantified from variation in 141,456 humans. Nature 2020; 581: 434-43.
26. Landrum MJ, Lee JM, Benson M, et al. ClinVar: improving access to variant interpretations and supporting evidence. Nucleic Acids Res 2018; 46: D1062-7.

JPTM
Journal of Pathology and Translational Medicine 2022; 56: 217-224
https://doi.org/10.4132/jptm.2022.03.15

CASE STUDY

Clinically undetected plasmacytoid urothelial carcinoma of the urinary bladder with non-mass-forming metastases in multiple organs: an autopsy case

Yuya Asano[1,2], Kosuke Miyai[2,3], Shinya Yoshimatsu[4], Makoto Sasaki[5], Katsunori Ikewaki[5], Susumu Matsukuma[2,4]

[1]National Defense Medical College, Saitama;
[2]Department of Pathology and Laboratory Medicine, National Defense Medical College, Saitama;
[3]Department of Pathology, Japan Self-Defense Forces Central Hospital, Tokyo;
[4]Department of Laboratory Medicine, National Defense Medical College Hospital, Saitama;
[5]Department of Anti-Aging and Vascular Medicine, National Defense Medical College, Saitama, Japan

This case report outlines a clinically undetected urinary bladder plasmacytoid urothelial carcinoma (PUC) with multiple metastases detected at autopsy. An 89-year-old man presented with edema in the lower limbs. Pleural fluid cytology revealed discohesive carcinomatous cells, although imaging studies failed to identify the primary site of tumor. The patient died of respiratory failure. Autopsy disclosed a prostate tumor and diffusely thickened urinary bladder and rectum without distinct tumorous lesions. Histologically, the tumor consisted of acinar-type prostate adenocarcinoma with no signs of metastasis. Additionally, small, plasmacytoid tumor cells were observed in the urinary bladder/rectum as isolated or small clustering fashions. These metastasized to the lungs, intestine, generalized lymph nodes in a non-mass-forming manner. Combined with immunohistochemical studies, these tumor cells were diagnosed PUC derived from the urinary bladder. Both clinicians and pathologists should recognize PUC as an aggressive histological variant, which can represent a rapid systemic progression without mass-forming lesions.

Key Words: Urothelial carcinoma; Plasmacytoid variant; Urinary bladder; Autopsy; Cancer of unknown primary

Received: December 13, 2021 **Revised:** February 21, 2022 **Accepted:** March 15, 2022
Corresponding Author: Kosuke Miyai, MD, PhD, Department of Pathology, Japan Self-Defense Forces Central Hospital, 1-2-24 Ikejiri, Setagaya-ku, Tokyo 154-8532, Japan
Tel: +81-3-3411-0151, Fax: +81-4-2996-5193, E-mail: mykusu228@nifty.com

Plasmacytoid urothelial carcinoma (PUC) was first reported in 1991 as a rare histologic variant of urothelial carcinoma (UC) characterized by isolated tumor cells that morphologically resemble plasma cells with eccentric nuclei and eosinophilic cytoplasm [1-3]. In addition to its high risk of peritoneal spread, positive margins at cystectomy, and tumor recurrence, PUC has been recognized as an independent prognostic factor for poor prognosis in patients with urinary bladder carcinoma [4]. PUC may pose a significant diagnostic problem, particularly when it occurs in its exclusively pure or predominant pattern in a limited biopsy, cytology, or transurethral resection specimen. Moreover, reflecting an infiltration pattern arranged as diffuse, thick sheets, cords, or nests of small discohesive tumor cells without forming a focal mass [5], it is challenging to detect PUC via imaging procedures [6,7]. Initial manifestations of PUC may include distant metastasis or peritoneal dissemination [8]. Thus, a generalized histological analysis is required to precisely assess the spreading/metastasis of the tumor. However, there are only a limited number of autopsy case reports on PUC [7-10]. Herein, we describe a case of urinary bladder PUC that was initially recognized as a "carcinoma of unknown origin" through pleural fluid cytology, but an autopsy revealed extensive locoregional spreading and distant metastasis of the tumor.

CASE REPORT

An 89-year-old Japanese man was admitted to our hospital with severely edematous lower limbs. The patient was diagnosed with prostate cancer at the age of 80 and received hormone therapy for 8 years. Because of atypical urothelial cells in urine smear

pISSN 2383-7837
eISSN 2383-7845

cytology, he underwent transurethral resection of bladder tumor (TURBT) 1 year and 4 months before admission, that revealed UC in situ with a stromal microinvasion (Fig. 1A). A follow-up abdominal computed tomography (CT) scan taken 3 months before admission showed thickening of the rectal wall; however, no significant deformation was found in the urinary bladder. At the time of admission, a high level of carbohydrate antigen 19-9 (2,771 U/mL; normal, < 37 U/mL) was detected in serum, whereas levels of carcinoembryonic antigen and prostate-specific antigen (PSA) were normal.

Following admission, bilateral pleural effusion progressed, and pleural fluid smear/cell block cytology revealed discohesive carcinomatous cells (Fig. 1B) that were immunoreactive for cytokeratin (CK) 7 and CK20 and negative for PSA and thyroid transcription factor-1. Various organs, including the stomach, bile duct, pancreas, and urinary tract, were speculated to be the origin of tumor. However, fluorodeoxyglucose positron emission tomography/CT scan taken 20 days after admission failed to detect any primary lesions (i.e., carcinoma of unknown origin). The patient's respiratory function gradually deteriorated because of aspiration pneumonia. The patient was treated with only palliative therapy and died 27 days after admission. An autopsy was performed on the same day (postmortem, 7 hours).

Grossly, a prostate tumor measuring 3.5 cm in the largest diameter, protruding into the urethra, was detected. Around this tumor, the rectal wall and posterior wall of the urinary bladder were diffusely thickened, but no other mass-forming lesions were observed in the whole body examined (Fig. 1C, D). Histologically, the prostate tumor showed fused-gland features of acinar-type adenocarcinoma, Gleason Grade Group 4, extending to the rectal wall and urethra. Examination of the thickened urinary bladder wall revealed diffuse infiltration of discohesive,

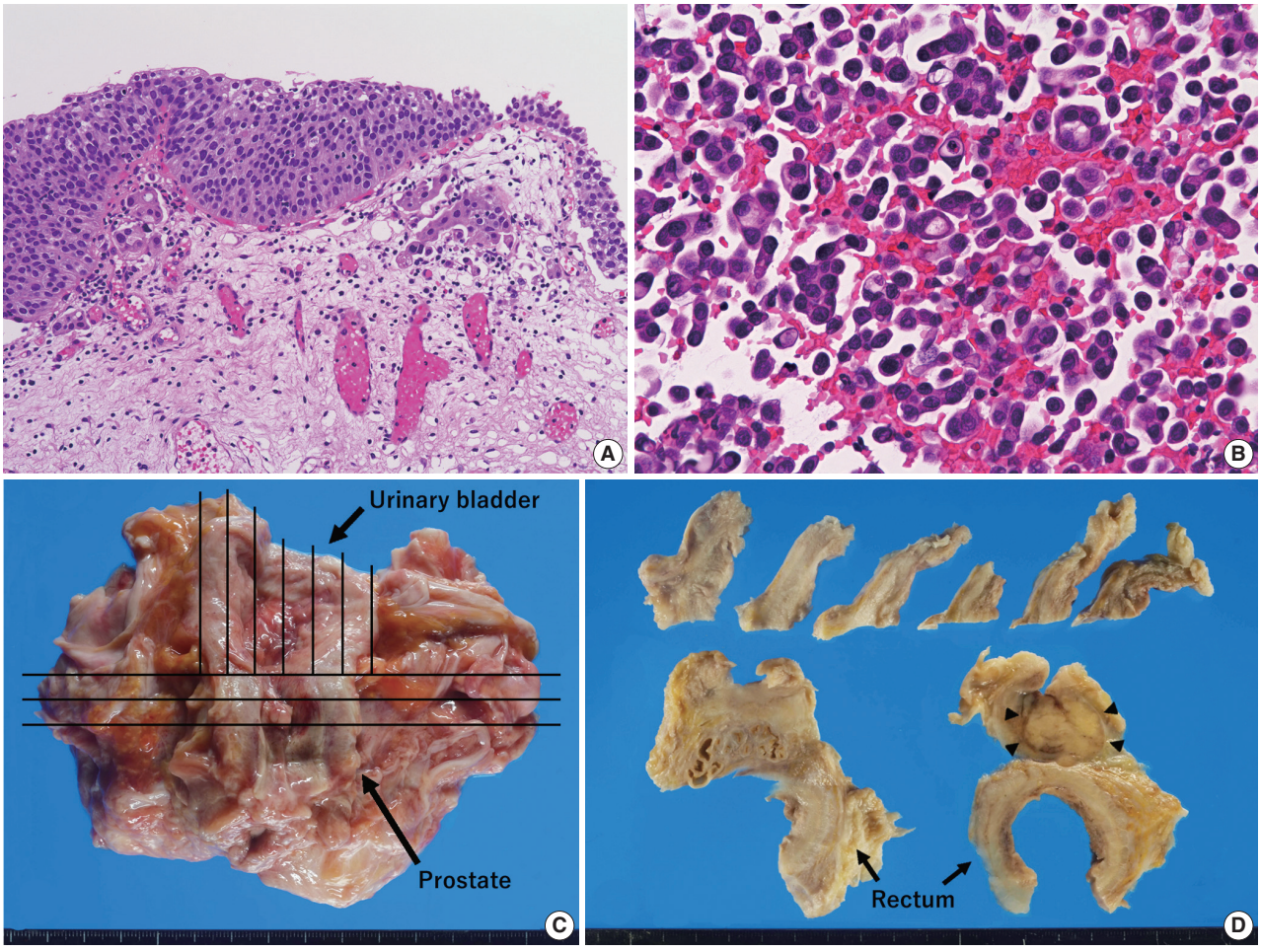

Fig. 1. Premortem microscopic findings. (A) Transurethral resection specimen showing urothelial carcinoma in situ with a stromal microinvasion. (B) Discohesive carcinomatous cells with signet-ring or plasmacytoid features in the cell block from pleural fluid was noted. Gross examination at autopsy. (C) Anterior view of the gross description of the pelvic organs. (D) A prostate tumor protruding into the urethra is detected (arrowheads). Around this tumor, the rectal wall and posterior wall of the urinary bladder are diffusely thickened.

https://doi.org/10.4132/jptm.2022.03.15

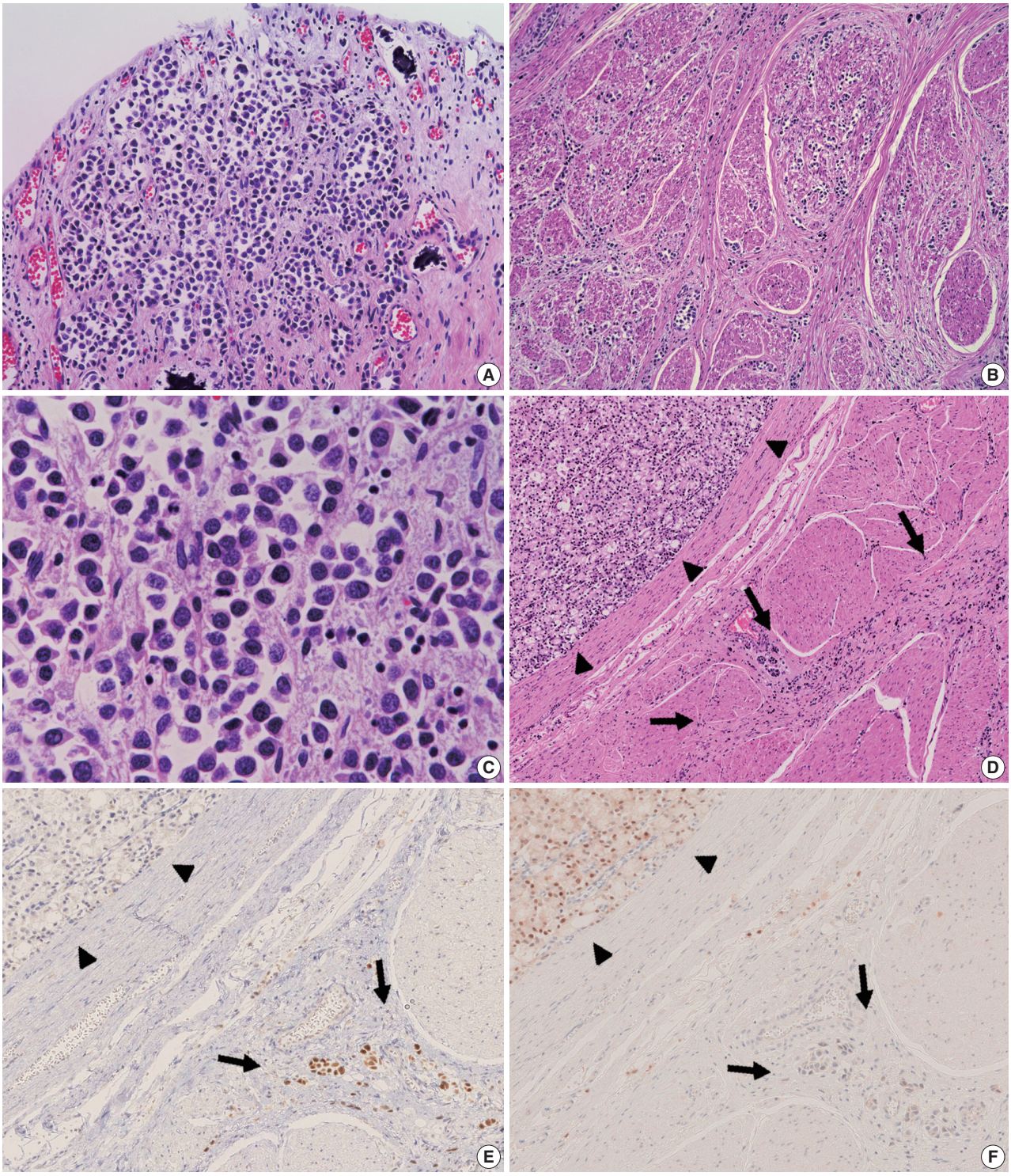

Fig. 2. Microscopic findings. (A, B) The thickened lesion in the urinary bladder wall, showing diffuse infiltration of discohesive, plasmacytoid tumor cells in a single file pattern and small nests in the edematous lamina propria (A) and muscularis propria (B). (C) The plasmacytoid tumor cells consisted of oval-to-round, eccentrically located nuclei and abundant densely eosinophilic and occasionally vacuolated/signet-ring-cell like cytoplasm. (D) Massive tumor extension into the thickened rectal wall, seminal vesicles, and periprostatic tissue (arrows) close to the prostate cancer (arrowheads) is observed. (E, F) Diffuse positive immunoreactivity for GATA binding protein 3 (E) and negative immunoreactivity for NK3 homeobox1 (F) in the plasmacytoid tumor cells (arrows, both E and F), and vice versa, in the prostate cancer cells (arrowheads, both E and F) is observed.

plasmacytoid tumor cells in a single file pattern and small nests in the edematous lamina propria (Fig. 2A), muscularis propria (Fig. 2B), and perivesical adipose tissue. The individual tumor cells displayed oval-to-round eccentrically located nuclei and abundant densely eosinophilic and occasionally vacuolated/signet-ring-cell-like cytoplasm (Fig. 2C). The tumor was exposed to the serosal surface of the urinary bladder and massively extended into the thickened rectal wall, seminal vesicles, and periprostatic tissue, surrounding the prostate cancer (Fig. 2D). Autopsy failed to detect any colorectal intramucosal lesions of the tumor.

Characteristics of primary antibodies used in immunohistochemical analysis are summarized in Table 1. Immunohistochemically, the plasmacytoid tumor cells were diffusely positive for CK7, CK20, p63, and GATA binding protein 3 (GATA3) and negative for NK3 homeobox 1 (Nkx3.1), while the opposite was observed in the prostate cancer cells (i.e., Nkx3.1+ and CK7/CK20/p63/GATA3-) (Fig. 2E, F). The plasmacytoid tumor cells were also negative for CDX2 and nuclear β-catenin. Immunoreactivity for E-cadherin was retained in the plasmacytoid tumor cells, and that for human epidermal growth factor receptor 2 (HER2) had a score of 2+ (Fig. 3A). PathVysion HER2 DNA probe kit (HER2 SpectrumOrange/CEP17 SpectrumGreen DNA probes, Abbott Molecular, Downers Grove, IL, USA) was used for fluorescence in situ hybridization analysis, as described previously [11]. Hybridization was performed between the denatured probes and denatured DNA on tissue sections at 37°C for 14–18 hours. The sections were counterstained with 4,6-diamidino-2-phenylindone. The number of fluorescence signals from both centromeric region of chromosome 17 (*CEP17*) and *HER2* probes in the 40 interphase tumor cell nuclei was counted. The *HER2*/*CEP17* ratio and mean *HER2* signal were less than 2.0 and 4.0, respectively (Fig. 3B). PUC in the present case showed no *HER2* amplification. Based on these findings, the urinary bladder tumor was diagnosed as PUC that histologically involved an area measuring 10×7 cm.

Non-mass-forming multiple metastases of PUC were found in the lungs (bilateral), jejunum, sigmoid colon, sacrum, and generalized lymph nodes and in peritoneal and pleural disseminations, with or without lymphatic invasion (Fig. 3C–E). No features of conventional UC were found in the primary and metastatic sites. Autopsy failed to detect distant metastases of the prostate cancer.

DISCUSSION

Emerging evidence demonstrates that PUC is associated with adverse clinicopathological features, advanced stage at cystectomy, and poor prognosis [3,12-16]. In a recent meta-analysis of eight case series, PUC of the bladder showed a higher frequency of pathological stage ≥T3, increased risk of perivesical/ureteral margin positivity, and lymph node metastasis, and elevated overall mortality rate compared to conventional UC [4]. While early tumor detection and accurate evaluation of tumor spreading are important for proper clinical management of PUC [3], its unique non-mass-forming progression makes it difficult to diagnose. Some reports indicate that PUCs tend to invade along the perirectal/perivesical fascial plane [12,15,16], which is usually challenging to detect using conventional CT/magnetic resonance imaging [6]. In the present case, autopsy showed an extensive local spreading to the perivesical fascial plane and generalized metastases of the tumor; however, it could not be detected via clinical imaging. PUC of the bladder is a rare disease; most histological data in previous case series were only from TURBT or

Table 1. Characteristics of primary antibodies in immunohistochemical analysis

Protein	Clone	Manufacturer, catalog number	Host	Antigen retrieval	Dilution
β-catenin	Monoclonal, β-catenin-1	Dako, Glostrup, Denmark, M3539	Mouse	Boil, 95°C 30 min, EDTA pH=9	1:200
CK7	Monoclonal, OV-TL 12/30	Dako, M7018	Mouse	Proteinase K, 37°C 15 min	1:200
CK20	Monoclonal, Ks20.8	Dako, M7019	Mouse	Proteinase K, 37°C 15 min	1:100
D2-40	Monoclonal, D2-40	Dako, M3619	Mouse	None	1:50
E-cadherin	Monoclonal, 4A2c7	Invitrogen, Carlsbad, CA, USA, 18-0223	Mouse	Boil, 95°C 30 min, EDTA pH=9	1:100
GATA3	Monoclonal, L50-823	Biocare Medical, Concord, CA, USA, 1-800-799-9499	Mouse	Boil, 95°C 30 min, EDTA pH=9	1:300
HER2	Polyclonal	Dako, K5204 (HercepTest II)	Rabbit	Boil, 95°C 40 min, specialized buffer	Ready-to-use
Nkx3.1	Monoclonal, EP356	Nichirei, Tokyo, Japan, 418281	Rabbit	Autoclave, 121°C 10 min, EDTA pH=9	Ready-to-use
p63	Monoclonal, 7JUL	Leica Biosystems, Newcastle Upon Tyne, UK, NCL-p63	Mouse	Boil, 95°C 30 min, EDTA pH=9	1:50
PSA	Monoclonal, ER-PR8	Dako, M0750	Mouse	None	1:100
TTF-1	Monoclonal, SPT24	Novocastra, Newcastle Upon Tyne, UK, NCL-TTF-1	Mouse	Boil, 95°C 30 min, EDTA pH=9	1:200

EDTA, ethylenediaminetetraacetic acid; CK, cytokeratin; GATA3, GATA binding protein 3; HER2, human epidermal growth factor receptor 2; Nkx3.1, NK3 homeobox 1; PSA, prostate-specific antigen; TTF-1, thyroid transcription factor-1.

https://doi.org/10.4132/jptm.2022.03.15

cystectomy specimens. We suggest that the lack of data regarding precise histological evaluation of such generalized disease (i.e., autopsy study) is one of the major factors that makes clinical/imaging analysis of PUC difficult.

Only four other autopsy cases of PUC have been reported to date [7-10]. The clinicopathological features of these cases (cases

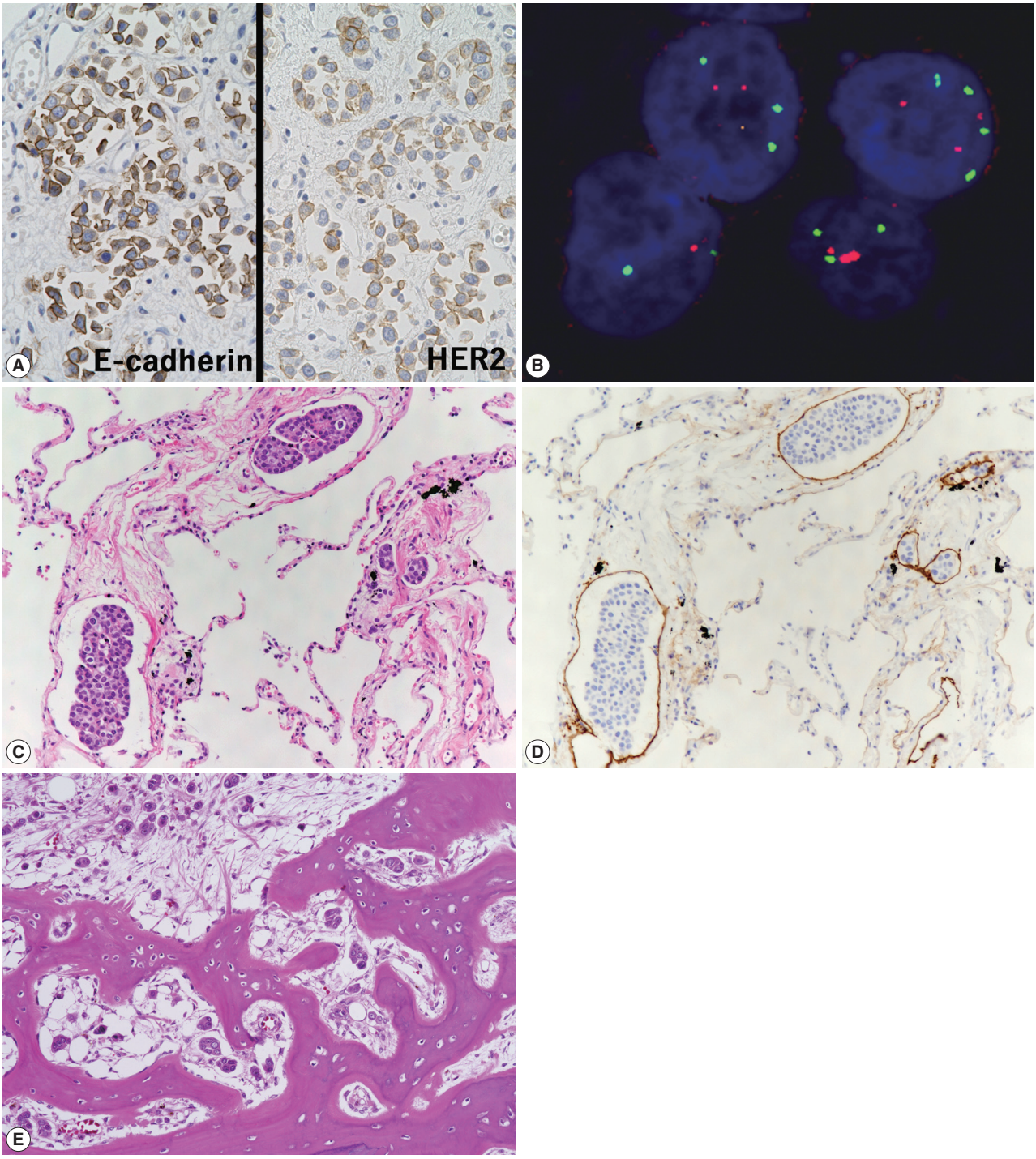

Fig. 3. (A) Retained immunoreactivity for E-cadherin and moderate-intensity immunoreactivity for human epidermal growth factor receptor 2 (HER2) were noted in cancer cells. (B) Fluorescence in situ hybridization for the copy number of *HER2* gene showing no *HER2* amplification in cancer cells. DAPI-counterstained interphase nuclei are observed; the red and green signals indicate the *HER2* and *CEP17* signals, respectively. (C) Metastatic small clusters or isolated cancer cells in the lungs. (D) Immunostaining for D2-40 highlighting lymphatic invasion of cancer cells. (E) Metastatic cancer cells in the sacral bone marrow.

https://jpatholtm.org/

Table 2. Clinicopathological features of the autopsy cases with plasmacytoid urothelial carcinoma

Case No.	Author	Age (yr)/ Sex	Primary tumor size/ Location	Operative procedure	Chemoradiotherapy	% PUC/ Total UC	Immunohistochemical analysis					Direct invasion	Distant metastasis	Prognosis
							CK7	CK20	E-cad	GATA3	HER2			
1	Simon et al. [7]	65/M	7 cm per gross/ bladder	TURBT and cysto-prostatectomy	MVAC (3 cycles), Atezolizumab	100	+	+	−	+	N/A	Rectal wall	Lungs, pleura, diaphragm, small/large intestine, gallbladder, thoracic and abdominal lymph nodes	DOD 9 mo[a]
2	Kohada et al. [8]	75/F	N/A/bladder	TURBT	GC (2 cycles), Pembrolizumab	N/A	−	−	+	+	+	Uterus, retroperitoneum	None	DOD 4 mo[a]
3	Ando et al. [9]	83/M	N/A/bladder	Nephro-ureterectomy	None	N/A	N/A	N/A	−	N/A	N/A	Rectal wall, prostate gland	Peritoneal dissemination and retroperitoneal lymphatic permeation	DOD 2 mo[b]
4	Tanaka et al. [10]	85/M	8×6 cm[c]/ bladder	TURBT	None	N/A	+	+	−	N/A	N/A	Prostate gland	Liver, spleen, kidneys, adrenal glands, bone marrow	DOC (AMI) 37 days[a]
5	Present case	89/M	10×7 cm[c]/ bladder	TURBT	None	100	+	+	+	+	−	Rectal wall, seminal vesicle, paraprostatic tissue	Lungs, right kidney and ureter, left testis, pancreas, liver hilum, right adrenal gland, small/large intestine, pleural/peritoneal dissemination, retroperitoneal tissue, bone marrow, thoracic and abdominal lymph nodes	DOD 1 year and 5 mo[a]

PUC, plasmacytoid urothelial carcinoma; UC, urothelial carcinoma; CK, cytokeratin; E-cad, E-cadherin; HER2, human epidermal growth factor receptor 2; M, male; TURBT, transurethral resection of bladder tumor; MVAC, methotrexate, vinblastine, doxorubicin and cisplatin; N/A, not available; DOD, death of disease; F, female; GC, gemcitabine and cisplatin; DOC, death of other cause; AMI, acute myocardial infarction.
[a]Period after TURBT; [b]Period after para-duodenum tissue biopsy, by which carcinoma of unknown origin was firstly detected; [c]At the time of autopsy.

https://doi.org/10.4132/jptm.2022.03.15

1–4) and the present case (case 5) are summarized in Table 2. In all five cases, the primary tumor location was the bladder, and four patients were men. The percentage of PUC in the total UC area was described in only one case (case 1); the tumor was a pure type PUC, similar to that in the present case. Immunohistochemically, three of four cases (75%) were positive for CK7 and CK20, three of three cases (100%) were positive for GATA3, and loss of E-cadherin staining was detected in three of five cases (60%). In cases 1, 2, and 4, PUC was diagnosed using TURBT specimens. In the present case, TURBT revealed only a minor amount of stromal invasion of cancer cells. However, no obvious detrusor muscle was detected in the whole specimen, indicating a high risk of residual tumor. In this context, if re-TURBT had been performed, the PUC invading the muscle layer might have been disclosed. All cases showed direct invasion of tumor to adjacent organs, and cases 1 and 3 showed progression along the perirectal fascial plane, similar to that seen in the present case. In all cases except case 2, multiple distant metastases were found in the intra-abdominal organs (cases 1, 3–5), thoracic cavity (cases 1 and 5), and bone (cases 4 and 5). PUC was the main cause of death in all cases except for case 4 (myocardial infarction), and all five patients died within 2 years from the initial diagnosis of the tumor.

In the present case, although plasmacytoid carcinomatous cells were detected during pleural fluid cytology, we could not consider those in relation to the conventional UC in the previous TURBT specimens. PUC is often observed at advanced stages with metastasis [6], and its differential diagnosis includes a wide variety of diseases such as signet-ring cell adenocarcinoma (especially colorectal origin due to the perirectal spreading pattern of PUC), carcinoma with rhabdoid features, lymphoma/myeloma, and melanoma [13]. The first case of PUC was also identified in a bone metastatic lesion and was reported to mimic a myeloma [1]. In such situations, the possibility of PUC should be recognized initially, and effective immunohistochemical analysis should be performed. GATA3 is the most sensitive marker for tumors derived from urinary epithelium, and CDX2/β-catenin might be useful to distinguish PUC from colorectal signet-ring adenocarcinoma [17]; hence, these markers should have been included in our immunohistochemical panel for pleural fluid cytology examination for diagnosing the present case. Although loss of E-cadherin expression is observed in 70%–80% of cases and is thought to be one of the diagnostic hallmarks of PUC [18], its frequency was found to be 57% in another case series [17]. Retention of cytoplasmic expression of E-cadherin is not sufficient to rule out PUCs.

Although there was moderate immunoreactivity for *HER2*, no gene amplification was detected in the tumor cells in the present case. A recent molecular study of 1005 UC cases revealed that *HER2* gene amplification was found in approximately 10% of the cases, and concluded that anti-HER2 antibody is expected to be applied to the novel standard treatment of UC [19]. Interestingly, *HER2* amplification is one of the features characterizing "luminal unstable" type in the recent consensus molecular classification, which is enriched in plasmacytoid histology of the bladder UC [20]. Further investigations directed towards HER2 status and the effectiveness of HER2-targeted therapy for this aggressive variant of UC are required.

In summary, we described a case of clinically undetected PUC that was initially identified as a "cancer of unknown primary" through pleural fluid cytology but autopsy revealed broad local spreading and multiple organ metastasis. This rare form of UC should be considered in the differential diagnosis of aggressive occult tumors. Data accumulation and analysis of additional autopsy case reports are essential to clarify the peculiar non-mass-forming spread of PUC, which can help in its early detection.

Ethics Statement

This single case report in exempted submission to Institutional Review Board and subsequent informed consent by the National Defense Medical College, Tokorozawa, Japan (Registration number, 4007; decision date, August 8, 2021).

Availability of Data and Material

The datasets generated or analyzed during the study are available from the corresponding author on reasonable request.

Code Availability

Not applicable.

ORCID

Yuya Asano https://orcid.org/0000-0002-0136-9905
Kosuke Miyai https://orcid.org/0000-0003-1776-3541
Shinya Yoshimatsu https://orcid.org/0000-0001-6761-4451
Makoto Sasaki https://orcid.org/0000-0002-0645-7015
Katsunori Iwasaki https://orcid.org/0000-0002-5721-2173
Susumu Matsukuma https://orcid.org/0000-0003-0409-7527

Author Contributions

Conceptualization: YA, KM. Data curation: YA, KM. Formal analysis: KM. Investigation: YA, KM, SY. Methodology: KM. Resources: SM. Supervision: MS, KI, SM. Visualization: KM. Writing—original draft: YA, KM. Writing—review & editing: SY, MS, KI, SM. Approval of final manuscript: all authors.

Conflicts of Interest

The authors declare that they have no potential conflicts of interest.

Funding Statement

No funding to declare.

Acknowledgments

We thank Mr. Susumu Tominaga and Ms. Chinami Onuma (National Defense Medical College) for their excellent technical assistance.

References

1. Sahin AA, Myhre M, Ro JY, Sneige N, Dekmezian RH, Ayala AG. Plasmacytoid transitional cell carcinoma: report of a case with initial presentation mimicking multiple myeloma. Acta Cytol 1991; 35: 277-80.
2. Zukerberg LR, Harris NL, Young RH. Carcinomas of the urinary bladder simulating malignant lymphoma: a report of five cases. Am J Surg Pathol 1991; 15: 569-76.
3. Ro JY, Shen SS, Lee HI, et al. Plasmacytoid transitional cell carcinoma of urinary bladder: a clinicopathologic study of 9 cases. Am J Surg Pathol 2008; 32: 752-7.
4. Kim DK, Kim JW, Ro JY, et al. Plasmacytoid variant urothelial carcinoma of the bladder: a systematic review and meta-analysis of clinicopathological features and survival outcomes. J Urol 2020; 204: 215-23.
5. Sood S, Paner GP. Plasmacytoid urothelial carcinoma: an unusual variant that warrants aggressive management and critical distinction on transurethral resections. Arch Pathol Lab Med 2019; 143: 1562-7.
6. Chung AD, Schieda N, Flood TA, et al. Plasmacytoid urothelial carcinoma (PUC): imaging features with histopathological correlation. Can Urol Assoc J 2017; 11: E50-7.
7. Simon CT, Skala SL, Killen PD, et al. Plasmacytoid urothelial carcinoma: a rapid autopsy case report with unique clinicopathologic and genomic profile. Diagn Pathol 2019; 14: 113.
8. Kohada Y, Kaiho Y, Ito J, et al. Progressive plasmacytoid variant bladder cancer with retroperitoneal dissemination: an autopsy case report. IJU Case Rep 2020; 3: 166-9.
9. Ando T, Watanabe K, Takahashi K, Mizusawa T, Sakai T, Katagiri A. Duodenal and rectal obstructions due to urothelial cancer infiltration from recurrent renal pelvic cancer in the bladder wall: an autopsy case. Urol Case Rep 2019; 27: 100903.
10. Tanaka A, Ohori M, Hashimoto T, et al. A case of plasmacytoid urothelial carcinoma of the bladder: rapid progression after transurethral resection. Hinyokika Kiyo 2012; 58: 101-3.
11. Miyai K, Ito K, Matsukuma S, Tsuda H. Frequent EGFR expression/*EGFR* amplification and lack of activating mutation in testicular choriocarcinoma. Pathol Int 2020; 70: 262-9.
12. Dayyani F, Czerniak BA, Sircar K, et al. Plasmacytoid urothelial carcinoma, a chemosensitive cancer with poor prognosis, and peritoneal carcinomatosis. J Urol 2013; 189: 1656-61.
13. Lopez-Beltran A, Requena MJ, Montironi R, Blanca A, Cheng L. Plasmacytoid urothelial carcinoma of the bladder. Hum Pathol 2009; 40: 1023-8.
14. Monn MF, Kaimakliotis HZ, Pedrosa JA, et al. Contemporary bladder cancer: variant histology may be a significant driver of disease. Urol Oncol 2015; 33: 18.
15. Cockerill PA, Cheville JC, Boorjian SA, et al. Outcomes following radical cystectomy for plasmacytoid urothelial carcinoma: defining the need for improved local cancer control. Urology 2017; 102: 143-7.
16. Li Q, Assel M, Benfante NE, et al. The impact of plasmacytoid variant histology on the survival of patients with urothelial carcinoma of bladder after radical cystectomy. Eur Urol Focus 2019; 5: 104-8.
17. Perrino CM, Eble J, Kao CS, et al. Plasmacytoid/diffuse urothelial carcinoma: a single-institution immunohistochemical and molecular study of 69 patients. Hum Pathol 2019; 90: 27-36.
18. Sangoi AR, Chan E, Stohr BA, Kunju LP. Invasive plasmacytoid urothelial carcinoma: a comparative study of E-cadherin and P120 catenin. Hum Pathol 2020; 102: 54-9.
19. Lae M, Couturier J, Oudard S, Radvanyi F, Beuzeboc P, Vieillefond A. Assessing *HER2* gene amplification as a potential target for therapy in invasive urothelial bladder cancer with a standardized methodology: results in 1005 patients. Ann Oncol 2010; 21: 815-9.
20. Kamoun A, de Reynies A, Allory Y, et al. A consensus molecular classification of muscle-invasive bladder cancer. Eur Urol 2020; 77: 420-33.

 https://doi.org/10.4132/jptm.2022.03.15

JPTM
Journal of Pathology and Translational Medicine 2022; 56: 225-230
https://doi.org/10.4132/jptm.2022.04.07

CASE STUDY

Hepatic carcinoma expressing inhibin: case report of a proposed novel entity and review of the literature

Antonia Syrnioti[1], Evangelia Athanasiou[2], Prodromos Hytiroglou[1]

[1]Department of Pathology, Aristotle University School of Medicine, Thessaloniki;
[2]"Microdiagnostiki" Laboratory, Thessaloniki, Greece

Hepatic carcinoma expressing inhibin is a recently described neoplasm with varied architecture, including trabecular, pseudoglandular, follicular/microcystic, organoid, solid and tubular patterns of growth. We report a case of hepatic carcinoma expressing inhibin that occurred in a 47-year-old woman presenting with epigastric and back pain. The tumor was located in the left hepatic lobe and measured 12 cm in diameter. On immunohistochemical stains, the neoplastic cells were positive for inhibin, as well as cytokeratins 7, 8/18 and 19. There was mild focal expression of synaptophysin, and lack of expression of hepatocytic markers. The histogenesis of hepatic carcinoma expressing inhibin is presently uncertain. From a practical point of view, this neoplasm can potentially cause diagnostic pitfalls by simulating other primary or metastatic tumors, such as hepatocellular carcinoma, cholangiocarcinoma, neuroendocrine tumors, and follicular carcinoma of thyroid gland. Performing inhibin immunostain could assist in the differential diagnosis of liver tumors with unusual histologic features.

Key Words: Carcinoma; Immunohistochemistry; Inhibin; Liver

Received: February 10, 2022 **Revised:** March 26, 2022 **Accepted:** April 7, 2022
Corresponding Author: Prodromos Hytiroglou, MD, Department of Pathology, Aristotle University School of Medicine, 54006 Thessaloniki, Greece
Tel: +30-2310-999-218, Fax: +30-2310-244-604, E-mail: pchytiro@auth.gr

Hepatic carcinoma expressing inhibin (HCEI) is a recently described neoplasm of uncertain histogenesis that exhibits histologic features simulating hepatocellular, cholangiocellular, thyroid, and neuroendocrine tumors. In addition to our original report in 2005 [1], fourteen cases of HCEI have been reported since 2017 [2-6], indicating that this neoplasm may be more common than previously thought. In most cases, the correct diagnosis was made in consultation; the contributors' diagnoses often were those of neuroendocrine tumors [2-5].

We report a new case of HCEI, review the literature on this proposed novel entity, and discuss its possible histogenesis.

CASE REPORT

Clinical summary

We have recently examined in consultation a left hepatic lobe tumor from a 47-year-old woman, who presented with epigastric and back pain of several months' duration. Physical examination revealed a palpable mass in the left upper abdominal quadrant. Her past medical history was unremarkable. The patient did not smoke or drink alcohol, had no history of liver disease, and was not on any medication. There was no family history of liver disease. On magnetic resonance imaging (MRI) of the upper abdomen, a lobulated mass was seen, which occupied almost the entire left hepatic lobe. The tumor appeared inhomogeneously enhanced after intravenous contrast administration. The remaining liver parenchyma appeared normal. There were no other abnormal findings in the pancreas, spleen, adrenal glands and kidneys. Chest X-ray was normal. Liver function tests, hematology work-up, and serum levels of tumor markers (carcinoembryonic antigen, CA19-9, CA125, and α-fetoprotein) were within normal limits. The patient underwent a left hepatic lobectomy. On postoperative chest computed tomography scan, as well as upper and lower abdominal MRI, there were no additional lesions or residual tumor.

Pathologic findings

On gross examination, the tumor was relatively well-circum-

pISSN 2383-7837
eISSN 2383-7845

scribed, displayed a tan-yellow cut surface, and measured 12 cm in greatest dimension (Fig. 1A). On microscopic examination, it exhibited trabecular, follicular and pseudoglandular architecture (Fig. 1B). The tumor cells were columnar or ovoid in shape, with eosinophilic cytoplasm and roundish nuclei with inconspicuous nucleoli (Fig. 1C). Mild nuclear pleomorphism and rare mitotic figures were found. The follicular structures contained amorphous eosinophilic material with peripheral vacuolization, reminiscent of thyroid follicles (Fig. 1B). Occasional fibrous septa were observed (Fig. 1B). Regions of hemorrhage and cystic degeneration were present. No necrosis was found. At the tumor border, there was invasive growth, with tongues and groups of neoplastic cells extending into the adjacent hepatic parenchyma (Fig. 1D). The hepatic parenchyma was otherwise unremarkable. No evidence of biliary intraepithelial neoplasia was present. The surgical margins of resection were free of tumor.

On immunohistochemical evaluation, the neoplastic cells were positive for cytokeratin (CK) 7 (Fig. 2A), CK8/18, and CK19 (Fig. 2B), as well as inhibin (Fig. 2C). There also was patchy mild positivity of tumor cells for synaptophysin (Fig. 2D). Membranous positivity with polyclonal carcinoembryonic antigen was present around pseudoglandular structures (Fig. 2E). The neoplastic cells were negative for HepPar-1, arginase-1, glypican-3, α-fetoprotein, glutamine synthetase, β-catenin (nuclear), CK20, epithelial membrane antigen, chromogranin, INSM1, thyroid transcription factor-1, thyroglobulin, human chorionic gonadotrophin, CA19-9, Melan A, CD10, CD56, CD99, vimentin, calretinin, estrogen and progesterone receptor proteins, PAX8, GATA3, CDX2, and trypsin. On immunohistochemical stains for Ki67 antigen, there was positivity in 10% of tumor cells (Fig. 2F).

Further immunohistochemical stains for CD34 and α-caldesmon were performed to explore the vascular architecture of the tumor. A rich, thin-walled vascular bed was evident on CD34 stains (Fig. 3A), while sparse larger vessels with venous features were seen on stains for α-caldesmon (Fig. 3B).

DISCUSSION

HCEI is an enigmatic neoplasm that was originally recognized because of the combination of its unusual histologic features with

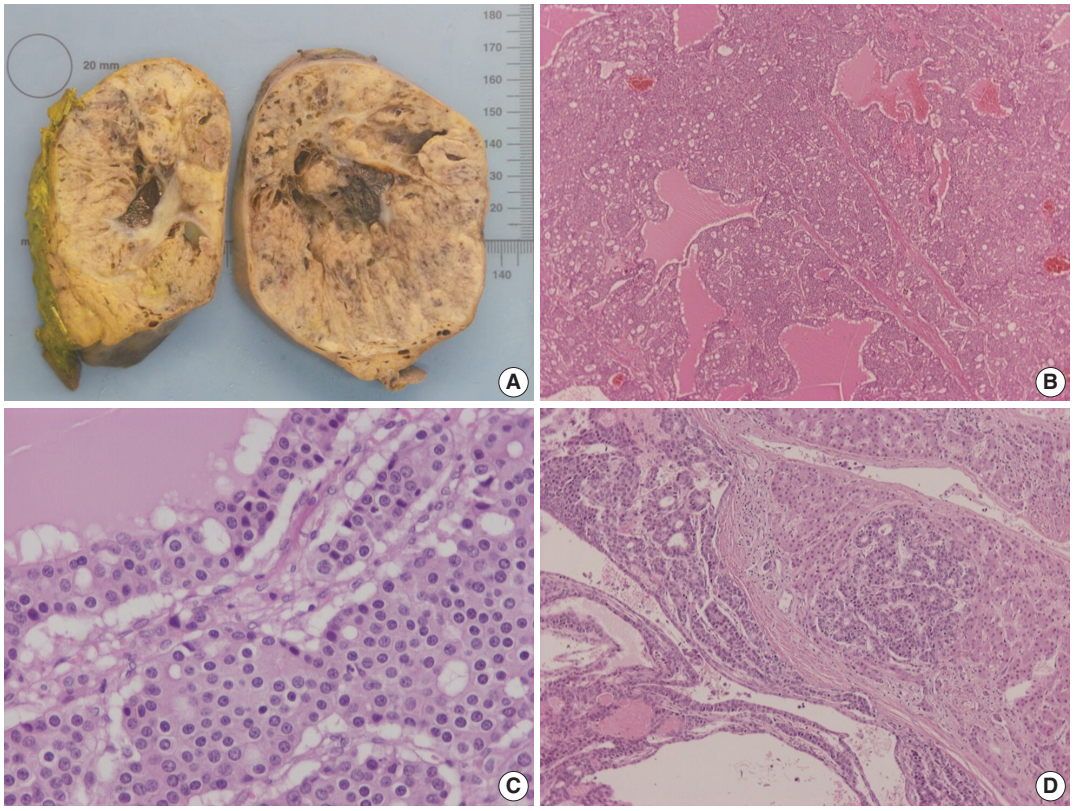

Fig. 1. Gross and microscopic features of the tumor. (A) Gross examination shows a large, relatively well-circumscribed tumor, with a tan-yellow cut surface and focal areas of hemorrhage and cystic degeneration. (B) Representative low power view of the tumor, demonstrating trabecular, follicular and pseudoglandular architecture. (C) On high power examination, the neoplastic cells are columnar or ovoid, with eosinophilic cytoplasm and mild nuclear pleomorphism. (D) Neoplastic cell invasion of the adjacent hepatic parenchyma is evident at the tumor margin.

https://doi.org/10.4132/jptm.2022.04.07

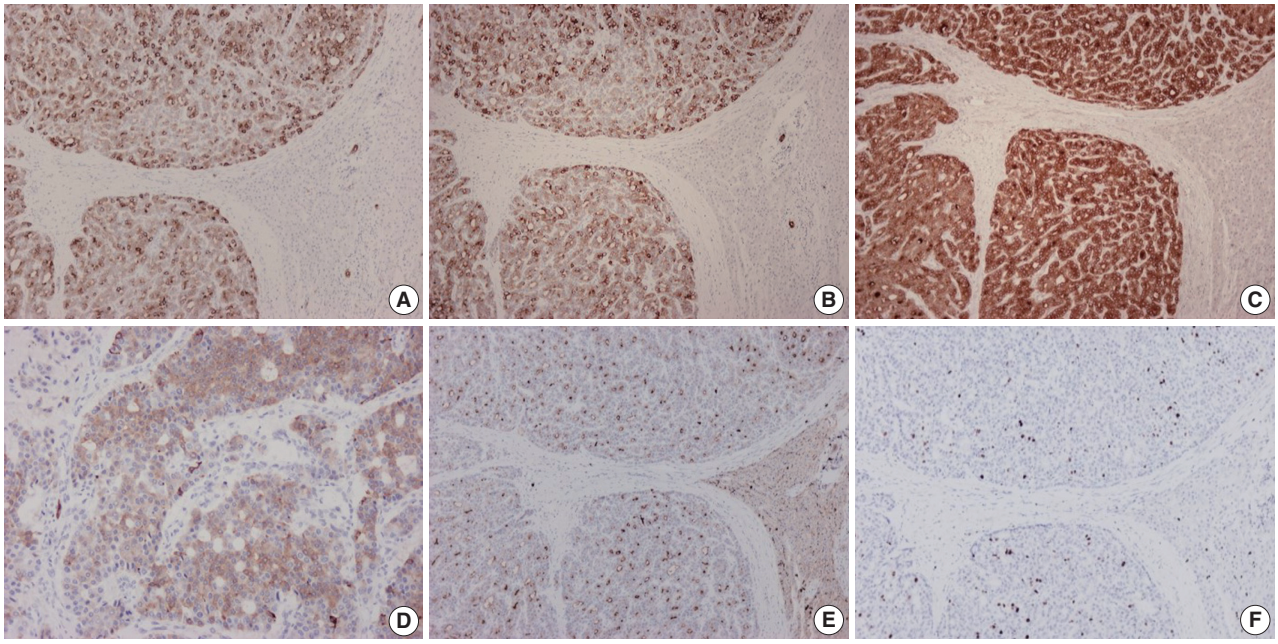

Fig. 2. Immunohistochemical findings of tumor cells. The neoplastic cells are positive for cytokeratin 7 (A), cytokeratin 19 (B), and inhibin (C). Patchy mild positivity of tumor cells for synaptophysin is also seen (D). Stain for polyclonal carcinoembryonic antigen demonstrates membranous positivity around pseudoglandular structures (E). Ten percent of tumor cells are positive for Ki67 antigen (F). Adjacent hepatic parenchyma is seen on the right side in all photomicrographs except for D.

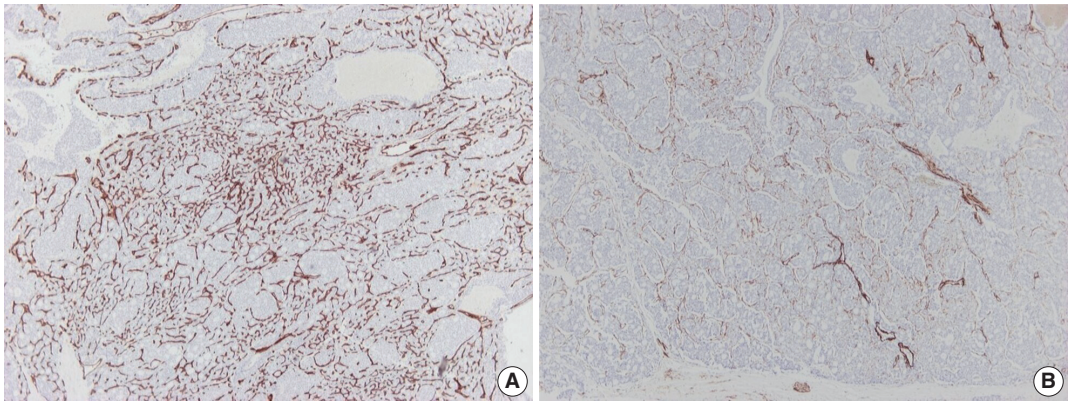

Fig. 3. Immunohistochemical findings of tumor vessels. A rich thin-walled vascular bed is observed on CD34 stain (A), while stain for α-caldesmon shows sparse larger vessels with venous features (B).

the immunohistochemical expression of inhibin [1]. Sixteen cases of HCEI have been thus far reported, including the present one (Table 1) [1-6]. Twelve cases occurred in women and four in men; the age range of the patients was 17 to 54 years. HCEI has been found to exhibit varied architecture, with trabecular, pseudoglandular, follicular/microcystic, organoid, solid and tubular patterns of growth. The neoplastic cells diffusely express inhibin. Prognosis is variable. The patient of our original report [1] received no further treatment following surgical resection, and is well, without evidence of disease, 20 years after presentation. The patient of our current report is also alive and without evidence of disease 9 months after presentation. However, three of the other 14 patients reported to date have died of the disease, 5 had disease progression, one had stable disease, 3 were disease-free at last follow-up, and two were lost to follow-up (Table 1).

Despite the small number of reported cases, there is sufficient evidence that HCEI is a distinct clinicopathologic entity [1-6]: (1) These tumors are relatively large (size range, 6.9 to 36 cm) when they become symptomatic, suggesting an indolent initial growth phase. (2) These tumors have characteristic histologic fea-

Table 1. Reported cases of hepatic carcinoma expressing inhibin

No.	Study	Age (yr)	Sex	Tumor location	Tumor size (cm)	Immunohistochemistry				Albumin ISH	*NIPBL/ACC1* fusion	Outcome	Non-tumorous liver status	OCP use	Serum AFP
						CK7	CK19	Synapto-physin	Chromo-granin						
1	Vrettou et al. (2005) [1]	24	F	Left lobe	14	+	+	–	–	N/A	N/A	Alive, NOD (> 19 yr)	Normal	Yes (10 yr)	N/A
2	Braxton et al. (2017) [2]	17	F	Right lobe	23	+	+	+ (weak)	+ (weak)	N/A	N/A	DOD (41 mo)	Normal	None	Normal
3	Braxton et al. (2017) [2]	44	F	Left lobe	16	+ (weak)	+	+	+ (weak)	N/A	N/A	Unknown	Normal	None	N/A
4	Braxton et al. (2017) [2]	25	F	Caudate lobe	7.5	+	+	+ (weak)	+ (weak)	N/A	N/A	DOD (30 mo)	Normal	None	Normal
5	Wen et al. (2021) [3]	37	F	N/A	6.9	+	+ (patchy)	- (focal)	–	+	N/A	NOD (2 yr)	N/A	N/A	N/A
6	Wen et al. (2021) [3]	28	F	N/A	15	+	N/A	+ (patchy)	–	+	N/A	NOD (5 mo)	N/A	N/A	N/A
7	Wen et al. (2021) [3]	19	F	N/A	14	+	+	N/A	– (focal)	+	N/A	DOD (2 yr)	N/A	N/A	N/A
8	Wen et al. (2021) [3]	34	F	N/A	20	+	N/A	–	–	+	N/A	NOD (1 yr)	N/A	N/A	N/A
9	Wen et al. (2021) [3]	44	F	N/A	23.5	+	+ (patchy)	+ (patchy variable)	+ (patchy)	+	N/A	Intrahepatic recurrence (1.5 yr)	N/A	N/A	N/A
10	Wen et al. (2021) [3]	33	F	N/A	15.5	+	+	+ (patchy)	+ (focal)	+	N/A	Metastases (at diagnosis)	N/A	N/A	N/A
11	Liang et al. (2021) [4]	26	M	Most of liver	36	+	N/A	+	–	+	N/A	Disease progression and metastases, AWD (15 mo)	N/A	N/AP	N/A
12	Argani et al. (2021) [5]	24	F	Right lobe	25.4	+	+	+ (patchy)	+ (focal)	+	+	Multifocal local recurrence and metastases, AWD (9 mo)	Normal	N/A	N/A
13	Argani et al. (2021) [5]	54	M	Right lobe	11.5	+	+	+ (patchy)	+ (focal)	+	+	Multifocal intrahepatic recurrence, AWD (10 mo)	Normal	N/AP	N/A
14	Argani et al. (2021) [5]	52	M	N/A	7.5	+	+	+ (patchy)	+ (focal)	+	+	Unknown	Normal	N/AP	N/A
15	Verhoeff et al. (2022) [6]	26	M	Right lobe	21	+	+ (patchy)	+ (patchy)	N/A	N/A	N/A	AWD (stable, by imaging, at 6 mo)	N/A	N/AP	N/A
16	Present case	47	F	Left lobe	12	+	+	+ (focal, weak)	–	N/A	N/A	NOD (9 mo)	Normal	None	Normal

Literature search was implemented using the following keywords in MEDLINE database (PubMed, English language): liver, carcinoma (or tumor), inhibin.
CK, cytokeratin; ISH, in situ hybridization; OCP, oral contraceptive; AFP, α-fetoprotein; F, female; N/A, not available; NOD, no evidence of disease; DOD, died of disease; M, male; N/AP, not applicable; AWD, alive with disease.

tures, including trabecular, pseudoglandular, follicular/microcystic, organoid, solid and tubular patterns of growth. 3) In addition to inhibin positivity, HCEI characteristically shows positivity for 'biliary' markers (CK7 and CK19), mild or patchy positivity for neuroendocrine markers (synaptophysin, chromogranin, CD56), and absence of staining for hepatocellular markers (HepPar-1, arginase-1, glypican-3, α-fetoprotein). Albumin mRNA has also been detected in 10 cases by in situ hybridization [3-5]. (4) Molecular studies recently performed in three cases [5] have detected a novel *NIPBL-NACC1* gene fusion in HCEI.

The histogenesis of HCEI remains elusive. Inhibin expression characterizes a limited range of normal cell types, including granulosa cells, luteinized thecal cells and hilus cells of the ovary, syncytiotrophoblastic cells and adrenocortical cells [1]. Theoretically, any of these cell types could be present in a heterotopic location, such as the liver, and give rise to tumors. However, tumors with the features of HCEI have not been described in the ovaries or adrenals. On the other hand, inhibin expression has occasionally been reported in tumor types without obvious connection to the normal cells mentioned above, such as mucinous cystic neoplasm of the liver and pancreas, as well as neuroendocrine tumors of clear cell type occurring in patients with von Hippel-Lindau disease [7]. It might be worth exploring whether there is any connection between these neoplasms and HCEI. Nevertheless, the possibility that inhibin expression may be triggered in cells with a biliary phenotype by *NIPBL-NACC1* gene fusion cannot be ruled out.

From a practical point of view, it is possible that HCEI has been underreported, due to its histologic and immunohistochemical similarities with hepatocellular carcinoma, cholangiocarcinoma, primary or metastatic neuroendocrine tumors and metastatic follicular carcinoma of the thyroid gland. The diagnosis of HCEI can be easily missed if pathologists do not think of performing inhibin immunostain. Reports of additional cases, including further immunohistochemical and molecular studies, will be useful to define this proposed new entity with certainty. In this context, it would be of interest to assess inhibin expression in neoplasms that have histologic similarities with HCEI, such as primary hepatic neuroendocrine tumors (including a recently described "primary hepatic neuroendocrine tumor with unusual thyroid follicular-like morphologic characteristics", which occurred in a 57-year old woman [8]), as well as tumors recently described as "thyroid-like intrahepatic cholangiocarcinoma", which occurred in three women and one man, between the ages of 26 and 59 years [9-12].

In conclusion, HCEI is an emerging entity that pathologists should be aware of. This neoplasm can potentially cause diagnostic pitfalls by simulating histologically other primary or metastatic hepatic tumors. Performing inhibin immunostain could be of great help in the differential diagnosis of liver tumors with unusual histologic features.

Ethics Statement

Informed consent was obtained from the individual participant included in this study. In our institution, case studies are exempted from Institutional Review Board submission.

Availability of Data and Material

The datasets generated or analyzed during the study are available from the corresponding author on reasonable request.

Code Availability

Not applicable.

ORCID

Antonia Syrnioti https://orcid.org/0000-0002-9232-6715
Evangelia Athanasiou https://orcid.org/0000-0002-3699-1999
Prodromos Hytiroglou https://orcid.org/0000-0003-3412-2914

Author Contributions

Conceptualization: AS, EA, PH. Data curation: AS, EA, PH. Formal analysis: AS, EA, PH. Methodology: AS, EA, PH. Supervision: PH. Writing—original draft: AS, EA, PH. Writing—review & editing: AS, EA, PH. Approval of final manuscript: all authors.

Conflicts of Interest

The authors declare that they have no potential conflicts of interest.

Funding Statement

No funding to declare.

References

1. Vrettou E, Hytiroglou P, Sikas N, Soultoyannis I, Goodman ZD. Hepatic adenocarcinoma expressing inhibin in a young patient on oral contraceptives. Virchows Arch 2005; 446: 560-5.
2. Braxton DR, Saxe D, Damjanov N, et al. Molecular and cytogenomic profiling of hepatic adenocarcinoma expressing inhibinA, a mimicker of neuroendocrine tumors: proposal to reclassify as "cholangioblastic variant of intrahepatic cholangiocarcinoma". Hum Pathol 2017; 62: 232-41.
3. Wen KW, Joseph NM, Srivastava A, et al. Inhibin-positive hepatic carcinoma: proposal for a solid-tubulocystic variant of intrahepatic cholangiocarcinoma. Hum Pathol 2021; 116: 82-93.
4. Liang TZ, Whang G, Chopra S. Primary hepatic carcinoma with inhibin positivity in a young male patient: a rare tumor previously only reported in females: case report and review of literature. Virchows Arch 2021; 478: 605-10.
5. Argani P, Palsgrove DN, Anders RA, et al. A novel NIPBL-NACC1 gene fusion is characteristic of the cholangioblastic variant of intrahepatic cholangiocarcinoma. Am J Surg Pathol 2021; 45: 1550-60.
6. Verhoeff K, Bacani J, Fung C, Canterbury LA. A Cholangioblastic variant of cholangiocarcinoma. ACG Case Rep J 2022; 9: e00746.

7. Sinkre PA, Murakata L, Rabin L, Hoang MP, Albores-Saavedra J. Clear cell carcinoid tumor of the gallbladder: another distinctive manifestation of von Hippel-Lindau disease. Am J Surg Pathol 2001; 25: 1334-9.
8. Ibrahim ME, Abadeer K, Zhai QJ, Nassar A. Primary hepatic neuroendocrine tumor with unusual thyroid follicular-like morphologic characteristics. Case Rep Pathol 2017; 2017: 7931975.
9. Chable-Montero F, Shah BS, Montante-Montes de Oca D, Angeles-Angeles A, Henson DE, Albores-Saavedra J. Thyroid-like cholangiocarcinoma of the liver: an unusual morphologic variant with follicular, trabecular and insular patterns. Ann Hepatol 2012; 11: 961-5.
10. Shah A, Chandibhamar BS, Gami A, Trivedi P. Case report of intrahepatic cholangiocarcinoma showing thyroid like follicular pattern: a rare morphological variant. . Eur J Med Case Rep 2020; 4: 280-4.
11. Fornelli A, Bondi A, Jovine E, Eusebi V. Intrahepatic cholangiocarcinoma resembling a thyroid follicular neoplasm. Virchows Arch 2010; 456: 339-42.
12. Chen SH, Zheng ZY, Wang HL, et al. Thyroid-like intrahepatic cholangiocarcinoma: report of a case and review of the literature. Int J Surg Pathol 2018; 26: 649-54.

https://doi.org/10.4132/jptm.2022.04.07

JPTM
Journal of Pathology and Translational Medicine 2022; 56: 231-237
https://doi.org/10.4132/jptm.2022.05.08

CASE STUDY

Primary pulmonary epithelioid inflammatory myofibroblastic sarcoma: a rare entity and a literature review

Priyanka Singh[1], Aruna Nambirajan[1], Manish Kumar Gaur[2], Rahul Raj[1], Sunil Kumar[2], Prabhat Singh Malik[3], Deepali Jain[1]

[1]Department of Pathology, All India Institute of Medical Sciences, New Delhi;
Departments of [2]Surgical Oncology and [3]Medical Oncology, Dr. BRA Institute Rotary Cancer Hospital, All India Institute of Medical Sciences, New Delhi, India

Epithelioid inflammatory myofibroblastic sarcoma (EIMS) is an aggressive subtype of inflammatory myofibroblastic tumor (IMT) harboring anaplastic lymphoma kinase (*ALK*) gene fusions and is associated with high risk of local recurrence and poor prognosis. Herein, we present a young, non-smoking male who presented with complaints of cough and dyspnoea and was found to harbor a large right lower lobe lung mass. Biopsy showed a high-grade epithelioid to rhabdoid tumor with ALK and desmin protein expression. The patient initially received 5 cycles of crizotinib and remained stable for 1 year; however, he then developed multiple bony metastases, for which complete surgical resection was performed. Histopathology confirmed the diagnosis of EIMS, with *ALK* gene rearrangement demonstrated by fluorescence in situ hybridization. Postoperatively, the patient is asymptomatic with stable metastatic disease on crizotinib and has been started on palliative radiotherapy. EIMS is a very rare subtype of IMT that needs to be included in the differential diagnosis of ALK-expressing lung malignancies in young adults.

Key Words: Epithelioid inflammatory myofibroblastic sarcoma; Inflammatory myofibroblastic tumor; Lung; Anaplastic lymphoma kinase; Crizotinib; Fluorescence in situ hybridization

Received: January 23, 2022 **Revised:** April 18, 2022 **Accepted:** May 8, 2022
Corresponding Author: Deepali Jain, MD, FIAC, Department of Pathology, All India Institute of Medical Sciences, New Delhi 110029, India
Tel: +91-1126549200, E-mail: deepalijain76@gmail.com

Inflammatory myofibroblastic tumor (IMT) is a distinctive mesenchymal tumor composed of neoplastic myofibroblastic tumor cells associated with inflammatory infiltrate of plasma cells, lymphocytes, and occasional eosinophils or neutrophils. IMTs present mainly in children and young adults, lack significant gender bias, and occur in a variety of anatomical locations [1]; lungs are one of the most common sites, accounting for ~1% of all adults and ~50% of pediatric lung tumors [2]. Fusions of the anaplastic lymphoma kinase (*ALK*) gene with various fusions partners, most commonly tropomyosin 3 (*TPM3*) or tropomyosin 4 (*TPM4*) gene, are observed in up to 60% of IMTs, correlating with diffuse cytoplasmic staining for ALK protein in tumor cells. Conventional IMTs show low-grade spindle cell tumor morphology lacking significant atypia, mitoses, or necrosis. Surgical resection is curative, and although one-fifth of cases will recur, < 5% of all IMTs metastasize [1,2].

Epithelioid inflammatory myofibroblastic sarcoma (EIMS) is a very rare subtype of IMT that has been associated with an aggressive course, rapid local recurrence, early metastases, and fatal outcome [1,3]. Unlike the bland spindle cell morphology of IMT, EIMS is composed of plump round to epithelioid tumor cells with prominent nucleoli and myxoid stroma with neutrophil-rich infiltrate [1] and show mitoses and necrosis. They harbor *ALK* gene fusions, most commonly with *RANBP2* (Ran specific binding protein 2) or, rarely, with *RRBP1* (ribosome binding protein 1). The fusions have been associated with a peculiar nuclear membrane (*RANBP2-ALK* fusion) or perinuclear accentuated cytoplasmic immunostaining (*RRBP1-ALK* fusion) for ALK protein [3-5]. EIMS occurs mainly in children and young adults, with a male gender predilection. These tumors have been most commonly reported in the mesentery and omentum [3,6], while primary pulmonary EIMS is extremely rare [7-9]. Herein, we report a primary pulmonary EIMS in a young male who was initially treated with ALK inhibitor monotherapy and subsequent surgery in the face of metastatic progression. In addition, we discuss the challenges associated with the diagnosis and treat-

pISSN 2383-7837
eISSN 2383-7845

ment of this rare entity.

CASE REPORT

A 25-year-old, non-smoking male presented with complaints of cough, significant weight loss, intermittent high-grade fever, and difficulty breathing for longer than 4 months. Imaging revealed a well-defined homogenous fluorodeoxyglucose (FDG)-avid mass of 6.9×4.2×6.1 cm involving the superior segment of the right lower lung lobe with no other pulmonary/pleural lesions or lymphadenopathy (Fig. 1A). Positron emission tomography scan showed another FDG-avid well-defined hypodense lesion of size 1.1×1.2 cm in segment IVA of the liver, likely metastasis. Biochemistry including serum tumor biomarkers was within normal range. A computed tomography–guided biopsy of the lung mass showed a poorly differentiated malignant tumor immunonegative for epithelial (pan-cytokeratin, epithelial membrane antigen), hematopoietic (CD45, myeloperoxidase, CD30), pneumocytic (thyroid transcription factor 1), melanocytic (human melanoma black 45, S-100), and mesothelial (calretinin, Wilms tumor protein 1) markers with retained INI-1 and BRG-1 expression. Tumor cells showed cytoplasmic ALK (VENTANA anti-ALK [D5F3] antibody developed by Roche Diagnostics [one 5 mL dispenser of VENTANA anti-ALK (D5F3) antibody contains approximately 70 µg of the rabbit monoclonal (D5F3) antibody; the antibody is diluted in 0.08 M phosphate buffered saline with 3% carrier protein and 0.05% ProClin 300, a preservative]) and cytoplasmic desmin. Myogenin was

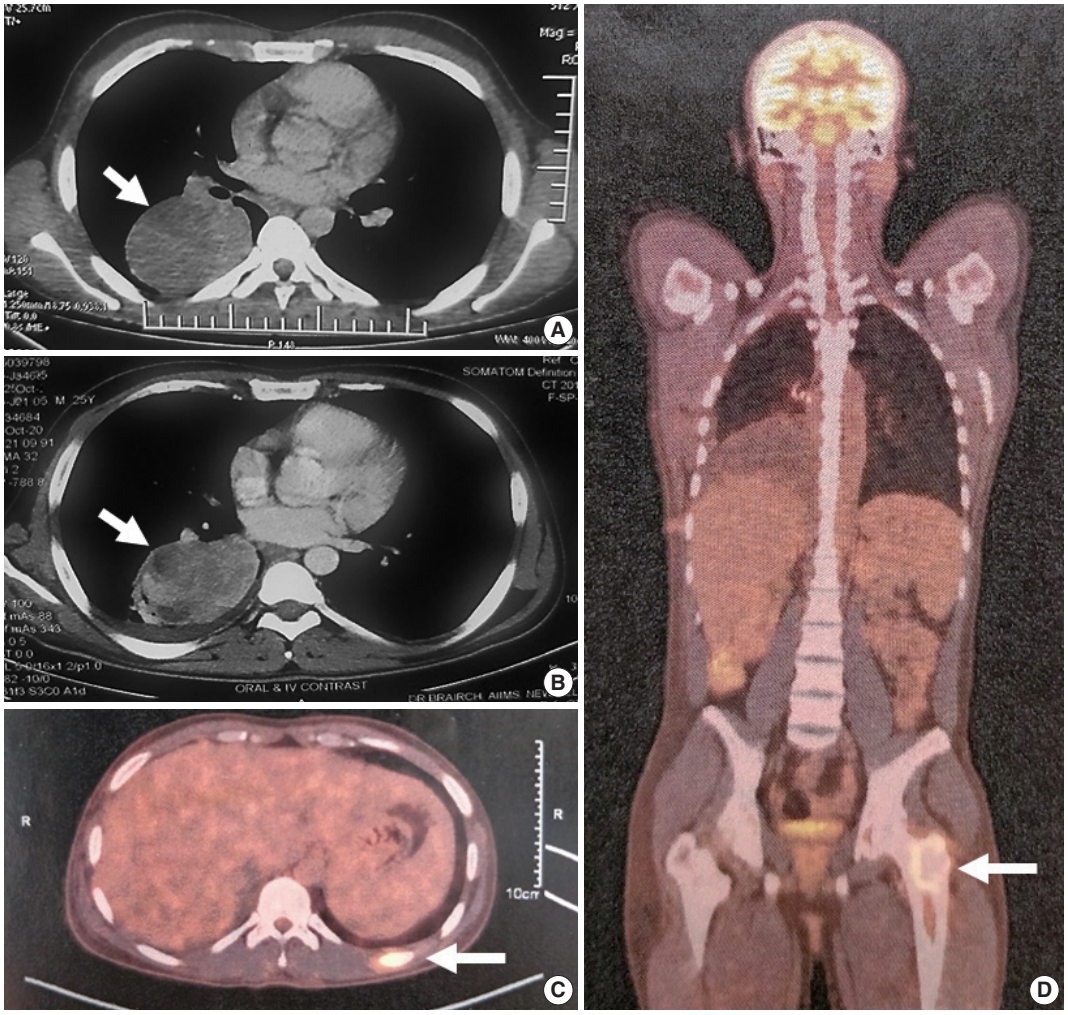

Fig. 1. Imaging features of the patient. (A) Computed tomography images show a homogeneous mass (arrow) with well-defined margin involving the superior segment of the right lower lobe. (B) Imaging at 6-months post-biopsy with the patient on crizotinib; the mass (arrow) was stable in size with few hypodense areas suggestive of necrosis. Positron emission tomography scan at 12-month post-biopsy with the patient continuing on crizotinib revealed new metastatic lesions in left 10th rib (arrow, C) and left proximal femur (arrow, D).

https://doi.org/10.4132/jptm.2022.05.08

negative. The possibility of EIMS was suggested, and resection/re-biopsy was advised for molecular confirmation due to limited remaining biopsy material.

After multidisciplinary thoracic oncology tumor board discussion, the patient was planned for surgical excision of the lung tumor and radiofrequency ablation of the liver lesion because of the young age of the patient with good performance status, solitary metastasis, and unconfirmed primary pathological diagno-

Fig. 2. Gross features of the resected pulmonary tumor. Resection specimen shows a well encapsulated, lobulated, uncut tumor (A). A cut section shows a circumscribed, fleshy tumor with a surrounding rim of lung parenchyma (arrow, B).

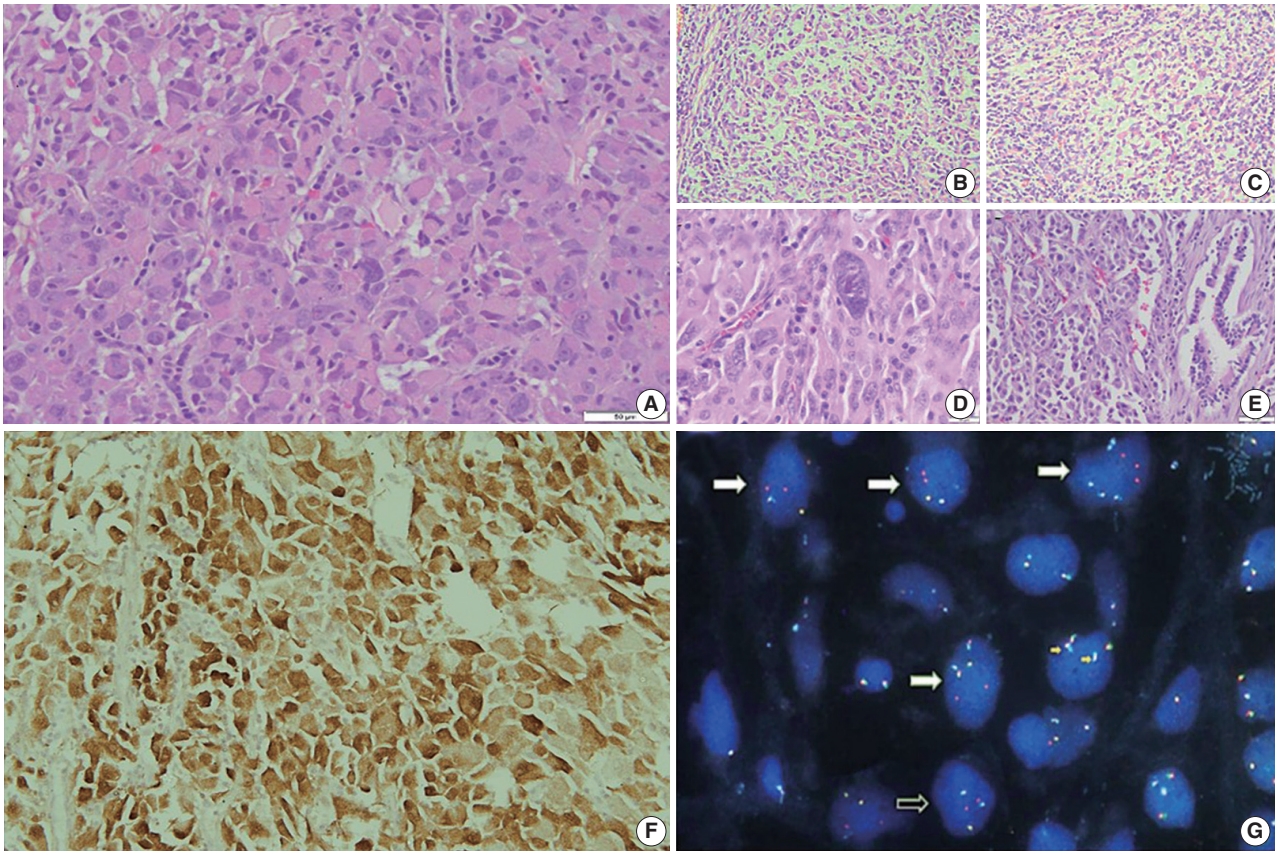

Fig. 3. Histomorphological and molecular features of the tumor. Hematoxylin and eosin-stained sections show rhabdoid phenotype tumor cells with moderate to abundant inclusion-like eosinophilic cytoplasm, prominent nucleoli, and fine granular chromatin with frequent mitoses in a myxoid stroma (A).The tumor cells show rich myxoid stroma and infiltration of mixed inflammatory cells (B, C, E) and prominent nuclear pleomorphism (D). The tumor cells show strong and diffuse cytoplasmic anaplastic lymphoma kinase (ALK) immunopositivity (F). (G) Fluorescence in situ hybridization using the ALK-ROS1 FLEXISH probe shows extra 3' signals (spectrum orange) of the *ALK* gene in tumor cells (white arrows, extra red signals unfused with green and/or aqua), indicating ALK gene rearrangement. The *ROS1* gene (indicated by fused red green-aqua signals, small yellow arrows) is intact.

sis. However, the patient was started on ALK inhibitor (crizotinib), and surgical intervention was deferred due to coronavirus disease 2019. Six months later, repeat imaging showed stable pulmonary disease (Fig. 1B) and complete resolution of the liver lesion. Crizotinib was continued and the patient was re-assessed for definitive surgical management. Repeat imaging 1 year after presentation showed increase in the size of the pulmonary mass (7.2×5.3×4.2 cm), and bone scan revealed metastasis in the right humerus (mid-shaft), left 10th rib, and left proximal femur (Fig. 1C, D). Pleural effusion or mediastinal lymph node metastasis (endobronchial ultrasound-guided transbronchial needle aspiration showed reactive lymphoid hyperplasia) was absent. Despite new bony metastases, because of the young age of the patient, surgical intervention was carried out as planned by means of video-assisted thoracoscopy-assisted right lower lobectomy.

Grossly, a well circumscribed, soft, fleshy tumor was identified in the lung parenchyma with focal areas of haemorrhage and necrosis (Fig. 2). Microscopy (Fig. 3) revealed a homogeneous tumor composed of ovoid to polygonal cells arranged in fascicles and sheets. The cells showed moderate to abundant eosinophilic cytoplasm with markedly pleomorphic nuclei, prominent nucleoli, and fine granular cytoplasm showing frequent mitoses (8 per 2 mm^2). Necrosis was present that had not been seen in the biopsy. Focal areas of myxoid change and lymphoplasmacytic infiltrate were noted. The immuno-profile of the tumor was similar to that of the biopsy except for focal cytokeratin expression in the resection, while histomorphology of the tumor was similar to that of the biopsy. The Ki-67 labeling index was ~30%–35% in the highest labeled areas. There was diffuse strong cytoplasmic staining for ALK protein. Fluorescence in situ hybridization assay using the FlexISH ALK/ROS1 DistinguISH Probe (ZytoVision, GmbH, Bremerhaven, Germany) showed one or more isolated 3' signals (extra orange signals) of the *ALK* gene without corresponding 5' signals (green signals) in the majority of tumor cells, indicative of *ALK* gene rearrangements [10], confirming the diagnosis of primary pulmonary EIMS. The *ROS1* gene represented by fused aqua-green-orange signals was intact (Fig. 3). The postoperative period was unremarkable, and the patient is currently asymptomatic 4-month post-surgery. He is continuing on crizotinib and is planned for palliative radiotherapy for the bony metastases.

DISCUSSION

Primary pulmonary EIMS is extremely rare, with only three cases reported previously in the English literature to the best of

Table 1. Clinicopathological features of reported cases of primary pulmonary epithelioid inflammatory myofibroblastic sarcoma including the current case

No.	Study	Age (yr)/ Sex	Anatomic site	Size (cm)	Clinical Presentation	Metastasis at presentation	Immunoprofile	Molecular confirmation (method)	Primary treatment	Outcome
1	Fu et al. [7]	21/M	Left lower lobe lung	10	Weight loss, fatigue	None	Desmin+, ALK (c), CD30–	*ALK* rearrangement (FISH)	Lobectomy	Bone metastases (pelvis, vertebrae) and underwent laminectomy; death 4 mo after resection
2	Sarmiento et al. [8]	71/M	Pleura based, left lower lobe	12.5	Dyspnoea, pleural effusion	None	NA	*ALK* rearrangement (FISH)	Lobectomy and adjuvant crizotinib	Progressed on crizotinib after 2 mo; near complete response to second line ALK inhibitor; remission after 1 yr at last follow-up
3	Kozu et al. [9]	57/M	Pleural cavity/ chest wall	NA	Pleural effusion and dyspnoea	N/A	Desmin+, cytokeratin+, ALK+ (c), CD30–	*RANBP2-ALK* fusion (PCR)	Crizotinib	NA
4	Present case	25/M	Lung Right lower lobe	7	Cough, loss of weight, fever, dyspnoea	Liver (solitary)	Desmin+, focal cytokeratin+, ALK+ (c), CD30–	*ALK* rearrangement (FISH)	Crizotinib	Complete resolution of liver metastases and stable pulmonary disease for 6 mo; bony metastases developed at 10 mo; lobectomy done and stable metastatic disease on crizotinib for 3 mo

ALK, anaplastic lymphoma kinase; (c), cytoplasmic; FISH, fluorescent in situ hybridization; NA, not available; *RANBP2*, Ran specific binding protein 2; PCR, polymerase chain reaction.

https://doi.org/10.4132/jptm.2022.05.08

Table 2. Differential diagnosis of poorly differentiated epithelioid to rhabdoid tumors

Entity	Incidence as lung mass	Epithelial markers	Mesenchymal markers	Other markers	ALK protein expression	Commonest *ALK* fusions
IMT [2]	Common	Pan CK+/–	SMA+, Desmin+	CD30–	Cytoplasmic (50%–60%)	TPM3-*ALK*, TPM4-*ALK*
ALCL [21]	Uncommon	EMA+	SMA+, Desmin–	CD30+	Nuclear and cytoplasmic	NPM-ALK
ALK+LBL [21]	Rare	EMA+	–	CD138+, CD38+, Mum1/IRF1+, IgA+, Bob1+	Cytoplasmic, nuclear and nucleolar	*CLTC-ALK* *ALK-SEC31A*
ALK-rearranged NSCLC	Common	CK+	–		Cytoplasmic	*EML4-ALK* [14]
Melanoma	Extremely rare	CK–	–	S-100+, Melan A+, HMB45+, SOX10+	ALK^{ATI} (seen in cutaneous melanoma) [22]	*EML4-ALK* [23]
Epithelioid mesothelioma [2]	Uncommon	CK5/6+/–, EMA+/–	Desmin–	Calretinin+/–, WT+, D2-40+	–	–
Rhabdomyosarcoma	Rare	CK/EMA–	Desmin+, Actin+	MyoD1+, Myogenin+ CD30–	Cytoplasmic	*NPM-ALK* [24], *EML4-ALK* [25]
Epithelioid leiomyosarcoma [1]	Rare	EMA+	SMA+, Desmin+, h-caldesmon+	CD34+/–CK+/–, EMA+/–	–	–
EIMS [2]	Rare	CK or EMA–/+	Desmin+, SMA+	CD30+	Nuclear membrane or cytoplasmic with perinuclear accentuation	*ALK-RRBP1* [3-5], *ALK-RANBP2*
Pleomorphic carcinoma [2]	<1%	NSCC component CK+, TTF-1 +, EMA+	Vimentin+	Surfactant protein A+, p53+	Rare	–

ALK, anaplastic lymphoma kinase; ALK ATI, anaplastic lymphoma kinase with alternative transcription initiation; IMT, inflammatory myofibroblastic tumor; CK/PanCK, cytokeratin; SMA, smooth muscle actin; TPM, tropomyosin; ALCL, anaplastic large cell lymphoma; EMA, epithelial membrane antigen; NPM, nucleophosmin; Mum1/IRF1, multiple myeloma 1/interferon regulatory factor 4 protein; CLTC, clathrin heavy chain; NSCLC, non–small cell lung carcinoma; EML4, echinoderm microtubule-associated protein-like 4; HMB45, human melanoma black 45; EIMS, epithelioid Inflammatory myofibroblastic sarcoma; *RRBP1*, ribosome binding protein 1; RANBP, Ran-binding protein; NSCC, non-small cell lung cancer; TTF-1, thyroid transcription factor 1.

our knowledge (Table 1) [7-9]. Including the present case, primary pulmonary EIMS occurs across a wide age range (21–71 years at diagnosis) with a male preponderance. The tumor presents as a solitary parenchymal mass or as pleural mass with a relatively short symptom duration (< 6 months) and is not uncommonly metastatic at presentation, with brain and skeleton appearing to be the preferred sites of metastases (Table 1).

Diagnosis of EIMS is challenging. The poorly differentiated epithelioid morphology can mimic anaplastic large cell lymphoma (ALCL), malignant melanoma, alveolar rhabdomyosarcoma, alveolar soft part sarcoma, epithelioid leiomyosarcoma, undifferentiated sarcoma, malignant mesothelioma, poorly differentiated carcinoma, and pulmonary pleomorphic carcinoma (containing a minimum 10% spindle and/or giant cells) and needs to be differentiated by relevant immunohistochemical markers (Table 2). Conventional IMTs are more common in the lung but are differentiated from EIMS by their bland spindle morphology, prominent lymphoplasmacytic cellular infiltrate, and absence of mitoses and pleomorphism. Rare cases of otherwise conventional IMTs that show increased mitotic activity, necrosis, and aggressive biological behavior are reported [11,12]; these should not be designated as EIMS in the absence of distinctive morphology of round to epithelioid cells, myxoid stroma, and mixed inflammatory infiltrate, as was observed in the present case. ALK protein expression is essential for diagnosis but is not specific as many other lung tumors express ALK protein due to underlying *ALK* gene rearrangements, as in ALCL, conventional IMTs, and non-small cell lung carcinoma (NSCLC), or to ALK copy number alterations as in rhabdomyosarcomas [13]. *ALK*-rearranged lung adenocarcinoma/NSCLC shows a variety of histological characteristics ranging from cribriform pattern, mucin-containing cells, presence of psammoma bodies, and solid signet-ring cells. None of the histological parameters are specific for a particular genotype [14-19]. Fluorescence in situ hybridization using break-apart probes is useful to confirm *ALK* gene rearrangements; however, polymerase chain reaction and/or sequencing of RNA transcripts is required for delineating *ALK* fusion partners. ALK protein expression in a nuclear membranous or perinuclear cytoplasmic pattern gives a clue to the presence of underlying *RANBP2* or *RRBP1* fusion partners with ALK, which are the most common fusions in EIMS; however, these fusions can also be observed in IMTs and ALCLs [20]. On the other hand, other fusion partners including *EML4*, the most common fusion partner in *ALK*-rearranged NSCLC, have also been report-

ed in EIMS associated with the more common cytoplasmic ALK staining pattern [26]. The various *ALK* gene rearrangement seen in NSCLC are EML4, TFG, KIF5B, KCL1, and multiple EML4 isoforms [27].

Thus, due to considerable genetic overlap with other ALKomas, EIMS is essentially a histopathological diagnosis, and definitive diagnosis can be difficult on a small biopsy, even with ancillary testing.

EIMS is an aggressive tumor with poor prognosis and local recurrence [1,3]. Review of previous reported pulmonary EIMS showed that surgical resection remained the mainstay of treatment when feasible (Table 1). These tumors do not respond to chemotherapy or radiotherapy [28,29]. Most ALK fusion proteins including those resulting from *RANBP2-ALK* fusions are sensitive to ALK tyrosine kinase inhibitor (TKI) inhibition in pre-clinical models [30], suggesting a role for targeted therapy. From the limited data available, EIMS does appear to respond to the ALK TKI crizotinib, as in our patient who experienced complete resolution of liver metastases. However, long-term responses or remissions are rare, with most EIMS patients progressing with metastatic disease within 3 to 6 months of crizotinib monotherapy [7-9], likely due to secondary resistance mechanisms [10]. A recent study demonstrated prolonged survival with a combination of ALK and CD30 targeted therapies [31]; however, CD30 expression appears to be uncommon in pulmonary EIMS (Table 1). EIMS is a very rare subtype of IMT that presents as a primary lung mass in young non-smokers, posing a considerable diagnostic challenge due to aggressive behavior with frequent metastases. There are limited data on treatment protocols; in the present case, targeted ALK inhibitor therapy combined with surgery achieved considerable disease control.

Ethics Statement

This study was approved by the Institutional Review Board with a waiver of informed consent (IRB No IEC-404/02.09.2016) and performed in accordance with the principles of the Declaration of Helsinki.

Availability of Data and Material

All data generated or analyzed during the study are included in this published article (and its supplementary information files).

Code Availability

Not applicable.

ORCID

Priyanka Singh https://orcid.org/0000-0002-0860-8016
Aruna Nambirajan https://orcid.org/0000-0001-7589-537X
Manish Kumar Gaur https://orcid.org/0000-0003-4403-9831
Rahul Raj https://orcid.org/0000-0003-2741-9496
Sunil Kumar https://orcid.org/0000-0002-9942-3403
Prabhat Singh Malik https://orcid.org/0000-0003-0205-8559
Deepali Jain https://orcid.org/0000-0001-5315-9814

Author Contributions

Conceptualization: PS. Data curation: PS. Formal analysis: PS. Supervision: DJ. Visualization: DJ. Writing—original draft: PS. Writing—review & editing: PS, AN, MKG, RR, SK, PSM, DJ. Approval of final manuscript: all authors.

Conflicts of Interest

D.J., a contributing editor of the *Journal of Pathology and Translational Medicine*, was not involved in the editorial evaluation or decision to publish this article. All remaining authors have declared no conflicts of interest.

Funding Statement

No funding to declare.

References

1. Yamamoto H. Inflammatory myofibroblastic tumor. In: WHO Classification of Tumours Editorial Board. WHO classification of tumors: soft tissue and bone tumours. Lyon: IARC Press, 2020; 109-11.
2. Tavora F, Glass C, Hornick JL, Jain D, Sheppared MN, Yi ES. Inflammatory myofibroblastic tumor. In: WHO Classification of Tumours Editorial Board. WHO classification of tumors: thoracic tumours. Lyon: IARC Press, 2021; 288-9.
3. Marino-Enriquez A, Wang WL, Roy A, et al. Epithelioid inflammatory myofibroblastic sarcoma: an aggressive intra-abdominal variant of inflammatory myofibroblastic tumor with nuclear membrane or perinuclear ALK. Am J Surg Pathol 2011; 35: 135-44.
4. Xu P, Shen P, Jin Y, Wang L, Wu W. Epithelioid inflammatory myofibroblastic sarcoma of stomach: diagnostic pitfalls and clinical characteristics. Int J Clin Exp Pathol 2019; 12: 1738-44.
5. Lee JC, Li CF, Huang HY, et al. ALK oncoproteins in atypical inflammatory myofibroblastic tumours: novel *RRBP1-ALK* fusions in epithelioid inflammatory myofibroblastic sarcoma. J Pathol 2017; 241: 316-23.
6. Garg R, Kaul S, Arora D, Kashyap V. Posttransplant epithelioid inflammatory myofibroblastic sarcoma: a case report. Indian J Pathol Microbiol 2019; 62: 303-5.
7. Fu X, Jiang J, Tian XY, Li Z. Pulmonary epithelioid inflammatory myofibroblastic sarcoma with multiple bone metastases: case report and review of literature. Diagn Pathol 2015; 10: 106.
8. Sarmiento DE, Clevenger JA, Masters GA, Bauer TL, Nam BT. Epithelioid inflammatory myofibroblastic sarcoma: a case report. J Thorac Dis 2015; 7: E513-6.
9. Kozu Y, Isaka M, Ohde Y, Takeuchi K, Nakajima T. Epithelioid inflammatory myofibroblastic sarcoma arising in the pleural cavity. Gen Thorac Cardiovasc Surg 2014; 62: 191-4.
10. Yoshida A, Bubendorf L, Varella-Garcia M. ALK testing with FISH. In: Tsao MS, Hirsch FR, Yatabe Y, eds. IASLC atlas of ALK and ROS1 testing in lung cancer. 2nd ed. North Fort Myers: Editorial Rx Press, 2016; 41-52.
11. Parker BM, Parker JV, Lymperopoulos A, Konda V. A case report: pharmacology and resistance patterns of three generations of ALK inhibitors in metastatic inflammatory myofibroblastic sarcoma. J Oncol Pharm Pract 2019; 25: 1226-30.

12. Rush NI, Sinnott M. Malignant inflammatory myofibroblastic tumor of the lung with IgG4-positive plasma cells. Ann Clin Pathol 2016; 4: 1069.
13. Du X, Shao Y, Qin HF, Tai YH, Gao HJ. *ALK*-rearrangement in non-small-cell lung cancer (NSCLC). Thorac Cancer 2018; 9: 423-30.
14. Kim H, Jang SJ, Chung DH, et al. A comprehensive comparative analysis of the histomorphological features of *ALK*-rearranged lung adenocarcinoma based on driver oncogene mutations: frequent expression of epithelial-mesenchymal transition markers than other genotype. PLoS One 2013; 8: e76999.
15. Inamura K, Takeuchi K, Togashi Y, et al. EML4-ALK lung cancers are characterized by rare other mutations, a TTF-1 cell lineage, an acinar histology, and young onset. Mod Pathol 2009; 22: 508-15.
16. Rodig SJ, Mino-Kenudson M, Dacic S, et al. Unique clinicopathologic features characterize *ALK*-rearranged lung adenocarcinoma in the western population. Clin Cancer Res 2009; 15: 5216-23.
17. Yoshida A, Tsuta K, Watanabe S, et al. Frequent *ALK* rearrangement and TTF-1/p63 co-expression in lung adenocarcinoma with signet-ring cell component. Lung Cancer 2011; 72: 309-15.
18. Nishino M, Klepeis VE, Yeap BY, et al. Histologic and cytomorphologic features of *ALK*-rearranged lung adenocarcinomas. Mod Pathol 2012; 25: 1462-72.
19. Popat S, Gonzalez D, Min T, et al. *ALK* translocation is associated with ALK immunoreactivity and extensive signet-ring morphology in primary lung adenocarcinoma. Lung Cancer 2012; 75: 300-5.
20. Cook JR, Dehner LP, Collins MH, et al. Anaplastic lymphoma kinase (ALK) expression in the inflammatory myofibroblastic tumor: a comparative immunohistochemical study. Am J Surg Pathol 2001; 25: 1364-71.
21. Campo E, Gascoyne RD. ALK-positive large B-cell lymphoma. In: Swerdlow SH, Campo E, Harris NL, et al. eds. WHO classification of tumours of haematopoietic and lymphoid tissues. Revised 4th ed. Lyon: IARC Press, 2017; 319-20.
22. Busam KJ, Vilain RE, Lum T, et al. Primary and metastatic cutaneous melanomas express ALK through alternative transcriptional initiation. Am J Surg Pathol 2016; 40: 786-95.
23. Couts KL, Bemis J, Turner JA, et al. ALK inhibitor response in melanomas expressing *EML4-ALK* fusions and alternate ALK isoforms. Mol Cancer Ther 2018; 17: 222-31.
24. Cessna MH, Zhou H, Sanger WG, et al. Expression of ALK1 and p80 in inflammatory myofibroblastic tumor and its mesenchymal mimics: a study of 135 cases. Mod Pathol 2002; 15: 931-8.
25. Gasparini P, Casanova M, Villa R, et al. Anaplastic lymphoma kinase aberrations correlate with metastatic features in pediatric rhabdomyosarcoma. Oncotarget 2016; 7: 58903-14.
26. Soda M, Choi YL, Enomoto M, et al. Identification of the transforming *EML4-ALK* fusion gene in non-small-cell lung cancer. Nature 2007; 448: 561-6.
27. Kim H, Chung JH. Overview of clinicopathologic features of *ALK*-rearranged lung adenocarcinoma and current diagnostic testing for *ALK* rearrangement. Transl Lung Cancer Res 2015; 4: 149-55.
28. Fabre D, Fadel E, Singhal S, et al. Complete resection of pulmonary inflammatory pseudotumors has excellent long-term prognosis. J Thorac Cardiovasc Surg 2009; 137: 435-40.
29. Sakurai H, Hasegawa T, Watanabe S, Suzuki K, Asamura H, Tsuchiya R. Inflammatory myofibroblastic tumor of the lung. Eur J Cardiothorac Surg 2004; 25: 155-9.
30. Childress MA, Himmelberg SM, Chen H, Deng W, Davies MA, Lovly CM. ALK fusion partners impact response to ALK inhibition: differential effects on sensitivity, cellular phenotypes, and biochemical properties. Mol Cancer Res 2018; 16: 1724-36.
31. Fordham AM, Xie J, Gifford AJ, et al. CD30 and ALK combination therapy has high therapeutic potency in *RANBP2-ALK*-rearranged epithelioid inflammatory myofibroblastic sarcoma. Br J Cancer 2020; 123: 1101-13.


JPTM
Journal of Pathology and
Translational Medicine